ON THE APPLICATION OF THE TWO-PARTICLE SELF-CONSISTENT METHOD TO SOME PROBLEMS IN MANY-BODY PHYSICS

By

Arya S.

(PHYS10201004003)

The Institute of Mathematical Sciences, Chennai

A thesis submitted to the

Board of Studies in Physical Sciences

In partial fulfillment of the requirements

for the degree of

DOCTOR OF PHILOSOPHY

of

HOMI BHABHA NATIONAL INSTITUTE

October, 2016

ON THE APPLICATION OF THE TWO-PARTICLE SELF-CONSISTENT METHOD TO SOME PROBLEMS IN MANY-BODY PHYSICS

By

Arya S.

(PHYS10201004003)

The Institute of Mathematical Sciences, Chennai

A thesis submitted to the

Board of Studies in Physical Sciences

In partial fulfillment of the requirements

for the degree of

DOCTOR OF PHILOSOPHY

of

HOMI BHABHA NATIONAL INSTITUTE

October, 2016

Homi Bhabha National Institute

Recommendations of the Viva Voce Committee

As members of the Viva Voce Committee, we certify that we have read the dissertation prepared by Ms. Arya S. entitled "On the application of the two-particle self-consistent method (TPSC) to some problems in many-body physics" and recommend that it maybe accepted as fulfilling the thesis requirement for the award of Degree of Doctor of Philosophy.

_____ Date: _____

Chairman - Prof. Guatam Menon

_____ Date: _____

Guide/Convener - Prof. Syed R. Hassan

_____ Date: _____

Examiner - Prof. Arghya Taraphder

_____ Date: _____

Member 1 - Prof. R. Shankar

_____ Date: _____

Member 2 - Prof. Sanatan Digal

Final approval and acceptance of this thesis is contingent upon the candidate's submission of the final copies of the thesis to HBNI.

We hereby certify that we have read this thesis prepared under our direction and recommend that it maybe accepted as fulfilling the thesis requirement.

Date:_____ _____

Place: IMSc, Chennai Guide: Prof. Syed R. Hassan

STATEMENT BY AUTHOR

This dissertation has been submitted in partial fulfillment of requirements for an advanced degree at Homi Bhabha National Institute (HBNI) and is deposited in the Library to be made available to borrowers under rules of the HBNI.

Brief quotations from this dissertation are allowable without special permission, provided that accurate acknowledgement of source is made. Requests for permission for extended quotation from or reproduction of this manuscript in whole or in part may be granted by the Competent Authority of HBNI when in his or her judgment the proposed use of the material is in the interests of scholarship. In all other instances, however, permission must be obtained from the author.

_____

Arya S.

DECLARATION

I, hereby declare that the investigation presented in the thesis has been carried out by me. The work is original and has not been submitted earlier as a whole or in part for a degree / diploma at this or any other Institution / University.

_____

Arya S

List of Publications arising from the thesis

Journal

1. S. Arya, P. V. Sriluckshmy, S. R. Hassan, and A.-M. S. Tremblay, "Antiferromagnetism in the Hubbard model on the honeycomb lattice: A two-particle self-consistent study"
   Physical Review B, Vol. 92, p 045111 (July 2015)

Others

1. S. Arya, M. S. Laad, and S. R. Hassan, "Exploring novel quantum criticality in strained graphene"
   arXiv : 1611. 04518 [cond-mat.str-el]

_____

Arya S.

Details of the modifications made in the thesis

Below, I summarize all the modifications I have made in my thesis "ON THE APPLICATION OF THE TWO-PARTICLE SELF-CONSISTENT METHOD (TPSC) TO SOME PROBLEMS IN MANY-BODY PHYSICS" based on the reports of the examiners and suggestions of the doctoral committee.

The page numbers given below correspond to the pages of the previous version of the thesis which was sent to the examiners for review. In addition to the changes mentioned below, typos and grammatical errors have been corrected. The examiner had suggested to enhance the size of figures in Chapter 3, especially from fig. (3.5) onwards. The overall size of all figures in this thesis has been enhanced for clarity.

1. On page 27, in the caption for Fig. (1.6), there was a typo. The corrected caption reads, 'Plots of the imaginary part of self-energy as a function of Matsubara frequency ...' instead of 'Plots of the imaginary part of self-energy as a function of interaction ...'

2. On page 32, Eq. (2.3) which was not an interaction term, as pointed out by the examiner, has been corrected.

3. On pages 64 (last paragraph) and 65 (first and third paragraphs), and in the caption of Fig. (3.11), the notation for magneto-volume has been modified to avoid confusion. The earlier notation was similar to the notation for Matsubara frequency, creating ambiguity, as pointed out by the examiner.

अज्ञानतिमिरान्धस्य ज्ञानाञ्जनशलाकया ।

चक्षुरुन्मीलितं येन तस्मै श्रीगुरवे नमः ॥

Salutations to the *Guru* (teacher), who, by applying the collyrium of knowledge to our blind inner eyes, removes the darkness of ignorance from them!

ACKNOWLEDGEMENTS

Without any ado, let me list out the people who have been a part of this journey so far.
From IMSc,
- the teachers who taught me during the first year of course work and the members of my monitoring committee, thank you very much for the experience I had as a new student here. Those were difficult times and I still value all the words of encouragement I got from you.
- the members of my doctoral committee, Prof. Gautam Menon, Prof. Sanatan Digal, I am thankful to you for all the pleasant interactions I had with you.
- the teachers who shared their knowledge with me during my stay in IMSc, Prof. R. Shankar, Prof. Mukul S. Laad and Prof. G. Baskaran, I am grateful to you for the time and patience you people most generously showered on me. It is indeed an honor to have interacted with physicists like you.
- all the administrative staff who were always ready to help, thank you for making my stay here smooth.
- system administrator P. Mangalapandi, thank you for all the discussions that helped me learn a lot about OpenMP and programming in general.
- friend and colleague Luckshmy, thank you for joining me and giving the much-needed push to my work when I was wallowing in listlessness. I will always respect your zest for research.
- Abhra, Tanmoy, Subhadeep, Renjan, Sasi *ettan*, Prasad, Rathul, Raja, Vasan, Majith, Kasi, Anvy, Jilmy, Anju thanks for all the moments of camaraderie we shared.
- Anoop *ettan* and Vinu *chettan*, thank you very much for all the wisdom you impart to, and the concern you show to the fledgling researcher that I am.
and
- Archana and Dibya, who I owe most of my good memories at IMSc to. Thank you so much for being the best friends and colleagues one could ever ask for.

- Prof. A.-M. Tremblay, our collaborator from Université de Sherbrooke
Sherbrooke, Québec, Canada, I am indebted to you for all the knowledge that you with utmost patience and kindness passed on to me.

From CUSAT, my alma mater,
- Prof. M. Sabir and Prof. Ramesh Babu Thayyulathil, it is my great fortune to have been your student and to have been initiated into 'theoretical physics' by you.
- Neeraj, Shijeesh, Navaneeth, Sajan, Sanal *ettan*, Arun *ettan*, Tharanath *ettan*, Anilesh, Linda, Monisha, Jerin thank you all for your company and the continued presence in my life.
From UC College, my alma mater,
- Reena Miss, I am indebted to you for your constant encouragement and affection.
- Ajith Sreenath, Nikhil, Varun, Meera, thanks for your consistent companionship.
and
- Sarada teacher, Ravi, Madhava, Nithin, Mani *chettan*, Manoj, Priya P, Athira *chechi*, thank you very much for all the care and affection.
- Devasia and Meghna, thank you so much for always being there, and for all the wisdom you impart!

- *Achan* and *Amma*, I will always be indebted to you for the love and freedom you bestowed on me as

parents.

- my guide and mentor Prof. S. R. Hassan a.k.a Hassan Sir, you are undoubtedly my best teacher and my real-life hero - the person I will always look up to, as a physicist and as a great human being. **THANK YOU** - now and always!

Contents

SYNOPSIS

Introduction : In the theoretical study of condensed matter systems, where correlations between constituent electrons lead to all sorts of interesting phenomena - the Hubbard model is the most ubiquitous of models. This model, in essence, contains a kinetic energy term which accounts for the hopping of electrons on a lattice and an onsite potential energy (U) penalizing double occupation of a site by electrons. The interaction term renders the exact solution of this model impossible in two and three dimensions. Out of the several approximation schemes implemented to solve this model, we focus on the Two-Particle Self-Consistent scheme (TPSC) [1, 2] . TPSC is a semi-analytical non-perturbative scheme to solve the single-band Hubbard model from weak to intermediate coupling. While being consistent with many physical principles, like conservation laws, Pauli principle and Mermin-Wagner theorem, this method can take into account the effects of long wavelength antiferromagnetic fluctuations. The results from this method agree well with those from Quantum Monte Carlo calculations.

The exact relation between self-energy and two particle correlation functions for the Hubbard model, $\Sigma_\sigma(1,\bar{1})G_\sigma(\bar{1},2) = -U\langle T_\tau c^\dagger_{-\sigma}(1)c_{-\sigma}(1)c_\sigma(1)c^\dagger_\sigma(2)\rangle$ is approximated in TPSC as $\Sigma^{(1)}_\sigma(1,\bar{1})G_\sigma(\bar{1},2) = U\frac{\langle n_\uparrow(1)n_\downarrow(1)\rangle}{\langle n_\uparrow(1)\rangle\langle n_\downarrow(1)\rangle}G_{-\sigma}(1,1^+)G_\sigma(1,2)$. 1 is shorthand for position and imaginary time $(\boldsymbol{r}_1,\tau_1)$ and $\bar{1}$ means summation over the position index and integration over imaginary time. When $\boldsymbol{r}_2 = \boldsymbol{r}_1, \tau_2 = \tau_1^+$, the exact relation is satisfied. Irreducible vertices in spin (U_{sp}) and charge (U_{ch}) channels are determined as functional derivatives of this self-energy. The implementation of this method rests on the existence of local sum rules satisfied by spin (χ^{sp}) and charge (χ^{ch}) susceptibilities. Using these sum rules and invoking self-consistency, we can compute the values of double occupancy, $\langle n_\uparrow n_\downarrow\rangle$, and irreducible vertices. By including spin and charge fluctuations, an improved approximation of the self-energy ($\Sigma^{(2)}$) can be made. TPSC can also be extended to compute the d-wave pairing susceptibility (χ^d), due to the presence of particle-hole fluctuations [3, 4, 5] .

This thesis discusses the application of TPSC to three cases - a) two-band Hubbard model on the honeycomb lattice b) Hubbard model on the square lattice with extended hopping to second and third nearest neighbors, (t-t'-t''-U model) and c) Hubbard model on the honeycomb lattice under uniaxial strain.

Antiferromagnetism in the Hubbard model on the honeycomb lattice : The existence of a quantum spin liquid phase between the semi-metal and antiferromagnet phases in the Hubbard model on the honeycomb lattice is a much debated topic [6, 7, 8] . Since TPSC is a semi-analytical, non-perturbative technique valid from weak to intermediate coupling, satisfying a number of physical principles including Mermin-Wagner theorem, we study this problem using TPSC. The honeycomb lattice is a triangular Bravais lattice with two sublattices. Therefore the formalism needs to be extended to the two-band case to deal with the Hubbard model on the honeycomb lattice. The Green function ($G_{\alpha\beta}$) and self-energy ($\Sigma_{\alpha\beta}$) are 2×2 matrices in the sublattice indices(a, b). The susceptibilities ($\chi_{\alpha\beta\gamma\delta}$) are 4×4 matrices. The procedure we follow is a generalization of the procedure in the case of the single-band Hubbard model. The existence of appropriate sum rules has to be ensured. Starting from the equation of motion of the Green function and using Dyson equation, we arrive at the exact relation satisfied by the self-energy matrix and matrix of two-particle correlation functions. The TPSC ansatz can be extended in a straightforward manner - from the first approximation of a local self-energy, we write down an irreducible spin vertex matrix $\mathcal{U}_{sp}$. This local and frequency independent matrix has non-zero entries ($\mathcal{U}_{sp}^{\alpha\alpha\alpha\alpha}$) when all the four sublattice indices are the same. We assume that the irreducible charge vertex $\mathcal{U}_{ch}^{\alpha\alpha\alpha\alpha}$ has a similar structure. These vertices can be determined numerically using spin and charge sum rules.

Ferromagnetic and antiferromagnetic spin susceptibilities can be defined in terms of the elements of the spin susceptibility matrix for non-interacting (χ^0) and interacting (χ^s) cases $\chi^{0,s}_{afm,fm} = \chi^{0,s}_{aaaa} \pm \sqrt{\chi^{0,s}_{aabb}\,\chi^{0,s}_{bbaa}}$. Thus, similar to the single band case, we can write down scalar expressions for the interacting susceptibilities in terms of the non-interacting susceptibilities. As antiferromagnetic spin fluctuations grow in amplitude, by performing an expansion around the susceptibility maximum at zero momentum and frequency ($\boldsymbol{q} = 0, i\nu = 0$), we can derive a scaling form for the retarded antiferromagnetic spin susceptibility. The ratio of the interacting susceptibility to the non-interacting susceptibility at ($\boldsymbol{q} = 0, i\nu = 0$), is taken as the measure of the correlation length in both the ferromagnetic and antiferromagnetic cases. We work at half-filling, for various values of temperature and interaction U. We numerically compute the double occupancy and the spin vertex. Correlation lengths in the ferromagnetic and antiferromagnetic channel are evaluated.

As we increase U, for lower values of temperature, the antiferromagnetic correlation length (ξ) increases rapidly. The critical interaction for the zero-temperature transition to the antiferromagnet, U_c, can be determined in two ways. The crossover plots to the

renormalized classical regime, where the correlation length (ξ) far exceeds the thermal de Broglie wavelength ($\xi_{th} \sim 1/T$), when extrapolated to zero temperature give the value of U_c. Similarly, from $\ln \xi$ vs. $\ln T$ plots we can determine U_c as well as the dynamical critical exponent z. The dynamical critical exponent is numerically evaluated to be $z = 1$. U_c is determined to be 3.79 ± 0.01, consistent with results from other methods. Since the estimates of the interaction strength for a Mott transition are greater than the value of U_c we obtain, the intermediate spin liquid phase can be ruled out.

Electron-doping in the Hubbard model with extended hopping on the square lattice : The theory behind high-T_c superconductors is a mystery, especially because of the lack of exact solutions to the Hubbard model, assumed to be the basic model containing the relevant physics of high - T_c superconductors. Starting from a strongly coupled antiferromagnetic Mott insulator at half-filling, upon doping the system with holes or electrons, antiferromagnetism is destroyed and superconductivity emerges. On the electron-doped side, antiferromagnetism is more prominent, compared to the hole-doped side where superconductivity is prominent. TPSC is especially suited to study electron-doped cuprates, as the coupling U lies in the weak to intermediate regime. Earlier studies of electron-doped cuprates using TPSC [3, 4] , gave results which were in remarkable agreement with experimental results.

The formalism of TPSC can be extended to study pairing correlations. The infinite Bethe-Salpeter series for the pairing susceptibility (χ_d) at zero momentum and frequency ($\boldsymbol{q} = 0, i\nu = 0$) is approximated by the first two terms, a direct term and a vertex term. The direct term describes direct pairing between interacting quasiparticles. The vertex term describes pairing mediated by spin and charge fluctuations. Hence spin fluctuations have to be large before this term can make a sizeable contribution to the pairing susceptibility. The temperature at which the ratio of the magnitudes of these two terms equals one, is taken as a measure of the superconducting transition temperature (T_c).

We revisit the problem of electron doping in the Hubbard model with extended hopping to the second nearest and the third nearest neighbors (t-t'-t''-U model) , on the two dimensional square lattice. This model agrees well with bandstructure calculations and ARPES results for the electron-doped cuprates. We study the transition temperature (T_i) from commensurate to incommensurate fluctuations as a function of filling by varying t' and t''. Antiferromagnetism seems to be stabilized in the presence of extended hopping. This extended hopping alters the noninteracting Fermi surface compared to the scenario when hopping is restricted to the nearest neighbor. Because of good agreement with

experimental results, from [4] , we choose $t' = -0.175$, and $t'' = 0.05$. The range of fillings studied is from half-filling, ($n = 1.0$) to $n = 1.2$ for interaction values till $U = 6.55$, for a range of temperatures. The antiferromagnetic correlation length increases as temperature decreases, and the value of interaction increases. The system has a crossover to the renormalized classical regime when the correlation length equals the thermal de Broglie wavelength ξ_{th}. The single particle density of states shows a pseudogap when this crossover occurs. For a fixed value of interaction, the antiferromagnetic fluctuations become less strong as we move away from half-filling and the crossover happens at even lower temperatures.

The pairing susceptibility, which is given as the sum of direct and vertex terms shows a dome-shaped variation with respect to filling. At half-filling, the large antiferromagnetic fluctuations create a pseudogap in the single particle density of states [4] , and away from half-filling the fluctuations decrease in magnitude. Previous results [3] of T_c showed a dome shaped variation with filling - there is an optimal doping where T_c is the maximum and T_c decreases on both sides of this doping. In contrast to this, we get a monotonic decrease in T_c as filling moves away from close filling. When $t' = t'' = 0$, at half-filling the noninteracting Fermi surface (FS) and the antiferromagnetic Brillouin zone (AFMBZ) coincide, and the pseudogap effects are significant all over the Fermi surface. As we turn on t' and t'', the FS intersects AFMBZ only at the hot spots, and the pseudogap does not have a catastrophic effect on pairing.

Hubbard model on the honeycomb lattice under uniaxial strain : The application of uniaxial strain to the tight-binding model without interactions on the honeycomb lattice was studied by Pereira and co. [9] . Once the strain reaches a threshold value $\epsilon = 0.23$, a gap opens up in the bandstructure, except when the strain is along the armchair direction. Thus there is a semi-metal to band insulator transition occurring in the system. We study this model using TPSC, after introducing an onsite Hubbard interaction. To do so, we use the multi-band formalism of TPSC developed earlier. In the multi-band case also, an improved approximation to self energy incorporating the effects of fluctuations in the particle-hole channel can be written down.

Since the application of strain changes the lattice vectors, the overlap between orbitals change and hence the hopping parameters change. The hopping parameters are no longer isotropic and the dispersion relation needs to be modified accordingly. We work with reciprocal lattice vectors corresponding to the undistorted lattice. The values of double occupancy as well as the spin and charge vertices can be determined from the spin and

charge sum rules by self-consistent calculations. We look at cases where strain is along the zigzag direction. When strain is really large, the antiferromagnetic correlation length does not show a dramatic increase as interaction increases and temperature decreases. The system remains an insulator.

For strain greater than the threshold where the gap opens up in the noninteracting case, if we remain close to the threshold, the antiferromagnetic correlation length becomes large for decreasing temperature and increasing interaction. This suggests that with the introduction of interaction, the band insulator becomes metallic. If we keep on increasing U, there is a transition from metal to an antiferromagnetic Mott insulator. The improved self energy including the effects of fluctuations lets us compute the interacting Green function. We can confirm this band insulator to metal to antiferromagnetic Mott insulator transition by looking at the interacting single particle density of states for various values of strain.

Summary : To conclude, we extend the formalism of TPSC to the multi-band case and study the semi-metal to antiferromagnet transition in the Hubbard model on the honeycomb lattice. The critical interaction strength for the transition is determined. We study electron-doping in the t-t'-t''-U model on the square lattice and look at pairing mediated by antiferromagnetic fluctuations. The pairing susceptibility has a dome shaped variation with filling, while the superconducting transition temperature decreases monotonically with filling as we move away from half-filling. Finally we study Hubbard interaction on the honeycomb lattice under strain using TPSC. Close to threshold strain where a band gap opens up, the Hubbard interaction turns the system into a metal before finally driving it into an antiferromagnetic insulator.

Bibliography

[1] Y. Vilk and A.-M. Tremblay, "Non-perturbative many-body approach to the hubbard model and single-particle pseudogap," *Journal de Physique I*, vol. 7, no. 11, pp. 1309–1368, 1997.

[2] A.-M. S. Tremblay, "Two-particle-self-consistent approach for the hubbard model," in *Strongly Correlated Systems*, pp. 409–453, Springer, 2012.

[3] B. Kyung, J.-S. Landry, and A.-M. S. Tremblay, "Antiferromagnetic fluctuations and d -wave superconductivity in electron-doped high-temperature superconductors," *Phys. Rev. B*, vol. 68, p. 174502, Nov 2003.

[4] B. Kyung, V. Hankevych, A.-M. Daré, and A.-M. S. Tremblay, "Pseudogap and spin fluctuations in the normal state of the electron-doped cuprates," *Phys. Rev. Lett.*, vol. 93, p. 147004, Sep 2004.

[5] S. R. Hassan, B. Davoudi, B. Kyung, and A.-M. S. Tremblay, "Conditions for magnetically induced singlet d-wave superconductivity on the square lattice," *Phys. Rev. B*, vol. 77, p. 094501, Mar 2008.

[6] Z. Meng, T. Lang, S. Wessel, F. Assaad, and A. Muramatsu, "Quantum spin liquid emerging in two-dimensional correlated dirac fermions," *Nature*, vol. 464, no. 7290, pp. 847–851, 2010.

[7] S. Sorella, Y. Otsuka, and S. Yunoki, "Absence of a spin liquid phase in the hubbard model on the honeycomb lattice," *Scientific reports*, vol. 2, 2012.

[8] S. Hassan and D. Sénéchal, "Absence of spin liquid in nonfrustrated correlated systems," *Physical review letters*, vol. 110, no. 9, p. 096402, 2013.

[9] V. M. Pereira, A. C. Neto, and N. Peres, "Tight-binding approach to uniaxial strain in graphene," *Physical Review B*, vol. 80, no. 4, p. 045401, 2009.

Publications in Refereed Journal:

a. Published:

(1) S. Arya, P. V. Sriluckshmy, S. R. Hassan, and A.-M. S. Tremblay, "Antiferromagnetism in the Hubbard model on the honeycomb lattice: A two-particle self-consistent study"
Physical Review B, Vol. 92, p 045111 (July 2015)

Presentations :

1. Talk titled 'Two-particle self-consistent approach in graphene' during 'Meeting on Transport in Topological Insulators' HRI, Allahabad on July 11, 2013.

2. Talk titled 'Antiferromagnetism in the Hubbard model on the honeycomb lattice' at the Condensed Matter Journal Club meeting at IMSc, on June 26, 2015.

Signature of Student:
Date:

List of Figures

Chapter 0

Introduction and Lexicon

0.1 What do I do ?

Disclaimer : This section is an attempt to explain my work to my parents and friends with minimum use of technical jargon.

The synergy we see all around us, is the result of interactions and correlations among the innumerable animate and inanimate objects in the universe. Imagine a world where there is no 'give and take', that would be a dull scenario, no matter how cliched it sounds. The astounding complexity, unpredictability and beauty of the world as it is, result from this process of give and take. And, as condensed matter theorists working on strongly correlated systems, we study a tiny part of this huge world.

Let me start with a very crude example. Consider a hypothetical research institute, and let their be N number of identical students in that institute. By 'identical', I mean they have some common attributes. They come to the institute, work, have lengthy discussions with their supervisors and peers, eat, drink coffee, sleep, watch movies or read books and so on. Suppose I follow one of the students for some days in succession. I get to know when he turns up at his desk, how long he works, how much time he spends in idle browsing on the internet, the usual schedule of his discussions with his supervisor, whether he avoids his supervisor by taking the least favored route to the common canteen during lunch, whether he has friends who he hangs out with and so on. Similarly, I can follow a pair of students to see when and where they hang out, whether they discuss their work, or share gossip, or share their knowledge about the latest of movies, or argue about who should govern the country and so on.

If the number of students is very large, I would not be able to follow everyone or every possible pair. I may have to devise some 'approximate' method to study trends.

That implies that I have to find a method apt to the particular problem I have at hand. Depending on what I want to know about the students, I can follow them during the day, or the night, on a sunny day or a rainy day. Or I may follow female students, or students above a certain age otherwise I watch them only during coffee time everyday. But, there is no guarantee that I can implement the same method to two extremely different case scenarios. If I follow the students during the day, I may be able to say what they would be upto during the evenings crudely. But, their nightlife for sure is beyond my study.

By doing the above exercise, I get a general idea about the students and the institute. And, I may arrive at conclusions about the style of work, their productivity and average amount of time spent a day drinking coffee or playing badminton, or how the weather affects these patterns and so on.

This is a very crude example, nevertheless, this sheds some light on what we attempt to do. Imagine a box of electrons and we are to write a 'story' about this box of electrons. For simplicity, let us assume that the interactions between the electrons are turned off. Suppose, we can (have the capability to) follow one particular electron and see what it is upto. If we are able to do this, we basically know the entire story. The other electrons are just copies of our electron and do the same things which our electron does. Since we have turned off the interactions, they all mind their own business, in fact, when they meet each other, they do not wish each other or exchange pleasantries, they just carry on as if their counterparts were not there. Studying this box of electrons is not hard, even if there are a large number of those.

Let us turn on interactions in the system. Now the game changes totally and the story has to be rewritten. The sheer number of electrons, their interactions and correlations, and many other interesting ingredients add different layers and twists to the stories. In fact, newer storylines may 'emerge' like ferromagnetism, superconductivity etc. A total description of the entire system in its finest details is beyond us. Hence, we can devise a 'model' which captures the crux of the system. This model is analogous to an 'outline' to the beginning of a story and our task is to complete the story.

Even with the outline at hand, we may have to resort to approximations, so that the outline is amenable and generates an interesting story. And, there may be different methods to make the outline tractable - for instance, our neighbor may have a totally different tool which he prefers to use to chisel the story. No matter what the approach is, it cannot neglect certain basic laws which we expect the system to comply with. If this condition is not respected, it might result in an 'unphysical' scenario in the story.

Just like following a single student or a pair of students in an institute, in a system of

electrons, I can look at quantities called the single particle Green function (or correlation function), or the two-particle Green function to study the system. The single particle Green function contains the entire information about the electron and is easy to calculate when there are no interactions. When interactions are present in the system, the Green function of a single electron gets modified. This additional contribution is called the self-energy. It is sometimes the most 'wanted' quantity in our studies and therefore is hard to track down easily. The two-particle Green functions are related to the 'responses' of the system - what happens when we shine light on the system or heat it. The way two particles propagate in the system is also different when there are interactions in the system.

Having said that, let me introduce the Hubbard model, the most ubiquitous among theoretical models in the study of condensed matter systems. Why do we need such theoretical models - these models help us describe real life materials in a theoretical language. The description in most cases is not exact, its usually very crude with the bare essentials which we can manage. Experimentalists perform experiments on materials, while theoreticians try to solve the model on a piece of paper or on a computer, and try to explain the experimental results, or try and predict new and interesting results. For instance, the Hubbard model came to the forefront when high temperature superconductivity was discovered.

Moving on, the Hubbard model is one of the simplest models which describe the interactions between electrons in a condensed matter system. Let us imagine a set of points on a square mesh. The square mesh is easy to imagine, in fact this 'mesh' can come in many varieties - square, triangle, cube etc. Assume the electrons are restricted to move only on the points on this mesh. The electrons have a 'spin' - an attribute which can come in two forms, we call them 'up' and 'down'. A 'site' on the mesh can have at most two electrons, if they have different spins - that is one electron has up spin and the other electron has down spin. Otherwise, a site can have an electron of either spin, or no electron at all. These are the only allowed scenarios. A site can never have two electrons of the same spin - this is ruled out by the famous Pauli exclusion principle. The allowed physical process is the 'hopping' of an electron from a site to its immediate neighbor. When a site is 'doubly occupied', the electrons interact with each other. This is not a good situation, the electrons do not like to be on the same site because of the repulsion they feel for each other.

An entity called the Hamiltonian for this system can be written, which is a description of the scenario - the model - in technical language. The Hubbard model thus includes, the

hopping of electrons from site to site and the interaction felt by two electrons on the same site. The model does not talk about interactions between electrons on two neighboring sites or anything. In that sense, we have a very simple model to start with. This is the outline of the story and it is complete when we 'solve' this model.

When we write down a model, there are certain parameters which describe the system, the temperature, the value of hopping, the value of interaction, the number of electrons, the shape of the mesh etc. By attempting to solve the model, we try to figure out the behavior of the system, or the real-life system which the model approximately describes. Crudely speaking, when interaction is increased in the Hubbard model, the system can change from a metal to an insulator. So, for a mesh with a single electron at every site, we can slowly crank the interaction up and see when the system becomes an insulator and so on.

In the case of the Hubbard model, when there is only hopping, the model is solvable. When there is no hopping and there is only onsite interaction between electrons, the model is solvable. For the most general case, the model despite its innocuous simplicity, is very hard to solve. So far, it has been solved only in one dimension (when the electrons are restricted to move on a line of points) and in infinite dimensions (imagining this is slightly tricky) [1, 2]. Many approximate methods have been devised to study it in two and three dimensions. And, I study this model with an approach named two-particle self-consistent (TPSC) approach. Using this method, we study the Hubbard model when the onsite interaction is of weak to intermediate strengths compared to the strength of hopping. This method introduces its own approximations, nevertheless so far it has been remarkably successful in completing many different stories! This thesis is the sum total of our attempts to study the Hubbard model in different scenarios using this method.

0.2 Lexicon

0.2.1 Bloch basis and Wannier basis

We are familiar with the description of electrons in a periodic potential by the Bloch basis, here the wave function is given by the product of a plane wave and a periodic function. The periodic function has the periodicity of the Bravais lattice.

$$\psi_{n\boldsymbol{k}}(\boldsymbol{r}) = e^{i\boldsymbol{k}\cdot\boldsymbol{r}}\, u_{n\boldsymbol{k}}(\boldsymbol{r}) \tag{1}$$

$$u_{n\boldsymbol{k}}(\boldsymbol{r}+\boldsymbol{R}) = u_{n\boldsymbol{k}}(\boldsymbol{r}) \tag{2}$$

$$\psi_{n\boldsymbol{k}}(\boldsymbol{r}+\boldsymbol{R}) = \psi_{n\boldsymbol{k}}(\boldsymbol{r}) \tag{3}$$

where $\boldsymbol{R}$ is a vector in the Bravais lattice and $\boldsymbol{k}$ is a vector in the Brillouin zone.

From the delocalized Bloch basis, we can make a unitary transformation to a localized basis called the Wannier basis. This is done with the tight-binding approximation in mind. This approximation works when the energy levels centered on each atom in the lattice give a somewhat accurate description of the lattice, and there is no significant overlap between the atomic energy levels. The Wannier basis can be reached by a Fourier transform as,

$$\phi_n(\boldsymbol{r}-\boldsymbol{R}) = \frac{1}{N^2}\sum_{\boldsymbol{k}} e^{-i\boldsymbol{R}\cdot\boldsymbol{k}}\psi_{n\boldsymbol{k}}(\boldsymbol{r}) \tag{4}$$

where N^2 is the number of sites on the lattice.

We work in the occupation number formalism making use of electron creation and annihilation operators. These operators can be either in the Bloch basis or in the Wannier basis. The creation and annihilation operators obey the following relations,

$$\{c_{\boldsymbol{k}}, c^\dagger_{\boldsymbol{p}}\} = \delta_{\boldsymbol{k},\boldsymbol{p}}\,, \quad \{c_{\boldsymbol{k}}, c_{\boldsymbol{p}}\} = 0\,, \quad \{c^\dagger_{\boldsymbol{k}}, c^\dagger_{\boldsymbol{p}}\} = 0 \tag{5}$$

and

$$\{c(\boldsymbol{r}_1), c^\dagger(\boldsymbol{r}_2)\} = \delta_{\boldsymbol{r}_1,\boldsymbol{r}_2}\,, \quad \{c(\boldsymbol{r}_1), c(\boldsymbol{r}_2)\} = 0\,, \quad \{c^\dagger(\boldsymbol{r}_1), c^\dagger(\boldsymbol{r}_2)\} = 0 \tag{6}$$

on a lattice. The number operator is given by $n_{\boldsymbol{k}} = c^\dagger_{\boldsymbol{k}} c_{\boldsymbol{k}}$ or $n(\boldsymbol{r}) = c^\dagger(\boldsymbol{r})c(\boldsymbol{r})$. The transformation is given by

$$c(\boldsymbol{r}) = \frac{1}{N}\sum_{\boldsymbol{k}} c_{\boldsymbol{k}} e^{i\boldsymbol{k}\cdot\boldsymbol{r}} \tag{7}$$

Either description is valid, but the choice is always made depending on which description aptly describes the system. For electrons moving in a periodic potential without interacting with each other, the Bloch description is suited. But, for instance when electrons on a single atom interact with each other the Wannier description seems to be more apt.

0.2.2 Correlation functions

Single-particle Green function or two-point correlation function

The single-particle Green function defines the probability amplitude of creating a particle of spin σ' at position $\boldsymbol{r'}$ at time τ' and annihilating a particle of spin σ at position $\boldsymbol{r}$ at time τ. The most general definition is,

$$\begin{aligned} G^{\sigma\sigma'}(\boldsymbol{r}\tau\,;\,\boldsymbol{r'}\tau') &= -\langle T_\tau c_{\boldsymbol{r}\sigma}(\tau) c^\dagger_{\boldsymbol{r'}\sigma'}(\tau')\rangle \\ &= -Tr\big[e^{-\beta H} T_\tau e^{\tau H} c_{\boldsymbol{r}\sigma} e^{-\tau H} e^{\tau' H} c^\dagger_{\boldsymbol{r'}\sigma'} e^{-\tau' H}\big] \end{aligned} \tag{8}$$

where T_τ means time ordering in imaginary time τ. The concept of imaginary time is a 'trick' used to deal with the factor $e^{-\beta H}$ appearing in expressions at finite temperature, temperature is treated as an 'imaginary' time once we compare this factor to the time evolution factor given by e^{-itH}. The imaginary time axis stretches from 0 to β, the inverse temperature. Let us take the most common case, $\sigma = \sigma'$. When the system has translational invariance and the Hamiltonian is time-independent, $G(\boldsymbol{r}\tau\,;\,\boldsymbol{r'}\tau') = G(\boldsymbol{r}-\boldsymbol{r'}\,,\tau-\tau')$. The single-particle Green function written in momentum space is,

$$G(\boldsymbol{k},\tau-\tau') = \sum_{\boldsymbol{r}} e^{-i\boldsymbol{k}\cdot\boldsymbol{r}} G(\boldsymbol{r}-\boldsymbol{r'}\,,\tau-\tau') \tag{9}$$

and even defined as,

$$G(\boldsymbol{k},\tau-\tau') = -\langle T_\tau c_{\boldsymbol{k}\sigma}(\tau) c^\dagger_{\boldsymbol{k}\sigma}(\tau')\rangle \tag{10}$$

$$= -Tr\big[e^{-\beta H} T_\tau e^{\tau H} c_{\boldsymbol{k}\sigma} e^{-\tau H} e^{\tau' H} c^\dagger_{\boldsymbol{k}\sigma} e^{-\tau' H}\big] \tag{11}$$

The fermionic single-particle Green function is anti-periodic in time. The Green function can be Fourier transformed to the imaginary frequency space as

$$G(\boldsymbol{k}, i\omega_n) = \int_0^\beta d\tau e^{ik_n\tau} G(\boldsymbol{k},\tau) \tag{12}$$

Here the frequencies are fermionic Matsubara frequencies which are given by $i\omega_n = (2n+1)\frac{\pi}{\beta}$. In the noninteracting case, this Green function is

$$G^0(\boldsymbol{k}, i\omega_n) = \frac{1}{i\omega_n - \varepsilon_{\boldsymbol{k}}} \tag{13}$$

By analytic continuation, $i\omega_n \to \omega + i\delta$, the retarded Green function and the energy spectrum of the problem can be determined. This is true for the interacting Green function also, however in most cases, analytic continuation is a nontrivial problem.

The noninteracting Green function is easy to determine and when interactions are introduced in the system the Green function changes. Writing down the interacting Green function in a form like Eq. (13) is tricky. This is where the concept of 'self-energy' comes into play. The energy of the particle gets changed from the noninteracting energy $\varepsilon_{\boldsymbol{k}}$ because of the interactions it undergoes in the many-particle system. The particle interacts with 'itself' through the changes it causes in the system due to its interactions with its counterparts [3], hence the name 'self-energy'.

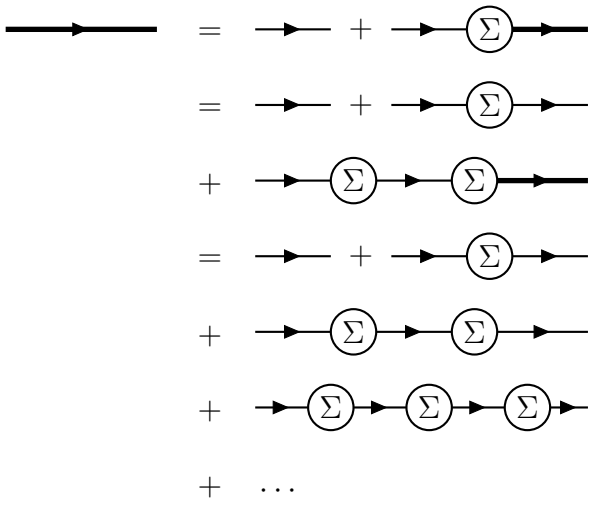

Figure 1: Diagrammatic representation of the Dyson equation. Here, the 'thin' line represents the noninteracting Green function G^0, the 'thick' line represents the interacting Green function G. Σ is the self-energy.

The interacting Green function may thus be written as,

$$G(\boldsymbol{k}, i\omega_n) = \frac{1}{i\omega_n - \varepsilon_{\boldsymbol{k}} - \Sigma(\boldsymbol{k}, i\omega_n)} \tag{14}$$

where $\Sigma(\boldsymbol{k}, i\omega_n)$ is the self-energy function. Written otherwise as,

$$G^{-1}(\boldsymbol{k}, i\omega_n) = (G^0)^{-1}(\boldsymbol{k}, i\omega_n) - \Sigma(\boldsymbol{k}, i\omega_n) \tag{15}$$

This is the famous Dyson equation connecting the noninteracting and interacting Green functions via the self energy function. The interacting Green function is visualized as the 'total' of the noninteracting Green function and all 'possible' encounters the particle can have on its trajectory (Fig. 1). All interaction effects are 'bundled' into the self energy and therefore it is the object most sought after in the study of a many-body system.

Two-particle Green function or four-point correlation function

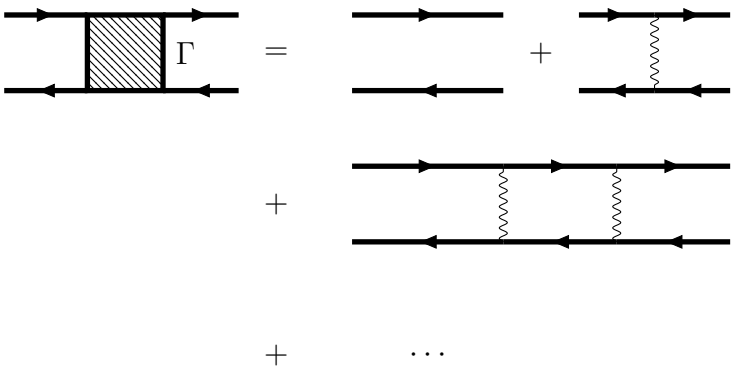

Figure 2: Diagrammatic representation of the Bethe-Salpeter equation for the particle-hole propagator. Here, the wiggly line represents the bare interaction and the hatched rectangle Γ represents the renormalized interaction.

Just like a single-particle correlation function was defined, a two-particle correlation function can also be introduced. This correlation function is of the form

$$\chi(1,2,3,4) = -\langle T_\tau c_{\boldsymbol{r}_4\sigma}(\tau_4) c^\dagger_{\boldsymbol{r}_3\sigma}(\tau_3) c_{\boldsymbol{r}_2\sigma}(\tau_2) c^\dagger_{\boldsymbol{r}_1\sigma}(\tau_1)\rangle \tag{16}$$

where $(1 = (\boldsymbol{r}_1, \tau_1))$.

This represents the probability amplitude for two particles introduced in the system at $(\boldsymbol{r}_1, \tau_1)$ and $(\boldsymbol{r}_3, \tau_3)$ to end up at $(\boldsymbol{r}_2, \tau_2)$ and $(\boldsymbol{r}_4, \tau_4)$. Depending on time ordering, this four-point correlation function may either be a particle-particle propagator or particle-hole propagator. From linear response theory, when small external perturbations like a magnetic field or an electric field act on the system, the response functions of the system

are given in terms of two-particle correlation functions [4]. Therefore, quantities like the magnetic susceptibility, electrical conductivity are described in terms of such two-particle correlation functions.

When there are no interactions in the system, the two-particle correlation functions can be factorized in terms of single-particle correlation functions - as the trajectory of a particle is not affected by other particles. The interacting response function can be written in terms of the noninteracting response function, just like we did in the case of the single-particle Green function. The analogue of the Dyson equation in the two-particle case is usually called the Bethe-Salpeter equation. The concept of the irreducible vertex aids us in doing this. The irreducible vertex is the so called renormalized interaction - the bare interaction between two particles gets modified as a result of the many possible events that can occur in the system, due to the sheer number of interacting particles in it.

This thesis deals with the application of two-particle self-consistent (TPSC) method to a handful of problems in many-body physics. Chapter 1 introduces the method as applied to the single-band repulsive Hubbard model, and presents some results for the half-filled case of the two-dimensional square lattice. Further, in Chapter 2 this method is generalized to the two-band case of graphene, to study the semi-metal to antiferromagnet transition of the half-filled Hubbard model on the honeycomb lattice. Using this generalized TPSC for the honeycomb lattice again, in Chapter 3, we study graphene under uniaxial strain. Going back to TPSC for the single-band Hubbard model, the pairing mediated by antiferromagnetic fluctuations in the Hubbard model on the square lattice with extended hopping to the second and nearest neighbors is studied in Chapter 4. A brief summary and outlook follow in Chapter 5.

Chapter 1

Introduction to the two-particle self-consistent method

1.1 Introduction

In the 1960s, in a series of papers titled, 'Electron correlations in narrow energy bands', John Hubbard introduced the eponymous Hubbard model [5–9]. It was visualized by Kanamori [10] and Gutzwiller [11] around the same time, but it was Hubbard's name that got attached to the model. Till then, the model of the free electron gas was successful in the description of the conduction bands of metals and alloys. But, for transition and rare-earth metals which had partially filled d and f bands, the correlations between electrons influence their properties. The free electron gas was found inadequate to describe these materials, even with the addition of electron correlations. Since the electron charge density is concentrated around the nuclei in the case of d and f bands, we can talk in terms of electrons being on some specific atom. The new model tried to combine the characteristics of the band model as well as the atomic model. Although it is stated that the theory is designed for the case of d and f electrons, the model in its simplest form contains electrons of two states per atomic site, spin up and spin down.

The Hubbard Hamiltonian is written as

$$H = H_0 + H_{int} \tag{1.1}$$

$$H_0 = -t \sum_{\langle ij \rangle \sigma} c^{\dagger}_{i\sigma} c_{j\sigma} + h.c \tag{1.2}$$

$$H_{int} = U \sum_{i} n_{i\uparrow} n_{i\downarrow} \tag{1.3}$$

The operator $c_{i\sigma}$ ($c^{\dagger}_{i\sigma}$) destroys (creates) an electron of spin σ on site i on the lattice. The number operator, $n_{i\sigma} = c^{\dagger}_{i\sigma}c_{i\sigma}$, gives the number of electrons with spin σ on site i of the lattice.

This Hamiltonian written in the Wannier basis comes from the tight-binding description of electrons in a material. The kinetic part (1.2) of the Hamiltonian describes the hopping of an electron in an orbital on a lattice site to the orbital on the neighboring site. The overlap between the orbitals determines the value of t. Whenever an orbital becomes occupied by two electrons of opposite spins, there is a potential energy penalty of U to be paid (1.3). This is the interaction part of the Hamiltonian. $\langle ij \rangle$ denotes that the lattice sites i and j are nearest neighbors.

There are two limits to the model - the two extremes which can be handled. When $U = 0$, and t is non-zero, the noninteracting model depicts the hopping of electrons from site to site, gaining kinetic energy. This situation describes a metal. Suppose $t = 0$, and U is non-zero, we reach the so-called atomic limit. The atoms are totally decoupled from each other and there are no charge fluctuations in the system. At half-filling ($n = 1.0$), when every site is occupied by an electron, suppose we slowly increase the interaction U. Then the electrons would hesitate to hop to the nearest neighbor site, because of the increasing potential energy penalty to be paid. Thus there is a transition from a metal to an insulator. This insulator is different from the band insulator we are familiar with and is known as a Mott insulator.

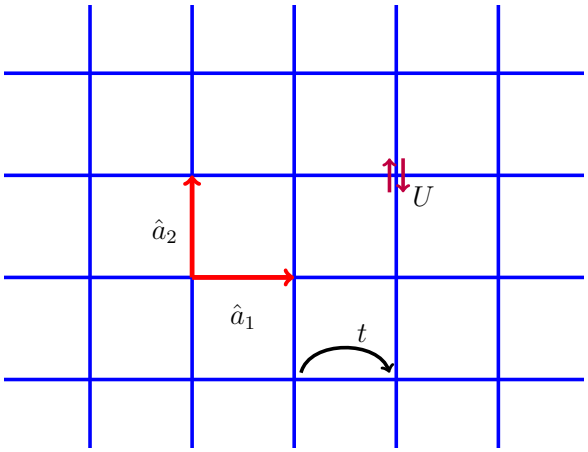

Figure 1.1: Hubbard model on the two dimensional square lattice, with the basis vectors shown in red. The hopping parameter t and the Hubbard interaction U are also indicated.

By a transformation from the Wannier basis to the Bloch basis, the noninteracting

tight-binding Hamiltonian for the square lattice can be written as,

$$H_0 = \sum_{\boldsymbol{k}\sigma} \epsilon_{\boldsymbol{k}} c^{\dagger}_{\boldsymbol{k}\sigma} c_{\boldsymbol{k}\sigma} \tag{1.4}$$

$$\epsilon_{\boldsymbol{k}} = -2t \left(\cos(\boldsymbol{k} \cdot a\boldsymbol{e_x}) + \cos(\boldsymbol{k} \cdot a\boldsymbol{e_y})\right)$$

$$\epsilon_{\boldsymbol{k}} = -2t \left(\cos k_x + \cos k_y\right) \tag{1.5}$$

where the distance between nearest neighbors a is taken as unity.

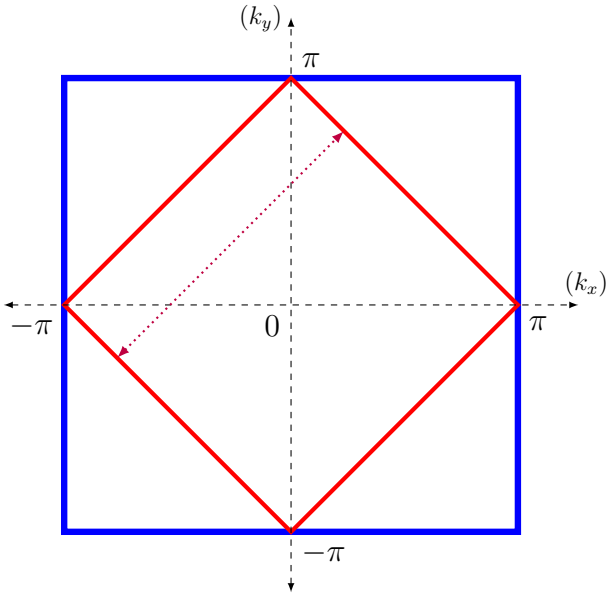

Figure 1.2: Brillouin zone of the two dimensional square lattice. The noninteracting Fermi surface at half-filling is shown in red. Given in purple is the nesting vector at half-filling given by (π, π), which maps one portion of the Fermi surface to the other.

1.2 Two-particle self-consistent approach

The Hubbard model has so far been solved exactly in one dimension [1] and infinite dimensions [2]. When it comes to two dimensions and three dimensions, where the model is applicable to real-life materials, the solutions are somewhat elusive.

The two-particle self-consistent method (TPSC) [12–14] is a non-perturbative, semi-analytical approach developed to study the single-band repulsive Hubbard model. In TPSC, when we compute solutions, analytics work till a point. Beyond that, we need self-consistent numerical calculations to reach the solutions. TPSC is valid from weak to

intermediate values of coupling. Hence, this method is not fit to study the Mott transition. TPSC satisfies many physical constraints, like the conservation of spin and charge, the Pauli exclusion principle and the Mermin-Wagner theorem [15, 16] which rules out finite temperature phase transitions in two dimensional systems. At finite temperature, the rapidly growing antiferromagnetic fluctuations and the resultant pseudogap in the single-particle density of states [17, 18] in the Hubbard model can be studied using this method. The results from this method have been shown to be in good agreement with solutions from Quantum Monte Carlo calculations [14]. The successful implementation of TPSC rests on the existence of appropriate sum rules. These sum rules are essential for the computation of irreducible vertices.

The two-particle self-consistent method has been extended to study the attractive Hubbard model in the weak to intermediate coupling regime [19, 20]. In this model, the pairing fluctuations in the renormalized classical regime cause a pseudogap in the single-particle density of states. Further, TPSC can also be extended to study the d- wave pairing mediated by antiferromagnetic fluctuations in the single-band Hubbard model [21–23]. By adding next-nearest neighbor interaction is added to the model, TPSC can be generalized to Extended TPSC (ETPSC) , letting one study competing spin and charge orders [24–26].

1.3 Spin and charge susceptibilities

If there is a small perturbation which couples to the spin or charge, we can calculate the linear response of the system. The response functions, the so called spin and charge susceptibilities are given by,

$$\chi_{sp}(1,2) = \langle T_\tau S_z(1) S_z(2) \rangle \tag{1.6}$$

$$\chi_{ch}(1,2) = \langle T_\tau n(1) n(2) \rangle - n^2 \tag{1.7}$$

Here, 1 is shorthand for $(\boldsymbol{r}_1, \tau_1)$. S_z is the z component of spin $S_z(1) = n_\uparrow(1) - n_\downarrow(1)$ and n is the charge, $n(1) = n_\uparrow(1) + n_\downarrow(1)$. The susceptibilities, from their definition, describe how much the spin or charge in the system at different sites 'talk to' each other. If there is some sort of spin order in the system, we would expect the spins to be 'correlated' and the spin susceptibility to diverge. If the charge susceptibility is large, there are charge fluctuations in the system, the system is expected to be a metal. Once the charge susceptibility is small, the charge fluctuations decrease and the system is an insulator.

The spin and charge susceptibilities when summed over all momenta and frequencies give us the following local spin and charge sum rules, these are just the local equal-time susceptibilities.

$$\begin{aligned}\chi_{sp}(0) &= \langle\, S_z S_z \,\rangle \\ &= \langle\, (\, n_\uparrow - n_\downarrow \,)^2 \,\rangle \\ &= \langle\, n_\uparrow n_\uparrow \,-\, n_\uparrow n_\downarrow \,-\, n_\downarrow n_\uparrow \,+\, n_\downarrow n_\downarrow \,\rangle \\ &= \langle n_\uparrow \rangle + \langle n_\downarrow \rangle - 2\langle n_\uparrow n_\downarrow \rangle \\ &= n - 2\langle n_\uparrow n_\downarrow \rangle \end{aligned} \tag{1.8}$$

Similarly for the charge susceptibility

$$\begin{aligned}\chi_{ch}(0) &= \langle\, n^2 \,\rangle - \langle n \rangle^2 \\ &= \langle\, (\, n_\uparrow + n_\downarrow \,)^2 \,\rangle - \langle n \rangle^2 \\ &= \langle n_\uparrow \rangle + \langle n_\downarrow \rangle + 2\langle n_\uparrow n_\downarrow \rangle - \langle n \rangle^2 \\ &= n + 2\langle n_\uparrow n_\downarrow \rangle - n^2 \end{aligned} \tag{1.9}$$

$n_\sigma = \frac{n}{2}$ is the average occupation number of the spin species σ, and n is the filling. While deriving these sum rules, the Pauli principle in the form $n_\sigma^2 = n_\sigma$ is made use of. No matter what approximation gives us the spin and charge susceptibilities, these quantities have to obey these rules - this is a basic physical constraint on the approximation.

In the noninteracting case, both the spin and charge susceptibilities are given by the same object, the Lindhard function. The Lindhard function or the noninteracting susceptibility is given by,

$$\chi_0(q) = -\frac{1}{\beta}\frac{1}{N^2}\sum_{k,\sigma} G^0(k)\, G^0(k+q) \tag{1.10}$$

$$= -\frac{1}{\beta}\frac{1}{N^2}\sum_{k,\sigma} \frac{1}{i\omega_n - \epsilon_{\boldsymbol{k}}}\;\frac{1}{i\omega_n + i\nu_n - \epsilon_{\boldsymbol{k}+\boldsymbol{q}}}$$

$$= -\frac{2}{N^2}\sum_{\boldsymbol{k}} \frac{n_F(\epsilon_{\boldsymbol{k}}) - n_F(\epsilon_{\boldsymbol{k}+\boldsymbol{q}})}{i\nu_n + \epsilon_{\boldsymbol{k}} - \epsilon_{\boldsymbol{k}+\boldsymbol{q}}} \tag{1.11}$$

where $q = (\boldsymbol{q}, i\nu_n)$ a shorthand for both the momentum $\boldsymbol{q}$ and the bosonic Matsubara frequency $i\nu_n$, $\beta = \frac{1}{T}$ is the inverse temperature. In Eq. (1.10) the summation is over all momenta $\boldsymbol{k}$, Fermionic Matsubara frequencies $(i\omega_n)$, and spin σ, while in Eq. (1.11)

the Matsubara summation has already been taken care of and the summation is just over all the momenta in the Brillouin zone. $n_F(\epsilon)$ is the Fermi distribution function, $n_F(\epsilon) = \frac{1}{e^{\beta\epsilon}+1}$.

The susceptibilities in the interacting case can be written in terms of the noninteracting susceptibilities using the Bethe-Salpeter equation. As mentioned previously, the Bethe-Salpeter equation is for the two-particle correlation function as the Dyson equation is to the single-particle correlation function, with the irreducible vertex being analogous to the self-energy. The irreducible vertex is momentum and frequency dependent in the most general case.

$$\chi_{sp}(q) = \frac{\chi_0(q)}{1 - \frac{\Gamma_{sp}(q)}{2}\chi_0(q)} \tag{1.12}$$

$$\chi_{ch}(q) = \frac{\chi_0(q)}{1 + \frac{\Gamma_{ch}(q)}{2}\chi_0(q)} \tag{1.13}$$

where $\Gamma_{sp,ch}$ are the irreducible vertices.

1.3.1 RPA vs. TPSC

Let us consider RPA or mean-field approximation, where the spin and charge vertices are both equal to the bare interaction U. The vertices are local and frequency independent. The spin and charge susceptibilities can be written as,

$$\chi_{sp}^{RPA}(q) = \frac{\chi_0(q)}{1 - \frac{U}{2}\chi_0(q)} \tag{1.14}$$

$$\chi_{ch}^{RPA}(q) = \frac{\chi_0(q)}{1 + \frac{U}{2}\chi_0(q)} \tag{1.15}$$

Let us take a look at some pitfalls that RPA has. First of all consider the denominator of the spin susceptibility, given by Eq. (1.14). When the denominator becomes zero, the spin susceptibility diverges, this means there is long-range spin order in the system. This scenario is prohibited by the Mermin - Wagner theorem which states that a continuous symmetry cannot be broken in two dimensions at finite temperature. In RPA, as we increase U, eventually we reach the mean - field transition value of interaction

$$U_{mf} = \frac{2}{\chi_0^{max}} \tag{1.16}$$

where χ_0^{max} is the maximum value of the susceptibility. This gives us a totally unphysical

result.

Similarly, let us consider the sum rules. The sum of the 'sum rules' Eqs. (1.8) and (1.9) is

$$\frac{T}{N^2}\sum_q \chi_{sp}(q) + \frac{T}{N^2}\sum_q \chi_{ch}(q) = 2n - n^2 \tag{1.17}$$

In RPA, the left hand side can be written after an expansion of the denominators as

$$\begin{aligned}\frac{T}{N^2}\sum_q \chi_{sp}^{RPA}(q) + \chi_{ch}^{RPA}(q) = \frac{T}{N^2}\sum_q \chi_0 + U(\chi_0(q))^2 + U^2(\chi_0(q))^3 \\ + \chi_0 - U(\chi_0(q))^2 + U^2(\chi_0(q))^3 + \cdots\end{aligned} \tag{1.18}$$

The RHS exceeds the physical result in RPA, because $\chi^0(q)$ is a positive quantity.

In RPA or mean-field theory, one factorizes the two particle Green function as the product of two single particle Green functions. For instance, the double occupancy $\langle n_\uparrow n_\downarrow\rangle = \langle n_\uparrow\rangle\langle n_\downarrow\rangle$. So at half-filling, RPA would give $\langle n_\uparrow n_\downarrow\rangle = \frac{1}{2}\times\frac{1}{2} = 0.25$. Now, imagine we turn on the onsite Hubbard interaction U. We expect the average probability of two electrons being on the same site to decrease in order to reduce the potential energy. Clearly, mean-field factorization of two-particle correlation functions is not an accurate approximation. This is where TPSC does a remarkable job in taking care of the correlation effects. The correlation effects due to two particles being on the same site is captured using TPSC.

Let us study the single-band Hubbard model on the square lattice at half-filling using the two-particle self-consistent method (TPSC), so that we get a precise idea regarding the implementation of this method. The interacting spin susceptibility and charge susceptibility are given in terms of the noninteracting Lindhard function by means of RPA like equations.

$$\chi_{sp}(q) = \frac{\chi_0(q)}{1 - \frac{U_{sp}}{2}\chi_0(q)} \tag{1.19}$$

$$\chi_{ch}(q) = \frac{\chi_0(q)}{1 + \frac{U_{ch}}{2}\chi_0(q)} \tag{1.20}$$

Here, U_{sp} and U_{ch} denote the irreducible spin and charge vertices or the renormalized interactions. The spin and charge susceptibilities have to obey local spin and charge sum rules (Eqs. (1.8) and (1.9)) . But, how should we go about calculating the irreducible

vertices? We introduce an ansatz for the renormalized interaction in the spin channel which includes correlation effects by construction.

$$U_{sp} = \frac{U\langle n_\uparrow n_\downarrow\rangle}{\langle n_\uparrow\rangle\langle n_\downarrow\rangle} \tag{1.21}$$

Then, by substituting this ansatz in Eq. (1.12), and looking at the local spin sum rule Eq. (1.8)

$$\begin{aligned} \frac{T}{N^2}\sum_q \chi_{sp}(q) &= \langle n_\uparrow\rangle + \langle n_\downarrow\rangle - 2\langle n_\uparrow n_\downarrow\rangle \\ \frac{T}{N^2}\sum_q \frac{\chi_0(q)}{1-\frac{1}{2}\frac{U\langle n_\uparrow n_\downarrow\rangle}{\langle n_\uparrow\rangle\langle n_\downarrow\rangle}\chi_0(q)} &= \langle n_\uparrow\rangle + \langle n_\downarrow\rangle - 2\langle n_\uparrow n_\downarrow\rangle \end{aligned} \tag{1.22}$$

The quantity, $\langle n_\uparrow n_\downarrow\rangle$, the double occupancy occurs on both sides of the equation and therefore we can try to obtain a self-consistent solution for this quantity. That is from where the method derives its name. We can either determine the spin vertex U_{sp} or the double occupancy $\langle n_\uparrow n_\downarrow\rangle$ self-consistently. We use the value of $\langle n_\uparrow n_\downarrow\rangle$ obtained by our self-consistent calculations in Eq. (1.9) and solve for U_{ch}. TPSC is designed in such a way that the spin and charge vertices attain a balance, where both the spin and charge sum rules are obeyed.

1.4 A peep into the derivation

(Detailed derivation can be found in Appendix A.)

From the equation of motion of the single-particle Green function, we can arrive at an exact relation between the self-energy, Σ and the two-particle correlation function.

$$\Sigma_\sigma(1,\bar{2})G_\sigma(\bar{2},2) = -U\langle n_{-\sigma}(1)c_\sigma(1)c^\dagger_\sigma(2)\rangle \tag{1.23}$$

where a bar over an index means that index will be summed over - i.e. a summation over the space index and an integration over the imaginary time index is assumed. In fact, when we evaluate the equation of motion of the single-particle Green function, this two-particle correlation matrix is the tricky term. The equation of motion of this two-particle correlation function would generate three-particle correlation functions and so on. The set of equations never closes. The self-energy is a quantity where all these interaction effects have been cleverly dumped, and hence it is very hard to evaluate.

This exact relation is the starting point of the approximation in TPSC. The Hartree-Fock factorization does a very crude job of approximating the double occupancy as $\langle n_\uparrow n_\downarrow \rangle = \langle n_\uparrow \rangle \langle n_\downarrow \rangle$. This works well when there is no interaction or when the interaction is very small. As soon as interactions become large, this is a very poor approximation. The exact result on the RHS involving the double occupancy has to be retained. Thus we can modify the approximation which resembles the Hartree-Fock approximation, but reproduces the exact result when $2 \to 1^+$. This is the TPSC ansatz where we write,

$$\Sigma_\sigma(1,\bar{2})G_\sigma(\bar{2},2) = \mathcal{A}\, G_{-\sigma}(1,1^+)G_\sigma(1,2) \tag{1.24}$$

We have replaced the bare interaction by a renormalized interaction such that the exact relation is reproduced when $2 \to 1^+$. This means,

$$\mathcal{A} = U\frac{\langle n_\uparrow n_\downarrow \rangle}{\langle n_\uparrow \rangle \langle n_\downarrow \rangle} \tag{1.25}$$

and

$$\Sigma_\sigma(1,2) = U\frac{\langle n_\uparrow n_\downarrow \rangle}{\langle n_\uparrow \rangle \langle n_\downarrow \rangle}\, G_{-\sigma}(1,1^+)\delta(1-2) \tag{1.26}$$

Thus the first approximation gives us a local frequency-independent self-energy. The spin and charge vertices are functional derivatives of the self-energy with respect to the single-particle Green function,

$$\Gamma_{sp}(1,2;3,4) = \frac{\partial \Sigma_\uparrow(1,2)}{\partial G_\downarrow(3,4)} - \frac{\partial \Sigma_\uparrow(1,2)}{\partial G_\uparrow(3,4)} \tag{1.27}$$

$$\Gamma_{ch}(1,2;3,4) = \frac{\partial \Sigma_\uparrow(1,2)}{\partial G_\downarrow(3,4)} + \frac{\partial \Sigma_\uparrow(1,2)}{\partial G_\uparrow(3,4)} \tag{1.28}$$

When we evaluate the spin vertex, we get a local, frequency-independent quantity because, $U_{sp} = U\frac{\langle n_\uparrow n_\downarrow \rangle}{\langle n_\uparrow \rangle \langle n_\downarrow \rangle}$. The higher order correlations from the derivative of $\frac{\langle n_\uparrow n_\downarrow \rangle}{\langle n_\uparrow \rangle \langle n_\downarrow \rangle}$ cancel because of the minus sign. But, as far as the charge vertex is concerned, this does not happen. For simplicity, we assume that the charge vertex U_{ch} is also local.

Once we have spin and charge fluctuations in the system, we can make use of these to get an improved approximation to the self-energy of the system. The self-energy including fluctuations in the longitudinal and transverse channels can be written as,

$$\Sigma^{(2)}_\sigma(k) = Un_{-\sigma} + \frac{U}{8}\frac{T}{N^2}\sum_q \left(3U_{sp}\chi_{sp}(q) + U_{ch}\chi_{ch}(q)\right) G^0_\sigma(k+q) \tag{1.29}$$

The first term in the expression is the average interaction energy of a particle of spin σ with the electrons of the opposite spin. The second term includes the effect of the spin and charge fluctuations on the self-energy.

1.5 Numerical procedure

1.5.1 Noninteracting susceptibility

Substituting the dispersion relation, Eq. (1.5) in Eq. (1.11) seems to be a straightforward way to evaluate the noninteracting susceptibility. Suppose we divide our Brillouin zone (BZ) into a grid with a total of N^2 momentum points and there are N_q numbers of Matsubara frequencies at which the noninteracting susceptibility is to be evaluated. Computing $\chi_0(q)$ by direct evaluation of Eq. (1.11) is tedious - for each pair of $(\boldsymbol{q}, i\nu_n)$, the value of the summand in Eq.(1.11) has to be evaluated at N^2 points in the BZ. The number of operations scales like $N^2 \times N_q \times N^2$.

Although we may make use of symmetries to reduce the number of operations, here we make use of another fact to simplify the numerics. The noninteracting susceptibility in the momentum- frequency space is in the form of a convolution

$$\chi_0(\boldsymbol{q}, i\nu_n) = -2\,\frac{T}{N^2}\sum_{\boldsymbol{k}, i\omega_n} G^0(\boldsymbol{k}, i\omega_n)\, G^0(\boldsymbol{k}+\boldsymbol{q}, i\omega_n + i\nu_n) \tag{1.30}$$

and in Fourier space, i.e., the position - imaginary time space it can be written as a product.

$$\chi_0(\boldsymbol{r}, \tau) = -2G^0(\boldsymbol{r}, \tau)G^0(-\boldsymbol{r}, -\tau) \tag{1.31}$$

$$= 2G^0(\boldsymbol{r}, \tau)G^0(\boldsymbol{r}, \beta - \tau) \tag{1.32}$$

where the inversion symmetry of the two dimensional square lattice as well as the antiperiodicity of the single particle Green function, $G^0(-\boldsymbol{r}, -\tau) = -G^0(\boldsymbol{r}, \beta - \tau)$ have been be invoked. Starting from $G(\boldsymbol{k}, \tau)$, we can evaluate $G(\boldsymbol{r}, \tau)$ using FFT,

$$G^0(\boldsymbol{r}, \tau) = \frac{1}{N^2}\sum_{\boldsymbol{k}} G^0(\boldsymbol{k}, \tau)e^{i\boldsymbol{k}\cdot\boldsymbol{r}} \tag{1.33}$$

where

$$G^0(\boldsymbol{k},\tau) = -e^{-\epsilon_{\boldsymbol{k}}\tau} n_F(-\epsilon_{\boldsymbol{k}}) \tag{1.34}$$

$$= -e^{-\epsilon_{\boldsymbol{k}}(\beta-\tau)} n_F(\epsilon_{\boldsymbol{k}}) \tag{1.35}$$

for $0 < \tau < \beta$.

Once we have $G^0(\boldsymbol{r},\tau)$, the calculation of $\chi_0(\boldsymbol{r},\tau)$ is straightforward. Then, by performing FFT $\chi_0(\boldsymbol{q}, i\nu_n)$ is obtained.

$$\chi_0(\boldsymbol{q}, i\nu_n) = \int_0^\beta d\tau e^{i\nu_n\tau} \sum_{\boldsymbol{r}} e^{-i\boldsymbol{q}\cdot\boldsymbol{r}} \chi_0(\boldsymbol{r},\tau) \tag{1.36}$$

There is one aspect we have to pay attention to. The imaginary time τ is a continuous parameter and performing a discrete Fourier transform on this dimension, gives wrong results at high frequencies. $\chi_0(\boldsymbol{q}, i\nu_n)$ has to decay at high frequencies, the results from FFTs which are periodic in $i\nu_n$ would not be appropriate.

In order to get around this difficulty, we make use of cubic splines [27]. Suppose we divide the imaginary time from 0 to β into $\mathcal{N}_t$ equal slices. Along each slice, $\chi_0(\boldsymbol{r},\tau)$ is approximated using by a cubic polynomial and the continuous Fourier transform is written as,

$$\begin{aligned} f(\nu) &= \sum_{n=1}^{\mathcal{N}_t} \int_{x_{n-1}}^{x_n} dx\ S_n(x) e^{i\nu x} \\ &= \frac{-S_{\mathcal{N}_t}(\beta) - S_0(0)}{i\nu} - \frac{-S'_{\mathcal{N}_t}(\beta) - S'_0(0)}{(i\nu)^2} \\ &+ \frac{-S''_{\mathcal{N}_t}(\beta) - S''_0(0)}{(i\nu)^3} - \left(1 - e^{i\nu\Delta x}\right) \sum_{n=0}^{\mathcal{N}_t - 1} S'''_n e^{i\nu x} \end{aligned} \tag{1.37}$$

where $x_0 = 0$ and $x_{\mathcal{N}_t} = \beta$. The first derivative of $\chi_0(\boldsymbol{r},\tau)$ at $\tau = 0$ and $\tau = \beta$ are provided in order to complete the set of equations needed to determine the unknowns - the spline coefficients. We can evaluate the derivatives of $\chi_0(\boldsymbol{r},\tau)$ from the derivatives of $G^0(\boldsymbol{r},\tau)$ and $G^0(\boldsymbol{r},\beta-\tau)$.

Here the expression has been simplified using integration by parts, and S_n represents the cubic spline for the n-th slice of imaginary time. S'_n, S''_n and S'''_n represent the first, second and third derivatives of the spline respectively. Since we are successively differentiating a cubic polynomial, S'''_n is proportional to the coefficient of the third degree term in the spline. Therefore, the final term in the expression (1.37) includes a discrete Fourier

transform which can be easily evaluated using FFTs. The noninteracting susceptibility at zero frequency can be computed as the integral of the spline over all the intervals. $\chi_0(q)$ is real and symmetric about the imaginary frequency axis. In fact, after FFT we have $\chi_0(q)$ for a momentum grid containing N^2 points, with $N_q = \mathcal{N}_t/2$ number of positive and negative Matsubara frequencies in the resulting data. In the evaluation of $G(\boldsymbol{r}, \tau)$, the number of operations required is $\mathcal{N}_t \times N^2 \log N^2$, and the three dimensional FFT Eq. (1.36) requires $N^2\mathcal{N}_t \log(N^2\mathcal{N}_t)$ operations.

1.5.2 Self-energy

If we take a look at Eq. (1.29), we can see that here also we have a convolution form for the second term involving spin and charge fluctuations. This helps us recast the expression in position - imaginary time space as a product using FFTs. We can come back to the momentum - frequency space using FFTs once more.

$$V(\boldsymbol{r}, \tau) = \frac{U}{8}\left(3U_{sp}\chi_{sp}(\boldsymbol{r}, \tau) + U_{ch}\chi_{ch}(\boldsymbol{r}, \tau)\right) \tag{1.38}$$

and this lets us rewrite the second term in the self-energy as

$$\frac{U}{8}\frac{T}{N^2}\sum_{q}\left(3U_{sp}\chi_{sp}(q) + U_{ch}\chi_{ch}(q)\right)G_\sigma(k+q) = \int_0^\beta e^{i\omega_n\tau}\sum_{\boldsymbol{r}} e^{-i\boldsymbol{k}\cdot\boldsymbol{r}}V(-\boldsymbol{r}, -\tau)G(\boldsymbol{r}, \tau) \tag{1.39}$$

where

$$V(\boldsymbol{r}, \tau) = \frac{U}{8}\left(3U_{sp}\chi_{sp}(\boldsymbol{r}, \tau) + U_{ch}\chi_{ch}(\boldsymbol{r}, \tau)\right) \tag{1.40}$$

We can compute $V(\boldsymbol{r}, \tau)$ accurately, by the following trick,

$$\begin{aligned} V(\boldsymbol{r}, \tau) = \frac{U}{8}\frac{T}{N^2}\sum_{\boldsymbol{q}, i\nu_n}\left[e^{i\boldsymbol{q}\cdot\boldsymbol{r}}e^{-i\nu_n\tau}\left(3U_{sp}\chi_{sp}(q) + U_{ch}\chi_{ch}(q)\right) - \left(3U_{sp} + U_{ch}\right)\chi_0(q)\right] \\ + \frac{U}{8}\left(3U_{sp} + U_{ch}\right)\chi_0(\boldsymbol{r}, \tau) \end{aligned} \tag{1.41}$$

This is done because, asymptotically $\chi_{sp}(q)$ and $\chi_{ch}(q)$ approach $\chi_0(q)$. The above 'trick' accomplishes one thing, the high frequency parts are removed in the Fourier transform, and this lets us use a smaller cutoff frequency.

Here also, we have to approximate the continuous Fourier transform over τ making

use of cubic splines. The derivatives of $V(-\boldsymbol{r}, -\tau)G^0(\boldsymbol{r}, \tau)$ with respect to τ need to be evaluated at $\tau = 0$ and $\tau = \beta$ for the evaluation of the spline coefficients. As $\chi_0(q)$, $\chi_{sp}(q)$ and $\chi_{ch}(q)$ are even functions of $i\nu$, only the derivative of the final term in Eq. (1.41) with respect to τ matters.

1.6 Results

This section gives a glimpse of the results from the TPSC method. Following the procedure mentioned in Refs. [13, 14, 27] we have attempted to replicate the results, in order to better grasp the various aspects of the method.

We work with the two dimensional square lattice, at half-filing ($n = 1.0$). t is taken as unity. For a particular value of temperature, T, at half-filling we can evaluate the noninteracting susceptibility using a combination of FFTs and cubic splines. For each value of U, we start with a guess value of the double occupancy. This is used to evaluate the spin susceptibility using (1.12). From the sum rule given by (1.8) the updated value of spin vertex can be obtained. This procedure is repeated till self-consistency is achieved. Using the value of double occupancy so obtained, making use of the charge sum rule (1.9) the irreducible charge vertex can be determined. Usually, we start with a very small value of U, the guess value of double occupancy being the value of double occupancy for the case of zero interaction. Then for the next value of U, the guess value we choose is the double occupancy obtained self-consistently for the previous value of U. For a smooth U grid, this ensures smooth numerical calculations.

Fig. 1.3 shows the plot of the noninteracting susceptibility $\chi_0(q)$ at zero-frequency for $T = 0.2$, at half-filling. At half-filling, because of nesting, the susceptibility peaks at (π, π) as can be seen from the plot.

1.6.1 Double occupancy and irreducible vertices

When we are in the paramagnetic regime we have spin rotational invariance. The average number of electrons with spin up as well as spin down is the same, $\langle n_\sigma \rangle = n_\sigma = \frac{n}{2}$. When there is no interaction between the electrons, the average value of double occupancy is given by $\langle n_\uparrow n_\downarrow \rangle = \langle n_\uparrow \rangle \langle n_\downarrow \rangle = \frac{n}{2} \times \frac{n}{2}$. At half-filling, therefore when $U = 0.0$, $\langle n_\uparrow n_\downarrow \rangle = \frac{1}{2} \times \frac{1}{2} = 0.25$. As the value of the interaction U increases, the probability of two electrons to be on the same site gets reduced because of the increased penalty to be paid. Therefore, the double occupancy $\langle n_\uparrow n_\downarrow \rangle$ decreases steadily with increasing U. This

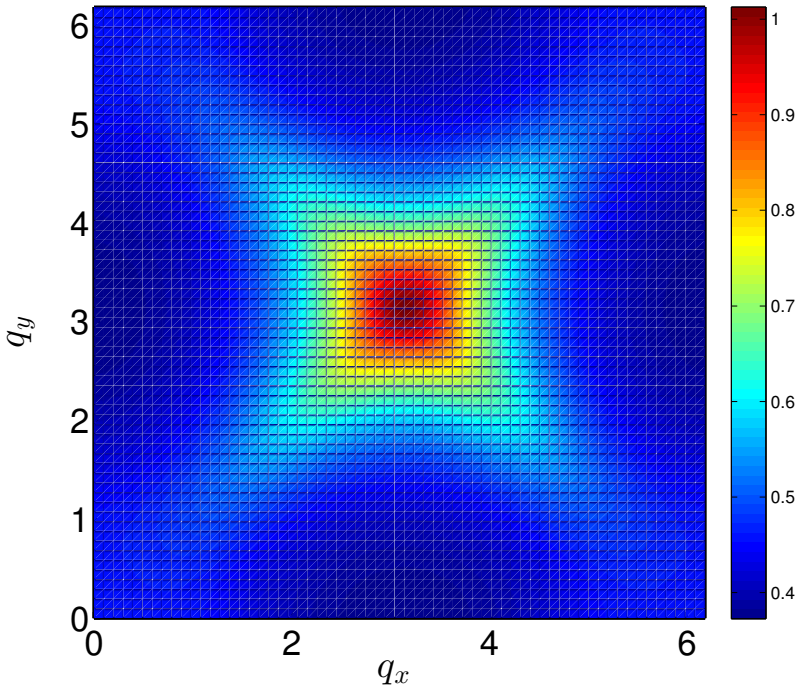

Figure 1.3: Plot of noninteracting susceptibility $\chi_0(q)$ at zero frequency, as a function of $\boldsymbol{q}$ for $T = 0.2$.

trend is clearly seen in the plot given in Fig. 1.4.

The curves for spin and charge vertices with respect to U are also given in Fig. 1.4. The spin and charge vertices are almost equal to U, for really small values of U. But, as the interaction increases, the spin vertex tends to saturate, while the charge vertex increases rapidly. In TPSC, the spin vertex can reach arbitrarily close to the mean-field transition value of interaction U_{mf}, but never crosses it. The saturation of the spin vertex is due to Kanamori-Brueckner screening. If the amplitude of the two-body wave function decreases, there is a reduced probability of a site being occupied by two electrons. This reduces the 'effect' of the interaction. The energy cost associated with this phenomenon would be the difference between the energy of the one-particle wave function with the maximum number of allowed particles and that of the one-particle wave function with just one particle in it. This is the bandwidth. Hence, the effective interaction U_{sp} saturates to a value of the order of the bandwidth. The rapid increase in the charge vertex shows that the charge fluctuations are suppressed, this means that the system is approaching a Mott transition.

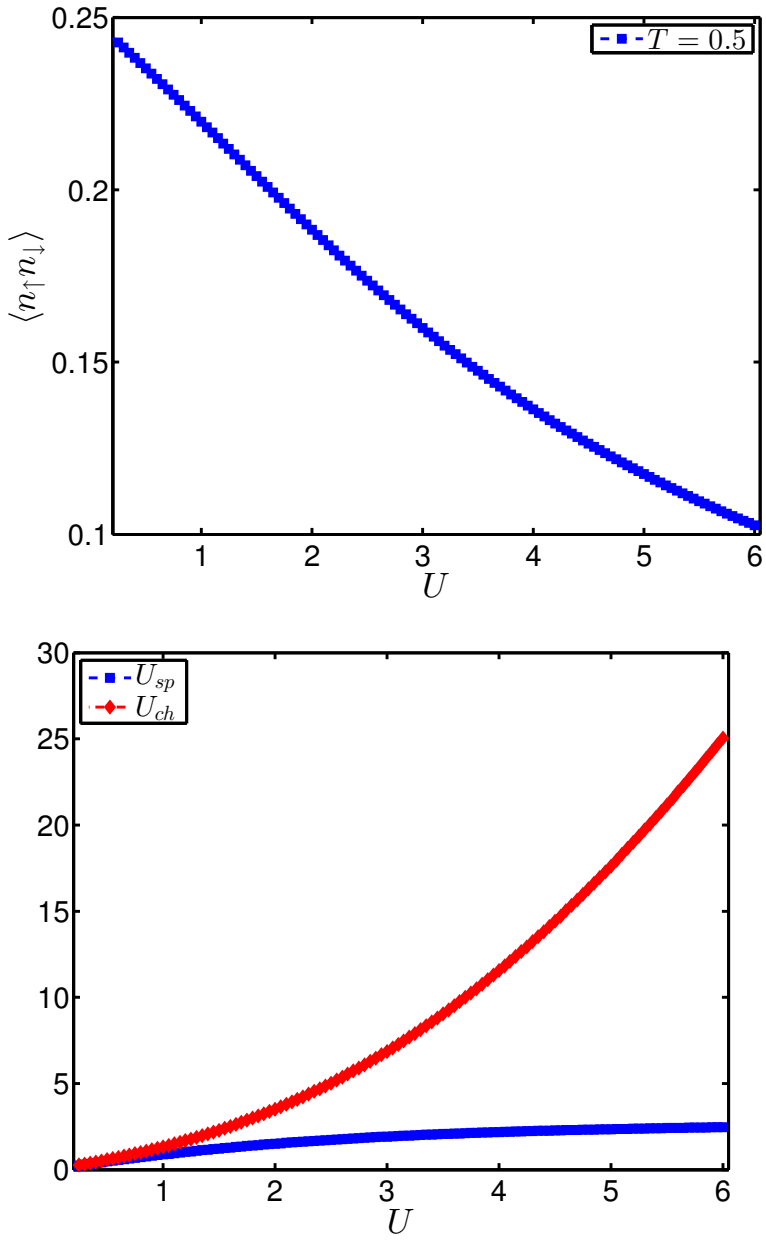

Figure 1.4: Plots of double occupancy $\langle n_\uparrow n_\downarrow \rangle$ and irreducible vertices U_{sp} and U_{ch} as functions of interaction U for $T = 0.5$.

1.6.2 Correlation lengths

The interacting spin and charge susceptibilities are given in terms of the noninteracting susceptibility by Eqs. (1.12) and (1.13), We study the interacting susceptibilities by studying a quantity called the correlation length, which we define as

$$\xi_{afm} = \sqrt{\frac{\chi_{sp}(\boldsymbol{Q}, 0)}{\chi_0(\boldsymbol{Q}, 0)}} \tag{1.42}$$

$$\xi_{ch} = \sqrt{\frac{\chi_{ch}(\boldsymbol{Q}, 0)}{\chi_0(\boldsymbol{Q}, 0)}} \tag{1.43}$$

where $\boldsymbol{Q} = (\pi, \pi)$, the wave vector at which the noninteracting susceptibility peaks in this case because of nesting.

In Fig. 1.5, we can see that, as the interaction increases, the charge correlation length ξ_{ch} decreases steadily. Also, the charge correlation decreases as temperature is decreased too. We have already seen the rapid growth of the charge vertex with increasing interaction. The plots of the charge correlation length give us the same information - that the charge fluctuations are suppressed as the interaction increases or as the temperature decreases. This reflects the tendency to Mott transition.

When we take a look at the antiferromagnetic correlation length, we see that the antiferromagnetic susceptibility increases as interaction increases. As we lower temperature, this increase in antiferromagnetic susceptibility is very large. This means that the antiferromagnetic fluctuations in the system are becoming huge. When the correlation length of these antiferromagnetic fluctuations exceed the thermal de Broglie wavelength, we say that the system has entered the 'renormalized classical regime'. This is the regime where the spin fluctuation energy is very small compared to the temperature. The quasiparticles are destroyed by these huge antiferromagnetic fluctuations and the single-particle density of states has a pseudogap when this crossover happens [17, 18]. The system is very close to the zero temperature quantum phase transition to antiferromagnetic order and even a small temperature is enough to produce huge fluctuations.

1.6.3 Self-energy

In order to have an idea about the self-energy we obtain from TPSC after the inclusion of the effects of spin and charge fluctuations, let us plot the imaginary part of the self-energy as a function of the fermionic Matsubara frequency, for various values of interaction. The

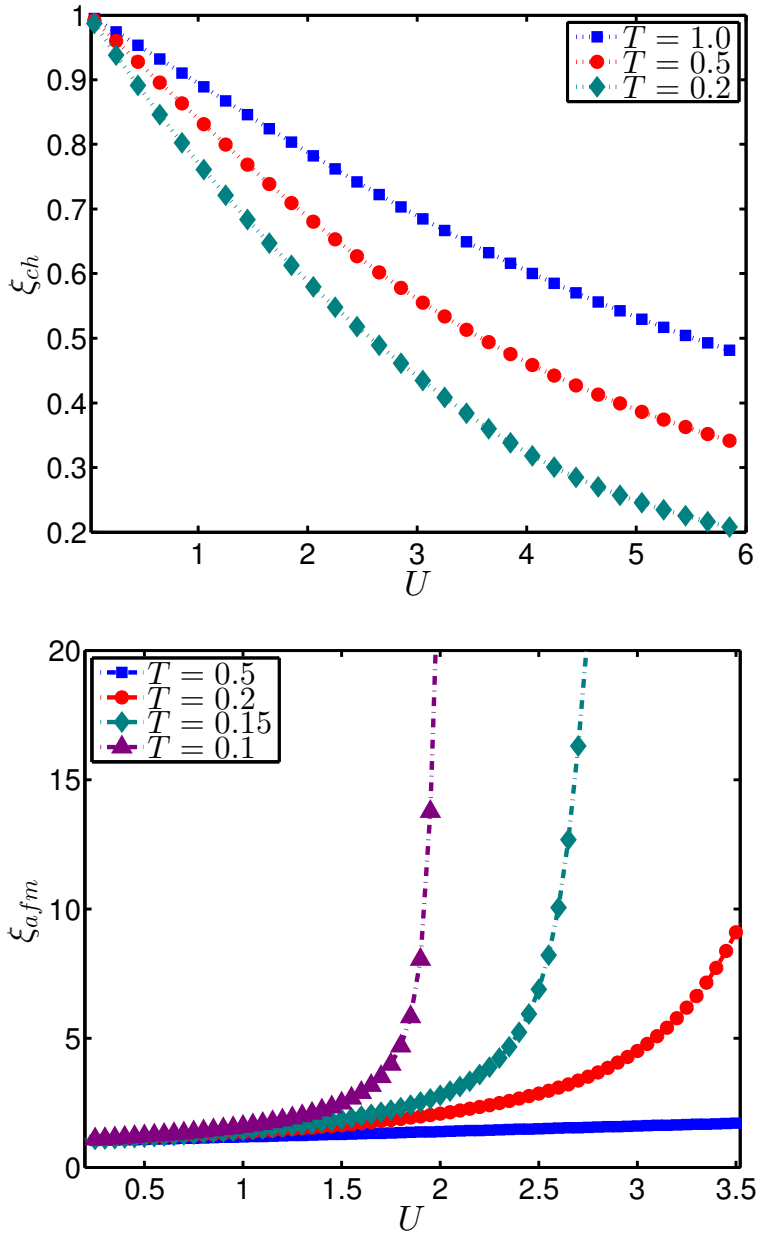

Figure 1.5: Plots of charge correlation length ξ_{ch} and antiferromagnetic correlation length ξ_{afm} with respect to interaction U for various temperatures.

plots in Fig. 1.6 have been generated for a temperature $T = 0.2$. $-\text{Im}\ \Sigma(\omega_n)$ is shown to increase as $\omega_n \to 0$, for $U \sim 5.0$. This indicates a pseudogap in the single-particle excitation spectrum, caused by the growing antiferromagnetic fluctuations.

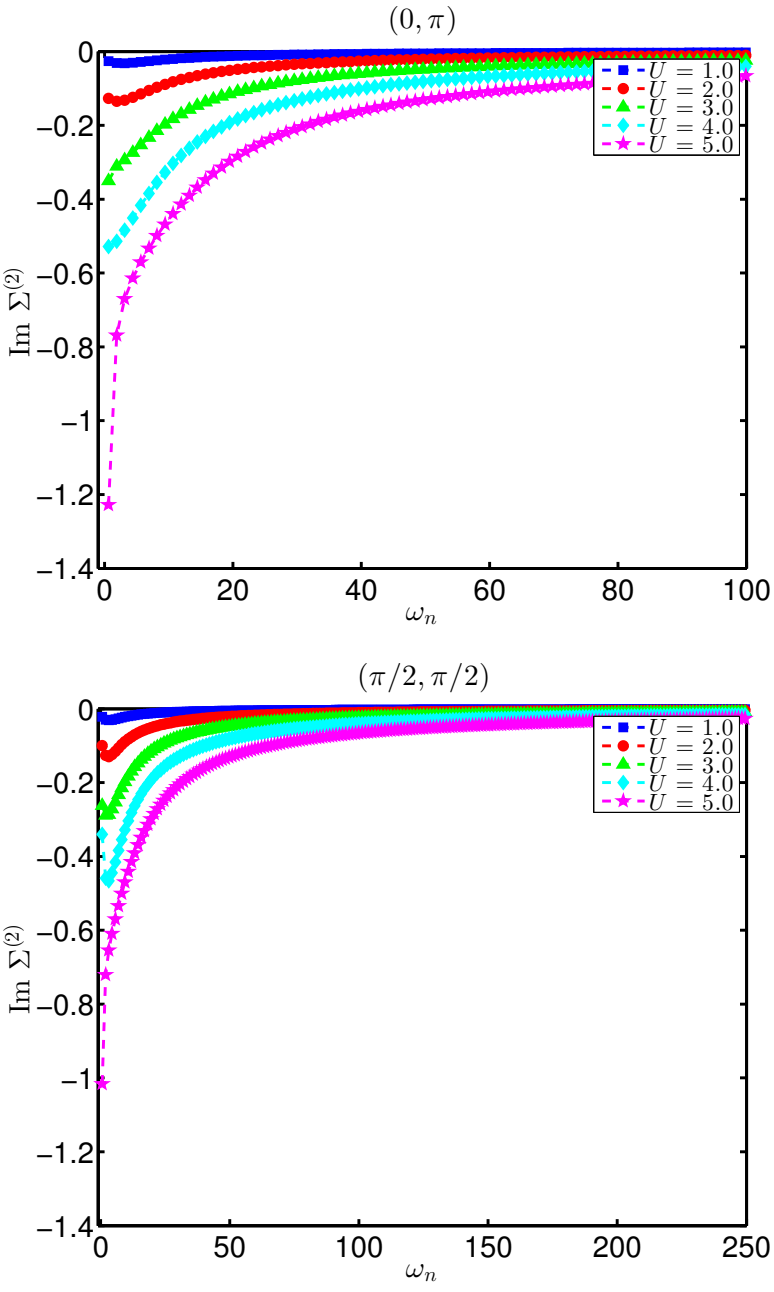

Figure 1.6: Plots of the imaginary part of self energy $\text{Im}\Sigma^{(2)}$ as a function of Matsubara frequency ω_n for various values of interaction U shown in the legend for $T = 0.2$. The plots show the self energy at two points on the Fermi surface at half-filling.

1.7 Summary

The two-particle self-consistent method (TPSC) is an approximation technique used to study the single-band Hubbard model, from weak to moderate values of interaction. Although it cannot capture the Mott transition, this method satisfies many physical constraints like the conservation of spin and charge and the Pauli exclusion principle exactly. Most important of all, the method is apt to capture the growing antiferromagnetic fluctuations in the system, without compromising the validity of the Mermin- Wagner theorem. Unlike RPA, this method does not generate the unphysical result of a phase transition at finite temperatures in two dimensions. The crossover to the 'renormalized' classical regime, when the correlation length of the antiferromagnetic fluctuations grows beyond the thermal de Broglie wavelength is captured by TPSC.

From an exact relation between the self-energy and two-particle correlation functions, the first approximation to the self-energy can be made, the self-energy is assumed to be local and frequency independent. From this we can derive the expression for the irreducible spin vertex, which is local and frequency independent. The charge vertex is also assumed to be local and frequency independent. The irreducible spin and charge vertices are determined self-consistently by a combined implementation of the Bethe-Salpeter equation, the local spin and charge sum rules and the TPSC ansatz. Therefore, TPSC is a non-perturbative and semi-analytical technique. From the results of spin and charge susceptibilities, we may calculate an improved approximation for the self-energy.

The results obtained for antiferromagnetic correlation length show the rapid growth of antiferromagnetic fluctuations for decreasing temperature and increasing interaction. The rapid increase in charge vertex shows the tendency to Mott transition, the same is validated by the decreasing charge correlation length. Further, from the imaginary part of self-energy, the pseudogap induced by these antiferromagnetic fluctuations can also be seen.

Chapter 2

Antiferromagnetism in the Hubbard model on the honeycomb lattice

2.1 Introduction

The concepts of 'symmetry' and 'symmetry breaking' are very crucial to the understanding of most phases of matter - usually by the breaking of some appropriate symmetry, long-range order sets in the system. Viewed against this background, the quantum spin liquid is an 'exotic' phase, in this phase of matter, long-range order is hindered in the ground state of the system. A good analogy can be made by citing the example of classical paramagnets, where thermal fluctuations prevent long-range order. In the case of a quantum spin liquid, even at zero temperature, the presence of quantum fluctuations prevent long-range order.

P. W. Anderson was behind the theoretical proposal of a spin liquid phase on the triangular lattice [28], following the concept of 'resonating valence bonds' introduced by Pauling [29]. Suppose we arrange spins on an equilateral triangular lattice and introduce an antiferromagnetic interaction between the spins. Its clearly visible that the spin on one site cannot simultaneously remain antiferromagnetically aligned to both its neighbors. So, if we imagine a triangular lattice, this geometric frustration prevents the formation of long-range order [30].

Later, Anderson used this concept of a resonating valence bond state in the context of high temperature superconductors, [31] prompting the extensive search of such a phase in materials. Since geometric frustration can act as a crucial ingredient for the occurrence of spin liquids, systems with geometric frustration are expected to host such phases. In three dimensions, the pyrochlore spin ices are expected to host this phase [32] whereas

experimental evidence for such a phase has been obtained in organic materials of the BEDT family, with a triangular lattice structure [33]. Also, the existence of such a phase in the Kagome lattice has also been theoretically proved [34].

Theoretically, if we take the Hubbard model on a lattice, and if we increase the interaction U, the model undergoes a phase transition from a Fermi liquid to an antiferromagnetic Mott insulator. Suppose, we add some frustration to the system, then quantum fluctuations would prohibit the antiferromagnetic long-range order and result in a spin liquid.

Usually, low-dimensional systems have large quantum fluctuations, so looking for such a phase in two-dimensional materials is deemed appropriate. The honeycomb lattice does not have any geometric frustration, but its lowest possible coordination number for a two-dimensional lattice, makes it a good candidate to search for a spin liquid phase. Meng and coworkers predicted the existence of such a spin liquid phase in the Hubbard model on the half-filled honeycomb lattice [35], by doing large scale Quantum Monte Carlo calculations. They claimed that for a small window of interaction values, a spin liquid phase exists in the system before the transition to the antiferromagnetic Mott insulator occurs. This theoretical result was confirmed later by further studies. However, Sorella *et al.* [36] worked on larger lattice sizes and ruled out the possibility of a spin liquid phase. So, whether the spin liquid phase exists in the half-filled Hubbard model on the honeycomb lattice is an interesting question to study.

A spin liquid can be considered as a Mott insulator without any long-range order. Methods like the Dynamical Mean Field Theory (DMFT) and its extensions (quantum cluster approaches) [37–39] are apt to study the Mott transition in the Hubbard model. Therefore, these methods can be implemented to study the 'so-called' intermediate spin liquid phase between the semimetal and the antiferromagnetic Mott insulator. Mott transition in the Hubbard model on the honeycomb lattice was confirmed by single-site DMFT studies as well as studies using quantum cluster approaches [40–46]. However, Hassan *et al.* [47] using CDIA (Cluster Dynamical Impurity Approximation) proved that the Mott transition was preempted by antiferromagnetic long-range order. The subtleties of various methods - cluster shape, various implementations of cluster methods [48–51], give varying results for the critical interaction strength.

The result from quantum cluster approaches can be taken as an upper bound to the critical interaction strength, since these approaches track down the Mott transition without any long-range order. But, if we have to locate the precise value of critical interaction strength for antiferromagnetism to set in, we need to apply a method which takes into

account the long wavelength antiferromagnetic fluctuations in the system. Since the interaction strength in the problem is of the order of $2/3$, TPSC as a non-perturbative, semi-analytical method valid from weak to intermediate coupling is well-suited to analyze the problem [13, 14]. The crossover plot can be obtained by picking the values at which the antiferromagnetic correlation length exceeds the thermal de Broglie wavelength. By extrapolating the crossover plot to zero temperature, we can have an estimate of the critical interaction strength U_c for the quantum phase transition.

2.2 Model

So far TPSC has been used to study the single-band Hubbard model. The honeycomb lattice is not a Bravais lattice - it can be visualized as a triangular Bravais lattice with two sublattices A and B. We first need to extend the formalism to the multi-band case of the Hubbard model on the honeycomb lattice.

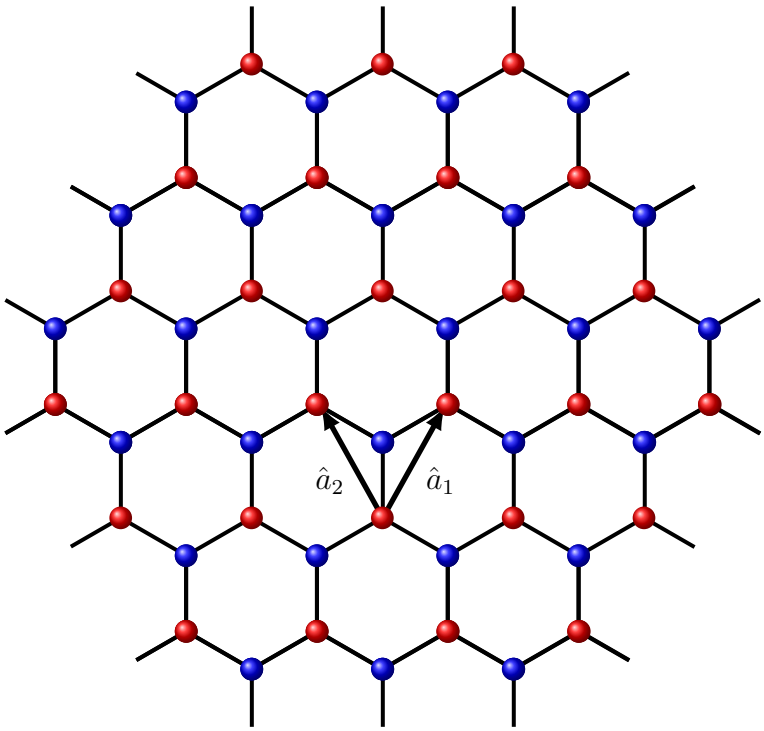

Figure 2.1: Honeycomb lattice which is a triangular Bravais lattice with two sublattices, indicated using red and blue circles. The lattice vectors $\boldsymbol{a}_1$ and $\boldsymbol{a}_2$ are also shown.

The Hubbard Hamiltonian on the honeycomb lattice is written as

$$H = H_0 + H_{int} \tag{2.1}$$

$$H_0 = -t \sum_{i,\Delta,\sigma} \left(a^\dagger_{i\sigma} b_{i+\Delta,\sigma} + h.c \right) \tag{2.2}$$

$$H_{int} = U \sum_{i \in A,B} (n_{ia\uparrow} n_{ia\downarrow} + n_{ib\uparrow} n_{ib\downarrow}) \tag{2.3}$$

where the hopping is from a site on sublattice A to a site on sublattice B or vice versa. The hopping from one site i can be to any of its three neighbor sites belonging to the other sublattice $i + \Delta$. In momentum space, the noninteracting Hamiltonian can be written as a 2×2 matrix with non-zero off-diagonal elements as

$$\mathbf{H}_0(\boldsymbol{k}) = \begin{bmatrix} 0 & f(\boldsymbol{k}) \\ f^*(\boldsymbol{k}) & 0 \end{bmatrix} \tag{2.4}$$

where

$$f(\boldsymbol{k}) = -t \left(1 + e^{-i\boldsymbol{k}\cdot\boldsymbol{a}_1} + e^{-i\boldsymbol{k}\cdot\boldsymbol{a}_2} \right) \tag{2.5}$$

The form of $f(\boldsymbol{k})$ can be understood by considering lattice points on a triangular lattice. Corresponding to each lattice point on the triangular lattice, there are two sites associated with the two sublattices. Each lattice point has six neighbors. Hopping to the three neighboring sites on the honeycomb lattice, can therefore be seen on the triangular lattice as i) hopping to the other sublattice belonging to the same lattice point and ii) hopping to the other sublattice belonging to two neighboring lattice points out of the six neighbors.

We may diagonalize this Hamiltonian to obtain the energy eigenvalues, $E_c(\boldsymbol{k}) = |f(\boldsymbol{k})|$ corresponding to the conduction band and $E_v(\boldsymbol{k}) = -|f(\boldsymbol{k})|$ corresponding to the valence band.

$$\mathbf{H}_0(k) = \begin{bmatrix} E_c(\boldsymbol{k}) & 0 \\ 0 & E_v(\boldsymbol{k}) \end{bmatrix} \tag{2.6}$$

where we basically switch to a diagonal basis description in terms of creation and anni-

hilation operators for the conduction and valence bands.

$$a^\dagger_{\boldsymbol{k}\sigma} = \frac{1}{\sqrt{2}}\left(v^\dagger_{\boldsymbol{k}\sigma} + c^\dagger_{\boldsymbol{k}\sigma}\right) \tag{2.7}$$

$$b^\dagger_{\boldsymbol{k}\sigma} = \frac{1}{\sqrt{2}} e^{i\phi_{\boldsymbol{k}}}\left(v^\dagger_{\boldsymbol{k}\sigma} - c^\dagger_{\boldsymbol{k}\sigma}\right) \tag{2.8}$$

where

$$e^{i\phi_{\boldsymbol{k}}} = \frac{f(\boldsymbol{k})}{|f(\boldsymbol{k}|}$$

2.2.1 Single-particle correlation function

The Green function is a 2×2 matrix in this case,

$$\mathbf{G} = \begin{pmatrix} G^{aa} & G^{ab} \\ G^{ba} & G^{bb} \end{pmatrix} \tag{2.9}$$

For instance, in the position - imaginary time representation, we have the following definition

$$G^{\rho\lambda}_{\sigma\sigma'}(1,2) = -\langle T_\tau \rho_\sigma(1)\lambda^\dagger_{\sigma'}(2)\rangle \delta_{\sigma\sigma'} \tag{2.10}$$

where $\rho, \lambda = a, b$ represent the sublattice indices. We have used a shorthand notation, 1 describes both the position ($\boldsymbol{r}_1$) and the imaginary time (τ_1). This 2×2 matrix form of the Green function has been written down, assuming spin rotational invariance.

In the momentum- imaginary frequency representation, we can write the noninteracting Green function as,

$$\begin{aligned} \mathbf{G}^0(\boldsymbol{k}, i\omega_n) &= \left[i\omega_n - \mathbf{H}_0\right]^{-1} \\ &= \begin{bmatrix} i\omega_n & -f(\boldsymbol{k}) \\ -f^*(\boldsymbol{k}) & i\omega_n \end{bmatrix}^{-1} \qquad (2.11) \\ &= \frac{1}{i\omega_n^2 - |f(\boldsymbol{k})|^2} \begin{bmatrix} i\omega_n & f(\boldsymbol{k}) \\ f^*(\boldsymbol{k}) & i\omega_n \end{bmatrix} \qquad (2.12) \end{aligned}$$

This can be viewed as,

$$G^{aa}(k) = \frac{1}{2}\left[G_{vv} + G_{cc}\right] \tag{2.13}$$
$$= \frac{1}{2}\left[\frac{1}{i\omega_n - E_v} + \frac{1}{i\omega_n - E_c}\right] \tag{2.14}$$
$$G^{ab}(k) = \frac{1}{2}e^{i\phi_{\boldsymbol{k}}}\left[G_{vv} - G_{cc}\right] \tag{2.15}$$
$$= \frac{1}{2}e^{i\phi_{\boldsymbol{k}}}\left[\frac{1}{i\omega_n - E_v} - \frac{1}{i\omega_n - E_c}\right] \tag{2.16}$$
$$\tag{2.17}$$

We also have

$$G^{ba}(k) = \frac{1}{2}e^{-i\phi_{\boldsymbol{k}}}\left[G_{vv} - G_{cc}\right] \tag{2.18}$$

Here also, we make use of a shorthand $k \to (\boldsymbol{k}, i\omega_n)$ for the momentum vector and the fermionic Matsubara frequency.

2.2.2 Two-particle correlation functions

The noninteracting as well as the interacting susceptibilities are 4×4 matrices with the following structure,

$$\chi = \begin{pmatrix} \chi^{aaaa} & \chi^{aaab} & \chi^{aaba} & \chi^{aabb} \\ \chi^{abaa} & \chi^{abab} & \chi^{abba} & \chi^{abbb} \\ \chi^{baaa} & \chi^{baab} & \chi^{baba} & \chi^{babb} \\ \chi^{bbaa} & \chi^{bbab} & \chi^{bbab} & \chi^{bbbb} \end{pmatrix} \tag{2.19}$$

Although the most general element of the noninteracting susceptibility is given by,

$$\chi_0^{\rho\lambda\eta\gamma}(q) = -\frac{T}{N^2}\sum_{k\sigma} G_\sigma^{(0)\eta\rho}(k)\, G_\sigma^{(0)\lambda\gamma}(k+q) \tag{2.20}$$

we can write a 2×2 matrix non-interacting susceptibility relevant for our purposes,

$$\boldsymbol{\chi}_0(q) = \begin{bmatrix} \chi_0^{aaaa}(q) & \chi_0^{aabb}(q) \\ \chi_0^{bbaa}(q) & \chi_0^{bbbb}(q) \end{bmatrix} \tag{2.21}$$

where

$$\chi_0^{\rho\rho\lambda\lambda}(q) = -\frac{T}{N^2} \sum_{k\sigma} G_\sigma^{(0)\lambda\rho}(k)\, G_\sigma^{(0)\rho\lambda}(k+q) \tag{2.22}$$

Here, $q \to (\boldsymbol{q}, i\nu_n)$ where the only difference is that $i\nu_n$ is the bosonic Matsubara frequency. The spin and charge susceptibilities in the position-imaginary time representation are,

$$\chi_{sp}^{\rho\rho\lambda\lambda}(1,2) = \langle T_\tau S_\rho^z(1) S_\lambda^z(2)\rangle \tag{2.23}$$

$$\chi_{ch}^{\rho\rho\lambda\lambda}(1,2) = \langle T_\tau n_\rho(1) n_\lambda(2)\rangle - \langle n_\rho\rangle\langle n_\lambda\rangle \tag{2.24}$$

The local spin and charge sum rules are obtained when we set $1 \to 2$ in (2.23) and (2.24) for the case $\lambda = \rho$

$$\frac{T}{N^2}\sum_q \chi_{sp}^{\rho\rho\rho\rho}(q) = \langle n_{\rho\uparrow}\rangle + \langle n_{\rho\downarrow}\rangle - 2\langle n_{\rho\uparrow} n_{\rho\downarrow}\rangle \tag{2.25}$$

$$\frac{T}{N^2}\sum_q \chi_{ch}^{\rho\rho\rho\rho}(q) = \langle n_{\rho\uparrow}\rangle + \langle n_{\rho\downarrow}\rangle + 2\langle n_{\rho\uparrow} n_{\rho\downarrow}\rangle - n_\rho^2 \tag{2.26}$$

The interacting spin and charge susceptibilities are given by

$$\boldsymbol{\chi}_{sp}(q) = \left[\mathbf{1} - \frac{1}{2}\boldsymbol{\chi}_0(q)\mathbf{U}_{sp}\right]^{-1} \boldsymbol{\chi}_0(q) \tag{2.27}$$

$$\boldsymbol{\chi}_{ch}(q) = \left[\mathbf{1} + \frac{1}{2}\boldsymbol{\chi}_0(q)\mathbf{U}_{ch}\right]^{-1} \boldsymbol{\chi}_0(q) \tag{2.28}$$

in terms of the noninteracting susceptibility. This is the matrix version of the scalar equation appearing in the single-band case. The elements of the matrix spin ($\mathbf{U}_{sp}$) and charge $\mathbf{U}_{ch}$ vertices appearing in the above expression can be obtained as the functional derivatives of the elements of the self-energy matrix with respect to the elements of the Green function matrix.

The crux of the TPSC ansatz lies in making an approximation to the self energy matrix, starting from the exact relation between the self-energy matrix and the two-particle correlation matrix.

2.3 A peep into the derivation

(Detailed derivation can be found in Appendix B.)

From the equation of motion of the Green function and the Dyson equation, in this case also, we can write the most general relation between the self energy and the two-particle correlation functions as

$$\mathbf{\Sigma}(1,\bar{2})\,\mathbf{G}(\bar{2},2) = \mathbf{u}(1,2) \tag{2.29}$$

where an element of the two-particle correlation matrix is

$$u^{\rho\lambda}_{\sigma\sigma'}(1,2) = -U\langle T_\tau \rho^\dagger_{-\sigma}(1)\rho_{-\sigma}(1)\rho_\sigma(1)\lambda^\dagger_{\sigma'}(2)\rangle\delta_{\sigma\sigma'} \tag{2.30}$$

Let us consider a single element in the most general relation between the self energy matrix and the two-particle correlation matrix. Suppose we have $2 \to 1^+$, which implies $\boldsymbol{r}_1 = \boldsymbol{r}_2$ and $\tau_2 = \tau_1 + \epsilon$ where ϵ is an infinitesimal increment for the right time ordering and in the multi-band case $\lambda = \rho$, then the RHS of the above equation can be written in terms of double occupancy at (1).

$$\begin{aligned}
[\mathbf{\Sigma}(1,\bar{2})\,\mathbf{G}(\bar{2},2)]^{\rho\lambda}_{\sigma\sigma'}\,\delta_{\sigma\sigma'}\delta_{\rho\lambda} &= u^{\rho\lambda}(1,2) && (2.31)\\
&= -U\langle T_\tau \rho^\dagger_{-\sigma}(1)\rho_{-\sigma}(1)\rho_\sigma(1)\lambda^\dagger_{\sigma'}(2)\rangle\delta_{\sigma\sigma'} && (2.32)\\
&= U\langle n_{\rho,\uparrow}(1)n_{\rho,\downarrow}(1)\rangle\delta_{\rho\lambda}\delta_{\sigma\sigma'} && (2.33)
\end{aligned}$$

We can extend the TPSC ansatz to the multi-band case and write

$$\Sigma^{\rho\eta}_\sigma(1,\bar{2})G^{\eta\lambda}_{-\sigma}(\bar{2},2) = \mathcal{A}\,G^{\rho\rho}_{-\sigma}(1,1^+)G^{\rho\lambda}_\sigma(1,2) \tag{2.34}$$

such that the exact expression involving the double occupancy is obtained on the RHS. When $2 \to 1^+$, we have

$$\begin{aligned}
\mathcal{A}\,G^{\rho\rho}_{-\sigma}(1,1^+)G^{\rho\lambda}_\sigma(1,1^+) &= \mathcal{A}\langle n_{\rho,-\sigma}(1)\rangle\langle n_{\rho,\sigma}(1)\rangle && (2.35)\\
&= U\langle n_{\rho,\uparrow}(1)n_{\rho,\downarrow}(1)\rangle\delta_{\rho\lambda} && (2.36)
\end{aligned}$$

Therefore, we have

$$\mathcal{A} = \frac{U\langle n_{\rho,\uparrow} n_{\rho,\downarrow}\rangle}{\langle n_{\rho,\uparrow}\rangle\langle n_{\rho,\downarrow}\rangle} \tag{2.37}$$

and

$$\Sigma_{\sigma}^{\rho\eta}(1,\bar{2}) G_{-\sigma}^{\eta\lambda}(\bar{2},2) = \frac{U\langle n_{\rho,\uparrow} n_{\rho,\downarrow}\rangle}{\langle n_{\rho,\uparrow}\rangle\langle n_{\rho,\downarrow}\rangle} G_{-\sigma}^{\rho\rho}(1,1^{+}) G_{\sigma}^{\rho\lambda}(1,2) \tag{2.38}$$

$$\Sigma_{\sigma}^{\rho\lambda}(1,2) = \frac{U\langle n_{\rho,\uparrow} n_{\rho,\downarrow}\rangle}{\langle n_{\rho,\uparrow}\rangle\langle n_{\rho,\downarrow}\rangle} G_{-\sigma}^{\rho\rho}(1,1^{+}) \delta(1-2)\delta_{\rho\lambda} \tag{2.39}$$

The irreducible vertices in the spin and charge channel are given by,

$$\Gamma_{sp}^{\kappa\eta\iota\upsilon}(1,2;3,4) = \frac{\partial\Sigma_{\uparrow}^{\kappa\eta}(1,2)}{\partial G_{\downarrow}^{\iota\upsilon}(3,4)} - \frac{\partial\Sigma_{\uparrow}^{\kappa\eta}(1,2)}{\partial G_{\uparrow}^{\iota\upsilon}(3,4)} \tag{2.40}$$

$$\Gamma_{ch}^{\kappa\eta\iota\upsilon}(1,2;3,4) = \frac{\partial\Sigma_{\uparrow}^{\kappa\eta}(1,2)}{\partial G_{\downarrow}^{\iota\upsilon}(3,4)} + \frac{\partial\Sigma_{\uparrow}^{\kappa\eta}(1,2)}{\partial G_{\uparrow}^{\iota\upsilon}(3,4)} \tag{2.41}$$

The spin vertex has a matrix structure where only the $aaaa$ and $bbbb$ terms are non-zero and equal to each other because of sublattice symmetry. This term denoted by $U_{sp} = U\frac{\langle n_{\uparrow} n_{\downarrow}\rangle}{\langle n_{\uparrow}\rangle\langle n_{\downarrow}\rangle}\rangle$ is local and frequency-independent. We assume the charge vertex has such a structure, despite the fact that we get higher order correlation functions if we evaluate the functional derivatives as shown in the above equations.

2.4 Ferromagnetic and antiferromagnetic spin susceptibilities

The ferromagnetic and the antiferromagnetic spin susceptibilities can be defined for both the noninteracting and interacting cases.

$$\chi_{fm}^{0,sp} = \chi_{0,\,sp}^{aaaa} - \sqrt{\chi_{0,\,sp}^{aabb}\,\chi_{0,\,sp}^{aabb}} \tag{2.42}$$

$$\chi_{afm}^{0,sp} = \chi_{0,\,sp}^{aaaa} + \sqrt{\chi_{0,\,sp}^{aabb}\,\chi_{0,\,sp}^{aabb}} \tag{2.43}$$

If we consider a 2×2 matrix $\mathbf{U}_{sp}$, from the structure of the self-energy only the diagonal $aaaa$ and $bbbb$ elements are non-zero. Therefore expanding the expression for the interacting spin susceptibility,

$$\boldsymbol{\chi}_{sp}(q) = \left[\mathbf{1} - \frac{1}{2}\boldsymbol{\chi}_0(q)\mathbf{U}_{sp}\right]^{-1}\boldsymbol{\chi}_0(q) \tag{2.44}$$

$$= \frac{1}{det}\left[\begin{array}{c|c} 1-\frac{U_{sp}}{2}\chi_0^{bbbb} & \frac{U_{sp}}{2}\chi_0^{aabb} \\ \hline \frac{U_{sp}}{2}\chi_0^{bbaa} & 1-\frac{U_{sp}}{2}\chi_0^{aaaa} \end{array}\right]\left[\begin{array}{c|c} \chi_0^{aaaa} & \chi_0^{aabb} \\ \hline \chi_0^{bbaa} & \chi_0^{bbbb} \end{array}\right] \tag{2.45}$$

$$= \frac{1}{det}\left[\begin{array}{c|c} (1-\frac{U_{sp}}{2}\chi_0^{bbbb})\chi_0^{aaaa} + \frac{U_{sp}}{2}\chi_0^{aabb}\chi_0^{bbaa} & \chi_0^{aabb} \\ \hline \chi_0^{bbaa} & (1-\frac{U_{sp}}{2}\chi_0^{aaa})\chi_0^{bbbb} + \frac{U_{sp}}{2}\chi_0^{bbaa}\chi_0^{aabb} \end{array}\right] \tag{2.46}$$

where making use of symmetry between the two sublattices $\chi_0^{aaaa} = \chi_0^{bbbb}$, we can write the determinant as

$$\begin{aligned} det &= \left(1 - \frac{U_{sp}}{2}\chi_0^{bbbb}\right)\left(1 - \frac{U_{sp}}{2}\chi_0^{aaaa}\right) - \left(\frac{U_{sp}^2}{4}\right)\chi_0^{aabb}\chi_0^{bbaa} \\ &= 1 - \frac{U_{sp}}{2}\chi_0^{aaaa} - \frac{U_{sp}}{2}\chi_0^{bbbb} + \frac{U_{sp}^2}{4}\left(\chi_0^{aaaa}\chi_0^{bbbb} - \chi_0^{aabb}\chi_0^{bbaa}\right) \\ &= 1 - U_{sp}\chi_0^{aaaa} + \frac{U_{sp}^2}{4}\left((\chi_0^{aaaa})^2 - \chi_0^{aabb}\chi_0^{bbaa}\right) \\ &= \left[1 - \frac{U_{sp}}{2}\left(\chi_0^{aaaa} + \sqrt{\chi_0^{aabb}\chi_0^{bbaa}}\right)\right]\left[1 - \frac{U_{sp}}{2}\left(\chi_0^{aaaa} - \sqrt{\chi_0^{aabb}\chi_0^{bbaa}}\right)\right] \end{aligned} \tag{2.47}$$

From the definition of antiferromagnetic spin susceptibility, we can write

$$\begin{aligned}
\chi^{sp}_{afm} &= \frac{1}{det}\left[\left(1-\frac{U_{sp}}{2}\chi_0^{bbbb}\right)\chi_0^{aaaa}+\frac{U_{sp}}{2}\chi_0^{aabb}\chi_0^{bbaa}+\sqrt{\chi_0^{aabb}\chi_0^{bbaa}}\right] \\
&= \frac{\left[\chi_0^{aaaa}-\frac{U_{sp}}{2}\chi_0^{aaaa}\chi_0^{bbbb}+\frac{U_{sp}}{2}\chi_0^{aabb}\chi_0^{bbaa}+\sqrt{\chi_0^{aabb}\chi_0^{bbaa}}\right]}{\left[1-\frac{U_{sp}}{2}\left(\chi_0^{aaaa}+\sqrt{\chi_0^{aabb}\chi_0^{bbaa}}\right)\right]\left[1-\frac{U_{sp}}{2}\left(\chi_0^{aaaa}+\sqrt{\chi_0^{aabb}\chi_0^{bbaa}}\right)\right]} \\
&= \frac{\left[\chi_0^{aaaa}+\sqrt{\chi_0^{aabb}\chi_0^{bbaa}}-\frac{U_{sp}}{2}\left(\chi_0^{aaaa}+\sqrt{\chi_0^{aabb}\chi_0^{bbaa}}\right)\left(\chi_0^{aaaa}-\sqrt{\chi_0^{aabb}\chi_0^{bbaa}}\right)\right]}{\left[1-\frac{U_{sp}}{2}\left(\chi_0^{aaaa}+\sqrt{\chi_0^{aabb}\chi_0^{bbaa}}\right)\right]\left[1-\frac{U_{sp}}{2}\left(\chi_0^{aaaa}-\sqrt{\chi_0^{aabb}\chi_0^{bbaa}}\right)\right]} \\
&= \frac{\left[\left(\chi_0^{aaaa}+\sqrt{\chi_0^{aabb}\chi_0^{bbaa}}\right)\left(1-\frac{U_{sp}}{2}\left(\chi_0^{aaaa}-\sqrt{\chi_0^{aabb}\chi_0^{bbaa}}\right)\right)\right]}{\left[1-\frac{U_{sp}}{2}\left(\chi_0^{aaaa}+\sqrt{\chi_0^{aabb}\chi_0^{bbaa}}\right)\right]\left[1-\frac{U_{sp}}{2}\left(\chi_0^{aaaa}-\sqrt{\chi_0^{aabb}\chi_0^{bbaa}}\right)\right]} \\
&= \frac{\chi_0^{aaaa}+\sqrt{\chi_0^{aabb}\chi_0^{bbaa}}}{1-\frac{U_{sp}}{2}\left(\chi_0^{aaaa}+\sqrt{\chi_0^{aabb}\chi_0^{bbaa}}\right)} \\
&= \frac{\chi_0^{afm}}{1-\frac{U_{sp}}{2}\chi_0^{afm}}
\end{aligned} \tag{2.48}$$

Similarly, we can derive the expression for ferromagnetic susceptibility in the interacting channel as

$$\chi^{sp}_{fm} = \frac{\chi_0^{fm}}{1-\frac{U_{sp}}{2}\chi_0^{fm}} \tag{2.49}$$

This simplification lets us reach scalar equations for the interacting ferromagnetic and antiferromagnetic susceptibilities, resembling those equations we had in the single-band case.

2.4.1 Scaling form of antiferromagnetic susceptibility

With the following definition,

$$M_{\alpha\beta}(\boldsymbol{k},\boldsymbol{q},i\nu_n) = \frac{n_F(E^{\alpha}_{\boldsymbol{k}})-n_F(E^{\beta}_{\boldsymbol{k}+\boldsymbol{q}})}{E^{\alpha}_{\boldsymbol{k}}+E^{\beta}_{\boldsymbol{k}+\boldsymbol{q}}+i\nu_n} \tag{2.50}$$

where $\alpha,\beta = \pm$ and $E^{\alpha}_{\boldsymbol{k}} = \alpha|f(\boldsymbol{k})|$, $f(\boldsymbol{k})$ is given by (2.5). If $\alpha = +$, that means $E^{\alpha}_{\boldsymbol{k}} = +|f(\boldsymbol{k})| = E_c(\boldsymbol{k})$. Similarly, for $\alpha = -$, we have $E^{\alpha}_{\boldsymbol{k}} = E_v(\boldsymbol{k})$.

The noninteracting susceptibilities can be written in the following form where, the

Matsubara summation over the frequencies has already been taken care of.

$$\chi_0^{aaaa}(\boldsymbol{q}, i\nu_n) = -\frac{2}{N^2}\frac{1}{4}\sum_{\boldsymbol{k}}\Big[M_{++}(\boldsymbol{k},\boldsymbol{q},i\nu_n) + M_{+-}(\boldsymbol{k},\boldsymbol{q},i\nu_n) + M_{-+}(\boldsymbol{k},\boldsymbol{q},i\nu_n) + M_{--}(\boldsymbol{k},\boldsymbol{q},i\nu_n)\Big] \tag{2.51}$$

$$\chi_0^{aabb}(\boldsymbol{q}, i\nu_n) = -\frac{2}{N^2}\frac{1}{4}\sum_{\boldsymbol{k}}(e^{i(\phi_{\boldsymbol{k}+\boldsymbol{q}}-\phi_{\boldsymbol{k}})})\Big[M_{++}(\boldsymbol{k},\boldsymbol{q},i\nu_n) - M_{+-}(\boldsymbol{k},\boldsymbol{q},i\nu_n) - M_{-+}(\boldsymbol{k},\boldsymbol{q},i\nu_n) + M_{--}(\boldsymbol{k},\boldsymbol{q},i\nu_n)\Big] \tag{2.52}$$

$$\chi_0^{bbaa}(\boldsymbol{q}, i\nu_n) = -\frac{2}{N^2}\frac{1}{4}\sum_{\boldsymbol{k}}(e^{-i(\phi_{\boldsymbol{k}+\boldsymbol{q}}-\phi_{\boldsymbol{k}})})\Big[M_{++}(\boldsymbol{k},\boldsymbol{q},i\nu_n) - M_{+-}(\boldsymbol{k},\boldsymbol{q},i\nu_n) - M_{-+}(\boldsymbol{k},\boldsymbol{q},i\nu_n) + M_{--}(\boldsymbol{k},\boldsymbol{q},i\nu_n)\Big] \tag{2.53}$$

If $\boldsymbol{q} = 0$ then

$$\sqrt{\chi_0^{aabb}(\boldsymbol{q}=0,i\nu_n)\,\chi_0^{bbaa}(\boldsymbol{q}=0,i\nu_n)} = \frac{2}{N^2}\frac{1}{4}\sum_{\boldsymbol{k}}\Big[M_{++}(\boldsymbol{k},\boldsymbol{q}=0,i\nu_n) - M_{+-}(\boldsymbol{k},\boldsymbol{q}=0,i\nu_n) - M_{-+}(\boldsymbol{k},\boldsymbol{q}=0,i\nu_n) + M_{--}(\boldsymbol{k},\boldsymbol{q}=0,i\nu_n)\Big] \tag{2.54}$$

Therefore the non-interacting anti-ferromagnetic susceptibility can be written as

$$\chi^0_{afm}(\boldsymbol{q}=0,i\nu_n) = -\frac{1}{N^2}\sum_{\boldsymbol{k}}\Big[M_{+-}(\boldsymbol{k},\boldsymbol{q}=0,i\nu_n) + M_{-+}(\boldsymbol{k},\boldsymbol{q}=0,i\nu_n)\Big] \tag{2.55}$$

and the non-interacting ferromagnetic susceptibility can be written as

$$\chi^0_{fm}(\boldsymbol{q}=0,i\nu_n) = -\frac{1}{N^2}\sum_{\boldsymbol{k}}\Big[M_{++}(\boldsymbol{k},\boldsymbol{q}=0,i\nu_n) + M_{--}(\boldsymbol{k},\boldsymbol{q}=0,i\nu_n)\Big] \tag{2.56}$$

The contribution to the anti-ferromagnetic susceptibility comes from the inter-band electron-hole pair excitations while that to the ferromagnetic susceptibility comes from intra-band electron-hole pair excitations as seen form the above result.

When the correlation length is large, a scaling form for the antiferromagnetic susceptibility can be written. The maximum of $\chi^0_{afm}(q)$ occurs at $\boldsymbol{q} = (0,0)$ at $i\nu_n = 0$. Starting from the relation Eq. (2.48), the numerator is replaced by the maximum $\chi^0_{afm}(\boldsymbol{q} = \boldsymbol{0}, i\nu_n = 0)$ and the denominator is expanded about the maximum. The antiferromagnetic susceptibility has a conical shape around $\boldsymbol{q} = \boldsymbol{0}$, as can be seen from the surface plot in

Fig. 2.2. Therefore the dependence is on $q = |\boldsymbol{q}| = \sqrt{q_x^2 + q_y^2}$. This can be numerically confirmed by fitting $\chi^0_{afm}(q)$ close to $\boldsymbol{q} = \boldsymbol{0}$ at zero frequency by a form $a + b|\boldsymbol{q}| + c|\boldsymbol{q}|^2$. The magnitude of coefficient $b = \frac{\partial \chi^0_{afm}}{\partial q}$ is numerically confirmed to be one order greater than that of the coefficient c. The scaling form for the retarded function can be obtained

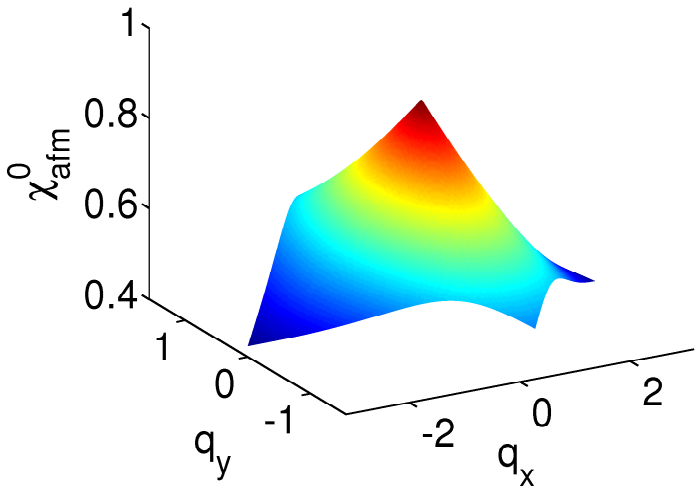

Figure 2.2: Plot of $\chi_0^{afm}(\boldsymbol{q}, i\nu_n = 0)$ for $T = 0.005$.

as,

$$\begin{aligned}
\chi^{sp}_{afm}(\boldsymbol{q}, \omega + i\delta) &= \frac{2\,\chi^0_{afm}(\boldsymbol{q} = \boldsymbol{0}, i\nu_n = 0)}{2 - U_{sp}\,\chi^0_{afm}(\boldsymbol{q}, i\nu_n)} \\
&= \frac{2}{\frac{2}{\chi^0_{afm}(\boldsymbol{q}=\boldsymbol{0}, i\nu_n=0)} - \frac{U_{sp}}{\chi^0_{afm}(\boldsymbol{q}=\boldsymbol{0}, i\nu_n=0)}\chi^0_{afm}(\boldsymbol{q}, i\nu_n)} \\
&= \frac{2}{U_{mf} - \frac{U_{sp}}{\chi^0_{afm}(\boldsymbol{q}=\boldsymbol{0}, i\nu_n=0)}[\chi^0_{afm}(\boldsymbol{q} = \boldsymbol{0}, i\nu_n = 0) + q\frac{\partial}{\partial q}\chi^0_{afm}(\boldsymbol{q}, i\nu_n)\Big|_{(\boldsymbol{q}=\boldsymbol{0}, i\nu_n=0)} + i\omega\frac{\partial}{\partial \omega}\chi^{0\prime\prime}_{afm}(\boldsymbol{q}, \omega)\Big|_{(\boldsymbol{q}=0, \omega=0)}]} \\
&= \frac{2}{U_{mf} - U_{sp} - \frac{U_{sp}}{\chi^0_{afm}(\boldsymbol{q}=0, i\nu_n=0)}\left[q\frac{\partial}{\partial q}\chi^0_{afm}(\boldsymbol{q}, i\nu_n)\Big|_{(\boldsymbol{q}=0, i\nu_n=0)} + i\omega\frac{\partial}{\partial \omega}\chi^{0\prime\prime}_{afm}(\boldsymbol{q}, \omega)\Big|_{(\boldsymbol{q}=0, \omega=0)}\right]}
\end{aligned} \tag{2.57}$$

where $\chi^{0\prime\prime}_{afm}$ is the imaginary part of the analytically continued antiferromagnetic susceptibility.

The microscopic length ξ_0 is defined as

$$\xi_0 = -\frac{1}{\chi^0_{afm}(\boldsymbol{q}=\mathbf{0}, i\nu_n=0)} \left.\frac{\partial \chi^0_{afm}(\boldsymbol{q}, i\nu_n)}{\partial q}\right|_{\boldsymbol{q}=\mathbf{0}, i\nu_n=0} \tag{2.58}$$

Using the following definitions for the mean-field critical interaction strength U_{mf}

$$U_{mf} = \frac{2}{\chi^0_{afm}(\boldsymbol{q}=\mathbf{0}, i\nu_n=0)} \tag{2.59}$$

and the variation of the spin vertex U_{sp} in TPSC from U_{mf}

$$\delta U = U_{mf} - U_{sp} \tag{2.60}$$

the correlation length is defined as

$$\xi = \xi_0 \frac{U_{sp}}{\delta U} \tag{2.61}$$

In TPSC, when the interaction increases, U_{sp} reaches arbitrarily close to U_{mf}, then the value of δU becomes very small. The correlation length increases rapidly when this happens, as can be seen from (2.61). We can rewrite the above equation (2.57) as

$$\chi^{sp}_{afm}(\boldsymbol{q}, \omega + i\delta) = \frac{2}{\delta U \left[1 + \left(\frac{U_{sp}}{\delta U}\xi_0\right) q - \left(\frac{U_{sp}}{\delta U}\xi_0\right) \left(\frac{1}{\xi_0} \frac{1}{\chi^0_{afm}(\boldsymbol{q}=\mathbf{0}, i\nu_n=0)} \frac{\partial}{\partial\omega} \chi^{0''}_{afm}(\boldsymbol{q}, \omega)\Big|_{(\boldsymbol{q}=\mathbf{0}, \omega=0)}\right) i\omega\right]} \tag{2.62}$$

Γ_0^{-1} is given as

$$\frac{1}{\Gamma_0} = \frac{1}{\xi_0 \chi^0_{afm}(\boldsymbol{q}=\mathbf{0}, i\nu_n=0)} \left.\frac{\partial \chi^{0''}_{afm}(\boldsymbol{q}, \omega)}{\partial\omega}\right|_{\boldsymbol{q}=\mathbf{0}, \omega=0} \tag{2.63}$$

we may write the scaling form as

$$\chi^{sp}_{afm}(\boldsymbol{q}, \omega + i\delta) = \frac{2\xi}{U_{sp}\xi_0} \frac{1}{1 + q\xi - \frac{i\omega\xi}{\Gamma_0}} \tag{2.64}$$

For our calculations, we can define practical measures of correlation length as

$$\xi^s_{afm} = \frac{\chi^{sp}_{afm}(\boldsymbol{q}=\boldsymbol{0}, i\nu_n = 0)}{\chi^0_{afm}(\boldsymbol{q}=\boldsymbol{0}, i\nu_n = 0)} \tag{2.65}$$

$$\xi^s_{fm} = \frac{\chi^{sp}_{fm}(\boldsymbol{q}=\boldsymbol{0}, i\nu_n = 0)}{\chi^0_{fm}(\boldsymbol{q}=\boldsymbol{0}, i\nu_n = 0)} \tag{2.66}$$

From Eq. (2.65), starting from the scaling form given by Eq. (2.64),

$$\xi^s_{afm} = \frac{2\xi}{U_{sp}\xi_0} \frac{1}{\chi^0_{fm}(\boldsymbol{q}=\boldsymbol{0}, i\nu_n = 0)} \tag{2.67}$$

$$= \frac{\xi}{\xi_0} \frac{U_{mf}}{U_{sp}} \tag{2.68}$$

For large correlation length, as $U_{sp} \sim U_{mf}$ the two definitions of correlation length essentially are the same.

2.5 Numerical procedure

We need to determine $\chi_0^{aaaa}(q)$ and $\chi_0^{aabb}(q)$. Because of sublattice symmetry, $\chi_0^{bbbb}(q) = \chi_0^{aaaa}(q)$. Once we know $\chi_0^{aabb}(q)$, $\chi_0^{bbaa}(q)$ can be written down. The definition of noninteracting susceptibility given by Eq. (2.22) is in the form of a convolution. The susceptibility in the Fourier space, the position - imaginary time space, is a product. Therefore, as in the case of the two-dimensional square lattice we can make use of FFTs in the numerical computation of the noninteracting susceptibilities. Using spin rotational symmetry, and then performing the Matsubara summation we can write down the expression for the susceptibilities given in Eqs. (2.51) and (2.52).

$$\begin{aligned}\chi_0^{aaaa}(\boldsymbol{r},\tau) &= -2G^{(0)aa}(\boldsymbol{r},\tau)G^{(0)aa}(-\boldsymbol{r},-\tau) \\ &= 2G^{(0)aa}(\boldsymbol{r},\tau)G^{(0)aa}(\boldsymbol{r},\beta-\tau) \qquad (2.69)\\ \chi_0^{aabb}(\boldsymbol{r},\tau) &= -2G^{(0)ab}(\boldsymbol{r},\tau)G^{(0)ba}(-\boldsymbol{r},-\tau) \\ &= 2G^{(0)ab}(\boldsymbol{r},\tau)G^{(0)ab}(\boldsymbol{r},\beta-\tau) \qquad (2.70)\end{aligned}$$

We can write

$$G^{\rho\lambda}(\boldsymbol{r},\tau) = \frac{1}{N^2}\sum_{\boldsymbol{k}} G^{\rho\lambda}(\boldsymbol{k},\tau)e^{i\boldsymbol{k}\cdot\boldsymbol{r}} \tag{2.71}$$

Using

$$G^{(0)aa}(\boldsymbol{k},\tau) = G^{(0)aa}(-\boldsymbol{k},\tau) \tag{2.72}$$
$$G^{(0)ab}(\boldsymbol{k},\tau) = G^{(0)ba}(-\boldsymbol{k},\tau) \tag{2.73}$$

The phase factor associated with G^{ab} changes sign when the sign of $\boldsymbol{k}$ changes, hence using the above relation

$$\begin{aligned} G^{(0)ba}(-\boldsymbol{r},\tau) &= \frac{1}{N^2}\sum_{\boldsymbol{k}} G^{(0)ba}(\boldsymbol{k},\tau)e^{i\boldsymbol{k}\cdot(-\boldsymbol{r})} \\ &= \frac{1}{N^2}\sum_{\boldsymbol{k}} G^{(0)ba}(\boldsymbol{k},\tau)e^{i(-\boldsymbol{k})\cdot\boldsymbol{r}} \\ &= \frac{1}{N^2}\sum_{-\boldsymbol{k'}} G^{(0)ba}(-\boldsymbol{k'},\tau)e^{i\boldsymbol{k'}\cdot\boldsymbol{r}} \\ &= \frac{1}{N^2}\sum_{\boldsymbol{k'}} G^{(0)ab}(\boldsymbol{k'},\tau)e^{i\boldsymbol{k'}\cdot\boldsymbol{r}} \\ &= G^{(0)ab}(\boldsymbol{r},\tau) \end{aligned} \tag{2.74}$$

For a particular $\boldsymbol{k}$, we can evaluate $f(\boldsymbol{k})$ and get the energy eigenvalues for the valence band and the conduction band. From this we can determine, $G^0_{vv}(\boldsymbol{k},\tau)$ and $G^0_{cc}(\boldsymbol{k},\tau)$. For $0 < \tau < \beta$

$$G_{vv}(\boldsymbol{k},\tau) = -e^{-E_v(\boldsymbol{k})\tau}n_F(-E_v(\boldsymbol{k})) \tag{2.75}$$
$$G_{cc}(\boldsymbol{k},\tau) = -e^{-E_c(\boldsymbol{k})\tau}n_F(-E_c(\boldsymbol{k})) \tag{2.76}$$
$$\tag{2.77}$$

$G^{(0)aa}(\boldsymbol{k},\tau)$ and $G^{(0)ab}(\boldsymbol{k},\tau)$ are given as

$$G^{(0)aa}(\boldsymbol{k},\tau) = \frac{1}{2}\left[G_{vv}(\boldsymbol{k},\tau) + G_{cc}(\boldsymbol{k},\tau)\right] \tag{2.78}$$
$$G^{(0)ab}(\boldsymbol{k},\tau) = \frac{1}{2}e^{-i\phi_{\boldsymbol{k}}}\left[G_{vv}(\boldsymbol{k},\tau) - G_{cc}(\boldsymbol{k},\tau)\right] \tag{2.79}$$

Using FFTs we can evaluate, $G^{(0)aa}(\boldsymbol{r},\tau)$ and $G^{(0)ab}(\boldsymbol{r},\tau)$. The procedure we applied for the computation of noninteracting susceptibility for the square lattice [27] can be extended in a straightforward manner. We can compute $\chi_0^{aaaa}(\boldsymbol{r},\tau)$ and $\chi_0^{aabb}(\boldsymbol{r},\tau)$ as the product of Green functions in the position-imaginary time space, and perform a 3D FFT to get $\chi_0^{aaaa}(\boldsymbol{q},i\nu_n)$ and $\chi_0^{aabb}(\boldsymbol{q},i\nu_n)$. Just as we did in the case of the square lattice, the

continuous transform along the imaginary time direction is approximated making use of cubic splines. The derivatives of $\chi_0^{aaaa}(\boldsymbol{r},\tau)$ and $\chi_0^{aabb}(\boldsymbol{r},\tau)$ needed for the evaluation of spline coefficients can be easily computed from the derivatives of $G_0^{(0)aa}(\boldsymbol{r},\tau)$ and $G_0^{(0)ab}(\boldsymbol{r},\tau)$.

2.6 Results

In generating the results given in this section, steps detailed in this flowchart, Fig. 2.3, were followed. We work at half-filling ($n = 1.0$). The real (momentum) space grid was of size $N \times N$, where $N = 50, 100, 200$ were taken. The noninteracting susceptibility obeys $\frac{T}{N^2}\sum_q \chi_0^{\rho\rho\rho\rho}(q) = \langle n_\rho \rangle = 0.5$, the number of Matsubara frequencies was fixed in such a way that this relation was satisfied to 1 percent accuracy. Fixing a temperature T, once we calculate the noninteracting susceptibility, the double occupancy can be computed self-consistently for a range of interaction values U. Once we have the double occupancy, the calculation of spin vertex is straightforward. We do not venture into the calculation of charge vertex here. The correlation lengths in the ferromagnetic and antiferromagnetic channels can be evaluated using the expressions Eqs. (2.66) and (2.65).

2.6.1 Double occupancy $\langle n_\uparrow n_\downarrow \rangle$

Because of bipartite symmetry, $\langle n_{a\uparrow} n_{a\downarrow} \rangle = \langle n_{b\uparrow} n_{b\downarrow} \rangle$. We denote the double occupancy by $\langle n_\uparrow n_\downarrow \rangle$ and plot it as a function of interaction U for various values of temperature in Fig .2.4. The results shown are for $N = 100$. From the inset, we can see that the temperature dependence of $\langle n_\uparrow n_\downarrow \rangle$ is very small.

When $U = 0$, at half-filling, the average number of up spin particles on a site is $\frac{1}{2}$. The case is the same for down spin particles also. Therefore, the average value of double occupancy can be written as the product of the probability of an up spin particle being on the site and the probability of a down spin particle being on the site. That means, $\langle n_\uparrow n_\downarrow \rangle = \langle n_\uparrow \rangle \times \langle n_\downarrow \rangle = \frac{1}{2} \times \frac{1}{2} = 0.25$. As we turn on the interaction, the double occupancy of a site becomes less favorable energetically. The double occupancy $\langle n_\uparrow n_\downarrow \rangle$ steadily decreases as we increase U.

2.6.2 Spin vertex U_{sp}

The spin vertex is given by $U_{sp} = \frac{U\langle n_\uparrow n_\downarrow \rangle}{\langle n_\uparrow \rangle \langle n_\downarrow \rangle}$ and is plotted in Fig. 2.5(for $N = 100$). For small values of U, U_{sp} is almost equal to U. As the interaction increases, the spin vertex

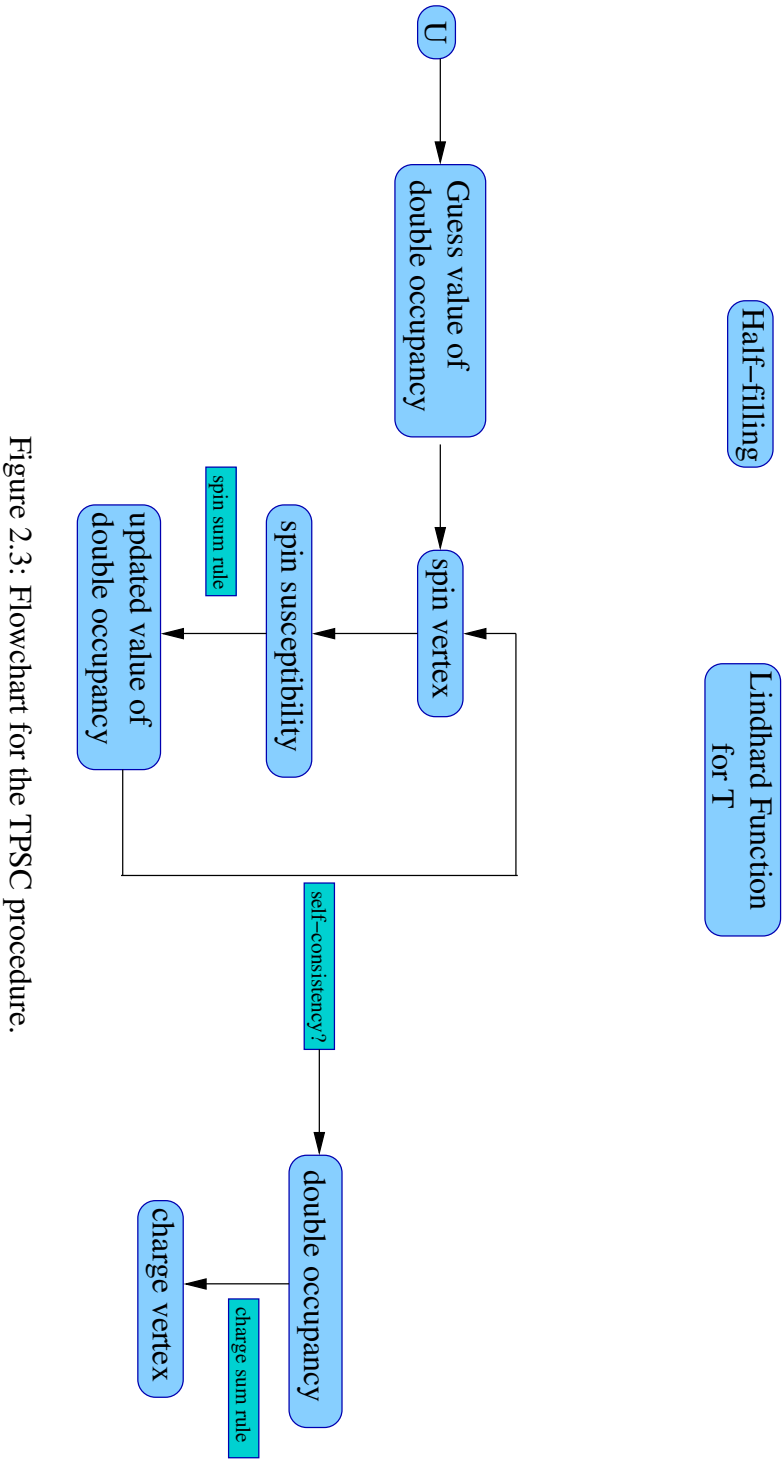

Figure 2.3: Flowchart for the TPSC procedure.

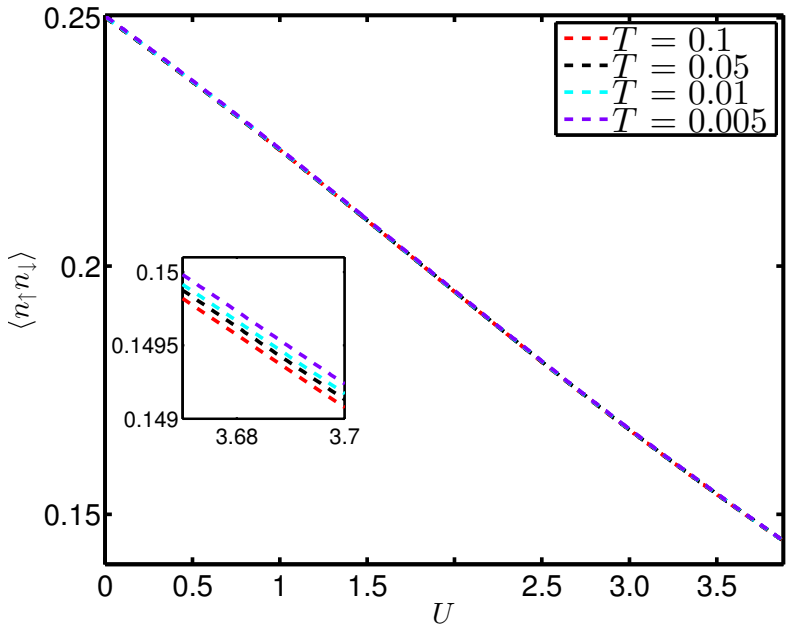

Figure 2.4: Plot of double occupancy $\langle n_\uparrow n_\downarrow \rangle$ as a function of interaction U for given temperatures. The temperature dependence is very small as seen from the inset.

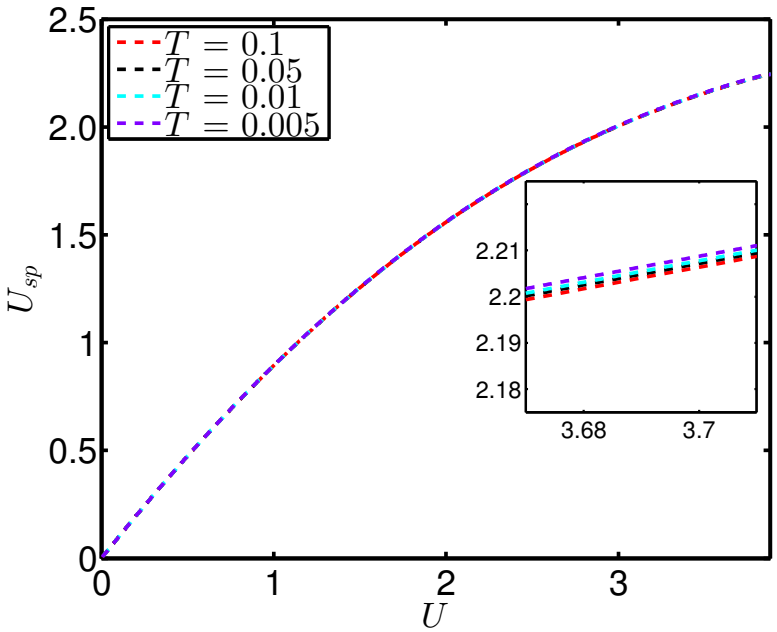

Figure 2.5: Plot of spin vertex U_{sp} as a function of interaction U for given temperatures. From the inset, its clear that this quantity is almost temperature independent.

increases and tends to saturate to a constant value. When U increases, the amplitude of the two-body wave function is reduced so as to decrease the probability of double

occupancy. This results in a reduced effective interaction. The maximum energy this can cost is the bandwidth, hence U_{sp} saturates to a value of the order of the bandwidth. This physics is a result of Kanamori-Brueckner screening [10, 13, 14].

Once we have the spin vertex, the interacting susceptibilities can be calculated using the Bethe - Salpeter equation. The susceptibilities in the ferromagnetic and antiferromagnetic channels can be computed from Eqs. 2.42 and 2.43.

2.6.3 Ferromagnetic correlation length

The ratio of the interacting susceptibility in the ferromagnetic channel to the corresponding noninteracting susceptibility at$(\boldsymbol{q} = \mathbf{0}, i\nu_n = 0)$, as defined in Eq. (2.66) is the measure of correlation length. This quantity denoted as ξ^s_{fm} is plotted as a function of interaction, for $T = 0.1$ and $T = 0.05$ in Fig. 2.6, again for $N = 100$. Although the

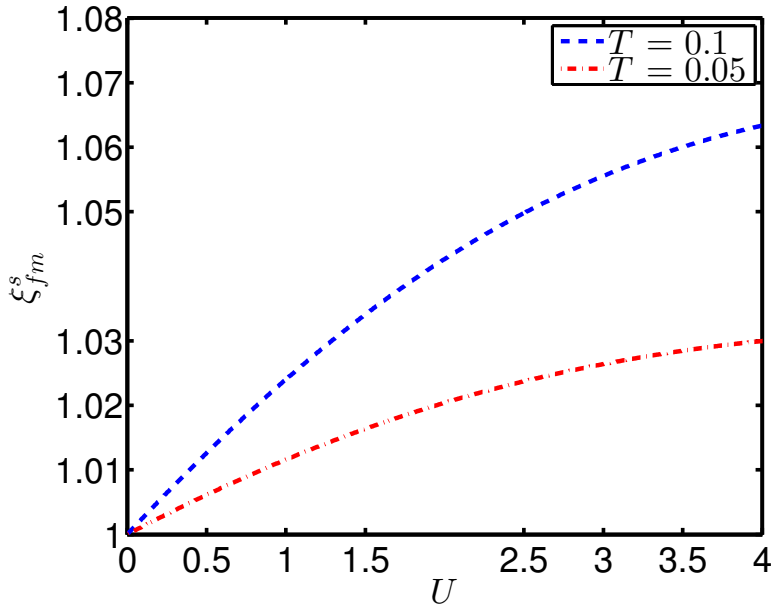

Figure 2.6: Plot of ferromagnetic correlation length ξ^s_{fm} as a function of interaction U for given temperatures.

correlation length increases, as the value of interaction increases, we see that a reduction in temperature results in a reduction in the correlation length.

2.6.4 Antiferromagnetic correlation length

First calculating the ratio of the interacting susceptibility to the noninteracting susceptibility in the antiferromagnetic channel (Eq. 2.65), ξ^s_{afm}, we multiply it by the microscopic

length ξ_0 (Eq. 2.58) to obtain the antiferromagnetic correlation length ξ. Fig. 2.7 shows a plot of ξ as a function of interaction, for various temperatures. Its clearly visible that, as we increase interaction U, the correlation length increases rapidly. This increase is even more dramatic as one goes to lower and lower temperatures. This is clearly in contrast to the behavior of the ferromagnetic correlation length (Fig. 2.6). These results are for $N = 100$.

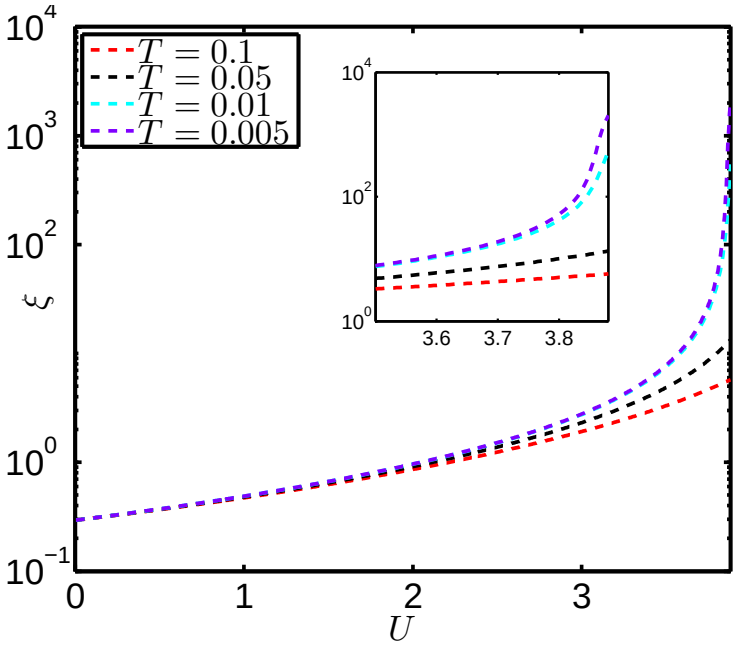

Figure 2.7: Semilogarithmic plot of antiferromagnetic correlation length $\xi = \xi_0\, \xi^s_{afm}$ as a function of interaction U for given temperatures.

2.6.5 Crossover temperature and U_c

For the quantum phase transition, when U is greater than the critical interaction strength, there is antiferromagnetic order in the system. At finite temperature, when U exceeds some particular value, we expect a 'crossover' to the renormalized classical regime. This crossover occurs when the spin fluctuation frequency ω_{sp} is smaller than the temperature thereby leading to large antiferromagnetic fluctuations.

In order to numerically determine the we use the condition that the correlation length exceeds the thermal de Broglie wavelength

$$\xi_{th} = \frac{v_F}{T}$$

where v_F is the Fermi velocity. Here v_F is at the Dirac point, since we are working at half-filling. The crossover points can be picked in two ways:

a) We fix the value of interaction U, and plot ξ vs. T as well as ξ_{th} vs. T. The point of intersection where $\xi = \frac{v_F}{T}$ gives us the crossover temperature T_X. The crossover plot is the plot of T_X as a function of U.

b) We fix the value of temperature T and scan the U axis for the value where the condition $\xi = \frac{v_F}{T}$ holds. A crossover plot can be generated where T is plotted vs U_X. The crossover plots given by both the methods for various system sizes are given in Fig. 2.8. The crossover plot can be extrapolated to zero temperature to obtain an estimate

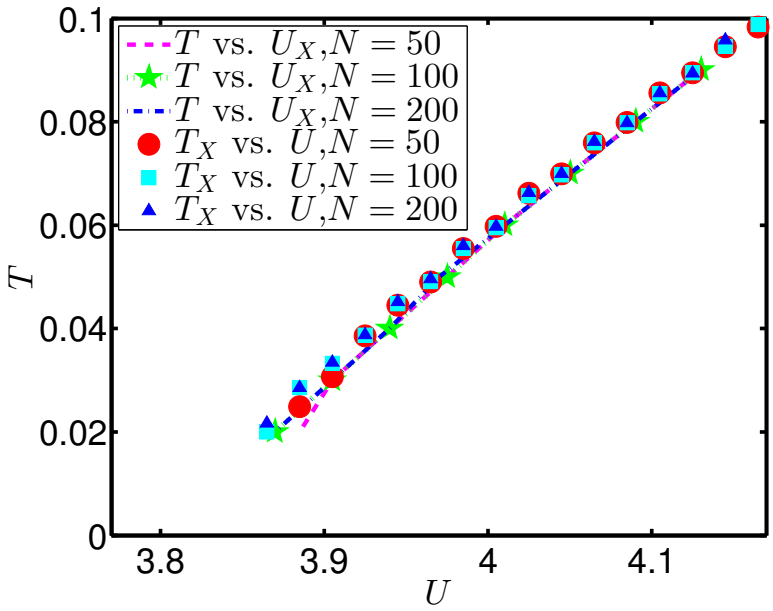

Figure 2.8: Crossover temperature as a function of U for given values of N.

of the critical interaction strength. The results which we obtain for linear and quadratic extrapolations are given in the Table 2.1.

2.6.6 Alternate determination of U_c and critical exponent z

The critical interaction strength U_c can be estimated by another method, which also lets us estimate the dynamical critical exponent z. In Fig. 2.9, we plot $\ln \xi$ as a function of $\ln T$ for $N = 100$ and $N = 200$. For $U < U_c$, $\ln \xi$ saturates at low temperatures and for $U > U_c$, $\ln \xi$ diverges at low temperatures. When $U = U_c$, ξ has pure power law behavior. We try to fit $\ln \xi$ vs $\ln T$ by a straight line for various values of U and pick the value of U which gives the best fit as U_c. The slope of this plot is taken as the estimate

		$N = 50$	$N = 100$	$N = 200$
T vs. U_X	linear	3.8	3.794	3.793
	quadratic	3.825	3.806	3.808
T_X vs. U	linear	3.779	3.775	3.775
	quadratic	3.809	3.795	3.789

Table 2.1: Table of the values of critical interaction strength obtained from linear and quadratic extrapolation of the crossover plots for various values of N.

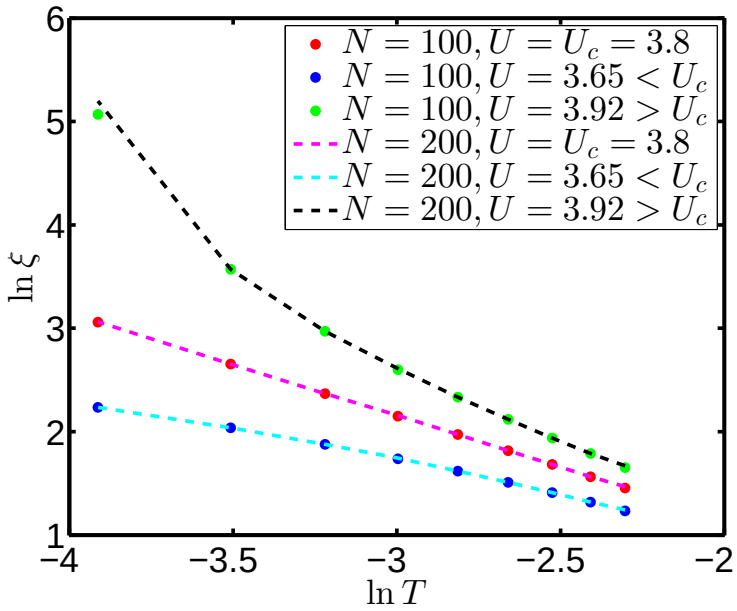

Figure 2.9: Plots of $\ln \xi$ as a function of $\ln T$ for various values of U ($N = 100$ and $N = 200$).

of z. For $N = 100$ and $N = 200$, the critical interaction strength thus determined is $U_c = 3.8 \pm 0.005$ and the dynamical critical exponent is $z = 1.00$. For $N = 50$, the largest correlation length is half the system size. Finite size effects cannot be neglected in this scenario, there $U_c = 3.85 \pm 0.005$ and $z = 0.87$.

2.6.7 ξ_0 and Γ_0^{-1}

From the expression for $\chi_0^{afm}(\boldsymbol{q}=\boldsymbol{0}, i\nu_n)$ given by Eq. (2.55) we may write the analytically continued $\chi_0^{afm}(\boldsymbol{q}=\boldsymbol{0}, \omega+i\delta)$ as

$$\begin{aligned}\chi^0_{afm}(\boldsymbol{q}=\boldsymbol{0}, \omega+i\delta) &= -\frac{1}{N^2}\sum_{\boldsymbol{k}}\Big[M_{+-}(\boldsymbol{k}, \boldsymbol{q}=0, \omega+i\delta) + M_{-+}(\boldsymbol{k}, \boldsymbol{q}=0, \omega+i\delta)\Big] \\ &= -\frac{1}{N^2}\sum_{\boldsymbol{k}}\left[\frac{2n_F(E^+_{\boldsymbol{k}})-1}{2E^+_{\boldsymbol{k}}+\omega+i\delta} + \frac{-2n_F(E^+_{\boldsymbol{k}})+1}{-2E^+_{\boldsymbol{k}}+\omega+i\delta}\right]\end{aligned} \tag{2.80}$$

In order to evaluate the imaginary part of this entity,

$$\text{Im }\chi^0_{afm}(\boldsymbol{q}=\boldsymbol{0}, \omega+i\delta) = -\pi\frac{1}{N^2}\sum_{\boldsymbol{k}}\tanh(\beta E^+_{\boldsymbol{k}}/2)\Big[\delta(2E^+_{\boldsymbol{k}}+\omega) - \delta(2E^+_{\boldsymbol{k}}-\omega)\Big] \tag{2.81}$$

The sum over $\boldsymbol{k}$ is rewritten in terms of an integral, and it is evaluated by a transformation to cylindrical coordinates,

$$\frac{1}{N^2}\sum_{\boldsymbol{k}} \to \int\frac{d^2k}{4\pi^2} \to \int_0^{\Lambda}\frac{kdk}{2\pi} \to \frac{1}{v_F^2}\int_0^{\Lambda_E}\frac{\varepsilon d\varepsilon}{2\pi}$$

Here Λ_E is the cutoff in energy. Assuming that $\omega > 0$, the second delta function in Eq. (2.81) contributes. We take a factor of 2 to account for the two Dirac points, and evaluate Eq. (2.81) as,

$$\text{Im }\chi^0_{afm}(\boldsymbol{q}=\boldsymbol{0}, \omega+i\delta) = \pi\frac{2}{v_F^2}\int_0^{\Lambda_E}\frac{\varepsilon d\varepsilon}{2\pi}\tanh(\beta\varepsilon/2)\,\delta(2\varepsilon-\omega) \tag{2.82}$$

In the limit of zero temperature, $\tanh(\beta\varepsilon/2) \to 1$, therefore

$$\begin{aligned}\text{Im }\chi^0_{afm}(\boldsymbol{q}=\boldsymbol{0}, \omega+i\delta) &= \frac{1}{v_F^2}\int_0^{\Lambda_E}\delta(2\varepsilon-\omega)\,\varepsilon d\varepsilon \\ &= \frac{1}{2v_F^2}\frac{\omega}{2}\end{aligned} \tag{2.83}$$

Now let us evaluate the real part, taking into account the two Dirac points

$$\text{Re } \chi^0_{afm}(\boldsymbol{q}=\boldsymbol{0},\omega+i\delta) = \frac{1}{N^2}\mathcal{P}\sum_{\boldsymbol{k}} \tanh(\beta E^+_{\boldsymbol{k}}/2)\left[\frac{4E^+_{\boldsymbol{k}}}{(2E^+_{\boldsymbol{k}})^2-\omega^2}\right] \tag{2.84}$$

$$= \mathcal{P}\frac{2}{v_F^2}\int_0^{\Lambda_E}\frac{\varepsilon d\varepsilon}{2\pi}\tanh(\beta\varepsilon/2)\left[\frac{4\varepsilon}{(2\varepsilon)^2-\omega^2}\right] \tag{2.85}$$

$$= \mathcal{P}\frac{1}{v_F^2}\int_0^{\Lambda_E}\frac{d\varepsilon}{\pi}\frac{(2\varepsilon)^2}{(2\varepsilon)^2-\omega^2} \tag{2.86}$$

where in the last line the zero temperature limit has been taken. By rewriting the numerator as $(2\varepsilon)^2-\omega^2+\omega^2$, we can simplify the integration as

$$\text{Re } \chi^0_{afm}(\boldsymbol{q}=\boldsymbol{0},\omega+i\delta) = \frac{1}{v_F^2}\int_0^{\Lambda_E}\frac{d\varepsilon}{\pi} + \frac{\omega^2}{v_F^2}\mathcal{P}\int_0^{\Lambda_E}\frac{d\varepsilon}{\pi}\frac{1}{(2\varepsilon)^2-\omega^2} \tag{2.87}$$

$$= \frac{1}{\pi v_F^2}\Lambda_E + \frac{\omega^2}{2\pi v_F^2}\mathcal{P}\int_0^{2\Lambda_E/\omega}\frac{dx}{\omega}\frac{1}{x^2-1} \tag{2.88}$$

We assume $\omega > 0$, to get

$$\text{Re } \chi^0_{afm}(\boldsymbol{q}=\boldsymbol{0},\omega+i\delta) = \frac{1}{\pi v_F^2}\Lambda_E - \frac{\omega}{2\pi v_F^2}\tanh^{-1}\left(\frac{\omega}{2\Lambda_E}\right) \tag{2.89}$$

$$\sim \frac{1}{\pi v_F^2}\Lambda_E - \frac{\omega^2}{4\pi v_F^2\Lambda_E} \tag{2.90}$$

From these results, we can estimate the values of Γ_0^{-1} and ξ_0.

$$\frac{1}{\Gamma_0} = \frac{1}{\xi_0}\frac{1}{\text{Re } \chi^0_{afm}(\boldsymbol{0},0)}\frac{\partial}{\partial\omega}\text{Im } \chi^0_{afm}(\boldsymbol{0},\omega+i\delta)\Big|_{\omega=0} \tag{2.91}$$

$$= \frac{1}{\xi_0}\frac{\frac{1}{4v_F^2}}{\Lambda_E\frac{1}{\pi v_F^2}} \tag{2.92}$$

$$= \frac{\pi}{4\xi_0\Lambda_E} \tag{2.93}$$

Taking $\Lambda_E = v_F\Lambda$, where the cutoff $\Lambda = \pi/a$, the above expression becomes,

$$\Gamma_0 = \frac{4\xi_0\Lambda_E}{\pi} = \frac{4\xi_0 v_F}{a} \tag{2.94}$$

From Lorentz invariance, we expect $\Gamma_0 = v_F$ and a is taken as unity. Therefore this means $\xi_0 \sim 0.25$.

Numerically, this can be confirmed by plotting ξ_0 and Γ_0 as a function of temperature as shown in Fig. 2.10. Γ_0 converges to the estimate $\sqrt{3}/2$ only for low temperatures and

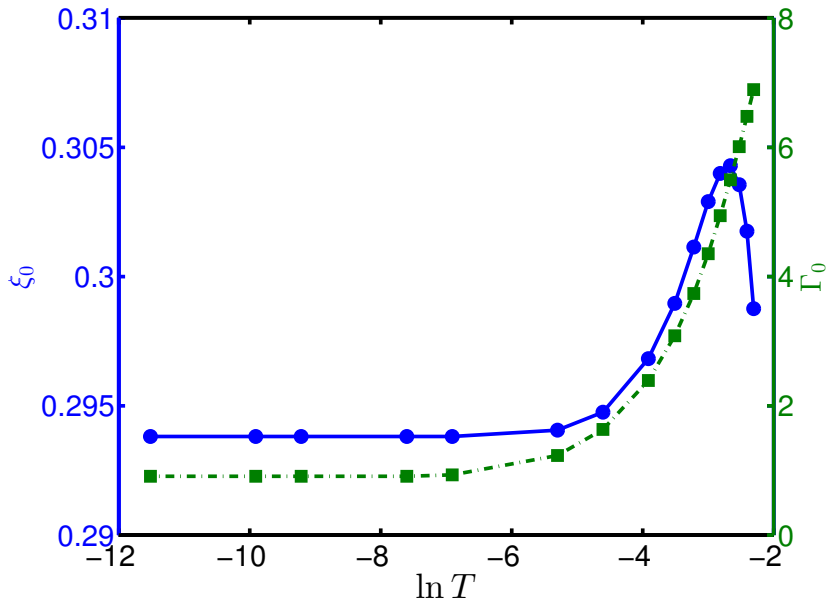

Figure 2.10: Plots of ξ_0 and Γ_0 as a function of T for the range $T = 0.001$ to 0.1. Each quantity has its own vertical axis, left for ξ_0 and right for Γ_0. ξ_0 is shown in blue, while the dot-dashed green curve shows Γ_0.

large lattice sizes $N = 2000$. The microscopic length ξ_0 is of the order of 0.25, and is almost temperature independent for low values of temperature.

2.7 Summary

The technique of TPSC has been extended to study the multi-band case of the Hubbard model on the honeycomb lattice. This non-perturbative method is valid from weak to intermediate coupling and satisfies crucial physical constraints like conservations laws for spin and charge, Pauli exclusion principle, Mermin-Wagner theorem. The spin and charge vertices are evaluated self-consistently using spin and charge sum rules. Along with the above mentioned physical laws, this method affirms the physics of Kanamori Brueckner screening for the renormalization of spin and charge vertices. The nearest-neighbor antiferromagnetic fluctuations grow as the interaction increases and as the temperature decreases. When the antiferromagnetic correlation length grows beyond the thermal de Broglie wavelength, the system has a crossover to the renormalized classical regime.

This crossover is the finite temperature signature of the zero temperature quantum phase transition and a pseudogap is expected to open up as the system enters this regime.

The critical interaction strength for the semimetallic to antiferromagnetic quantum phase transition as determined from the extrapolation of the crossover plot as well as the scaling form of the antiferromagnetic correlation length is $U_c = 3.79 \pm 0.01$. This estimate is consistent with the estimates from large scale quantum Monte Carlo calculations and functional renormalization group calculations [36, 52–54]. Since the estimates for the Mott transition, U_{Mott} are larger than the estimated value of U_c, the intermediate spin liquid phase can be ruled out.

Chapter 3

Exploring novel quantum criticality in strained graphene

3.1 Introduction

Tuning the value of strain applied to matter can generate novel effects which are interesting, so is the case with graphene. Such 'strain engineering' may aid us in uniting the mechanical and electronic properties of graphene, this can be exploited for the fabrication of devices. As shown by experimental studies, controlled and reversible strain upto 20 percent can be applied on graphene [55]. The effects of electron - electron interactions on the electronic structure modified by strain demands attention, as this interplay might lead to new and interesting phase transitions and responses.

The starting point of our study is the tight-binding analysis of uniaxial strain in graphene performed by Pereira and coworkers [56]. Our idea is to study the effects of the introduction of the Hubbard interaction U. Since graphene is a two-dimensional material, long-range antiferromagnetic fluctuations are very relevant. The interplay of the growing antiferromagnetic fluctuations (especially at low temperatures), with the strain induced anisotropy in the electronic structure might produce interesting physics. TPSC with its proven track record in capturing the physics of long-wavelength antiferromagnetic fluctuations is again the method of choice for this study.

The two main results of the tight-binding analysis done by Pereira and coworkers are i) the application of strain generates a gap in the band structure, when the applied strain exceeds a threshold value and ii) the strain along every direction does not produce a band gap. For instance, a strain along the armchair direction never produces a gap. In this work, we focus only on strain along the zigzag direction.

3.2 Tight-binding analysis

We follow the analysis given in Reference [56]. Upon the application of uniaxial tensional strain, naturally the bond lengths change. As a result, the overlap between the orbitals on nearest neighbor sites change. This can be written down as a change in the hopping parameters of the tight-binding Hamiltonian. The change in the lattice vectors modifies the reciprocal lattice vectors also, but in our study we do not consider the change in the reciprocal lattice. We work with modified hopping parameters and the reciprocal lattice of the undistorted lattice in our calculations.

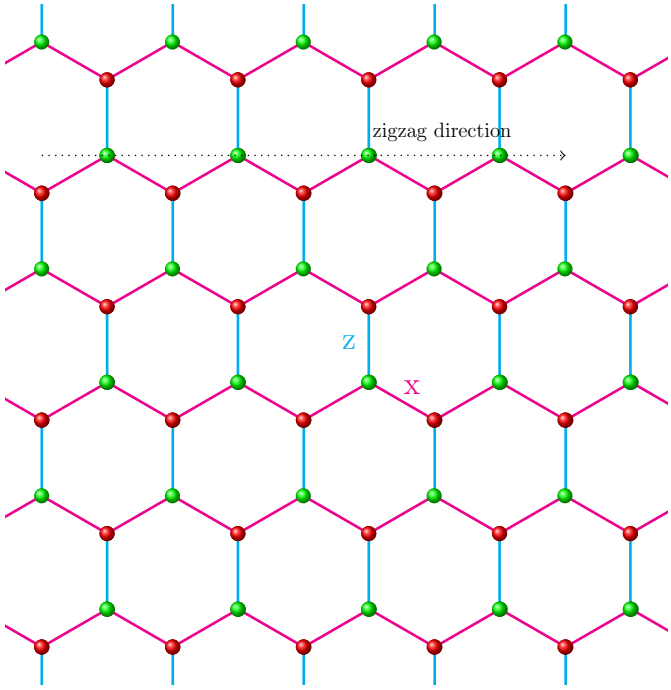

Figure 3.1: Honeycomb lattice showing zigzag direction in magenta, the z-bonds are colored in cyan.

Suppose the coordinate system is chosen such that the x-axis lies along the zigzag direction of the lattice. The tension $\boldsymbol{T}$ can be written in terms of the components as

$$\boldsymbol{T} = T\cos(\theta)\,\hat{x} + T\sin(\theta)\hat{y} \tag{3.1}$$

From Hooke's law relating stress τ_{ij} and strain ϵ_{ij}

$$\tau_{ij} = C_{ijkl}\epsilon_{kl} \tag{3.2}$$

$$\epsilon_{ij} = S_{ijkl}\tau_{ij} \tag{3.3}$$

where C_{ijkl} and S_{ijkl} are the components of the stiffness tensor and the compliance tensor respectively. Usually the components of these tensors depend on the choice of the coordinate system. But, as graphene is elastically isotropic, the choice of coordinate system does not matter. So we go to the coordinate system, where $\boldsymbol{T} = T\hat{x}'$. We assume the x -axis is along the direction in which strain is applied. We have,

$$\begin{aligned}\epsilon'_{ij} &= S_{ijkl}\tau'_{kl} \\ &= TS_{ijkl}\delta_{kx}\delta_{lx} \\ &= TS_{ijxx}\end{aligned} \tag{3.4}$$

Only five components of the compliance tensor are independent in graphite out of which S_{xxxx} and S_{xxyy} are relevant to us. Therefore we may write,

$$\epsilon'_{xx} = TS_{xxxx} \tag{3.5}$$

$$\epsilon'_{yy} = TS_{xxyy} \tag{3.6}$$

The above set of equations is easy to understand - when strain is applied along the x' direction, there is a deformation along that direction. There is a corresponding deformation along the perpendicular y' direction - transverse deformation. The strain tensor

$$\boldsymbol{\epsilon}' = \epsilon \begin{pmatrix} 1 & 0 \\ 0 & -\sigma \end{pmatrix} \tag{3.7}$$

where $\sigma = -S_{xxyy}/S_{xxxx}$ is the Poisson ratio and the strain is rewritten as $\epsilon = TS_{xxxx}$. The value of Poisson ratio in our computations is $\sigma = 0.165$.

Rewriting the strain tensor in the coordinate system we initially chose,

$$\boldsymbol{\epsilon} = \epsilon \begin{pmatrix} \cos^2\theta \, - \, \sigma \, \sin^2\theta & (1+\sigma) \, \cos\theta \, \sin\theta \\ (1+\sigma) \, \cos\theta \, \sin\theta & \sin^2\theta \, - \, \sigma \, \cos^2\theta \end{pmatrix} \tag{3.8}$$

Here, θ is the angle the direction of application of strain makes with the zigzag direction. $\theta = 0$ is the zigzag direction and $\theta = \pi/2$ is the armchair direction.

From the relation connecting the deformed vector $\boldsymbol{r}$ to the original vector $\boldsymbol{r}^0$,

$$\boldsymbol{r} = (1 + \epsilon) \cdot \boldsymbol{r}_0$$

we can evaluate the changed bond vectors. The bond lengths are the magnitudes of the bond vectors ($\boldsymbol{\delta}_i$ and i = 1, 2, 3) and these are given by

$$|\boldsymbol{\delta}_1| = 1 + \frac{3}{4}\epsilon_{11} - \frac{\sqrt{3}}{2}\epsilon_{12} + \frac{1}{4}\epsilon_{22} \tag{3.9}$$

$$|\boldsymbol{\delta}_2| = 1 + \epsilon_{22} \tag{3.10}$$

$$|\boldsymbol{\delta}_3| = 1 + \frac{3}{4}\epsilon_{11} + \frac{\sqrt{3}}{2}\epsilon_{12} + \frac{1}{4}\epsilon_{22} \tag{3.11}$$

The change in the hopping parameter is assumed to be given by

$$t = te^{-3.37(l/a_0 - 1)} \tag{3.12}$$

t is the hopping parameter in the undistorted lattice. In the undistorted lattice, the hopping parameters along all the bonds are the same, and is equal to $t_i = t$ for $i = 1, 2, 3$. In general, when strain is applied, the parameters change and are no longer equal to each other. l is the bond length and a_0 is the distance between nearest carbon atoms taken as unity in our computations. t is also taken as unity.

The dispersion relation can be written in terms of the modified hopping as,

$$\varepsilon_{\boldsymbol{k}} = \pm \left| t_2 + t_3 e^{-i\boldsymbol{k}\cdot\boldsymbol{a}_1} + t_1 e^{-i\boldsymbol{k}\cdot\boldsymbol{a}_2} \right| \tag{3.13}$$

When the strain is along the zigzag direction, $\theta = 0$, we have $|\boldsymbol{\delta}_1| = |\boldsymbol{\delta}_3|$ and therefore $t_1 = t_3$.

$$|\boldsymbol{\delta}_1| = 1 + \frac{3}{2}\epsilon - \frac{1}{4}\epsilon\sigma \tag{3.14}$$

$$|\boldsymbol{\delta}_2| = 1 - \epsilon\sigma \tag{3.15}$$

$$|\boldsymbol{\delta}_3| = 1 + \frac{3}{2}\epsilon - \frac{1}{4}\epsilon\sigma \tag{3.16}$$

For the gap to open up, the threshold strain needed along the zigzag direction is $\epsilon \approx 0.235$. Fig. 3.2 shows plots of the bandstructure and density of states(DOS) for the tight-binding model on the honeycomb lattice for various values of strain applied along the zigzag direction. The strain values for which the plots are made fall under the critical strain

required to produce a gap. The plots in Fig. 3.3 show the corresponding plots when the strain exceeds the critical strain, the band gap is clearly visible from the plots.

3.2.1 Energy minimum under the application of strain

When strain is applied on the lattice, the Dirac point starts moving from the K point towards the direction of the M point. This is shown in Fig. 3.4. Once the gap opens up, the minimum of the energy thus lies at the M point in the Brillouin zone. For the case where $t_1 = t_3$, the position of the minimum can be found out by minimizing $\varepsilon_{\boldsymbol{k}}^2$ which is given by,

$$\begin{aligned}\varepsilon_{\boldsymbol{k}}^2 &= t_2^2 + 2t_1^2 + 4t_1 t_2 \cos\left(\frac{\sqrt{3}}{2}k_x\right)\cos\left(\frac{3}{2}k_y\right) + 2t_1^2\cos\left(\sqrt{3}k_x\right) \\ &= t_2^2 + 4t_1 t_2 \cos\left(\frac{\sqrt{3}}{2}k_x\right)\cos(\frac{3}{2}k_y) + 4t_1^2\cos^2\left(\frac{\sqrt{3}}{2}k_x\right) \end{aligned} \tag{3.17}$$

Minimizing this expression with respect to k_x and k_y, we can find the position of the minimum as,

$$\boldsymbol{k}_{min} = \left(\pm\frac{2}{\sqrt{3}}\cos^{-1}\left(-\frac{t_2}{2t_1}\right), 0\right) \tag{3.18}$$

Numerically, we can locate the momentum value $\boldsymbol{k}_{min}$ by dividing the Brillouin zone into a $N \times N$ mesh, and looking for the minimum energy. But, as we introduce strain, pinpointing $\boldsymbol{k}_{min}$ might be a bit tricky. If we choose the same Brillouin zone mesh for all values of strain, the momentum value corresponding to the zero energy may not lie on the mesh. We have to modify the value of N with strain and choose the appropriate value of N which gives us an energy close to zero. This is applicable till the threshold strain, because once the threshold strain is crossed and the gap opens up, the minimum is at the M point. To check the correctness of our choice of N, for a fine grid of ω, we plotted the non-interacting spectral function as $A(\boldsymbol{k}_{min}, \omega) = -\frac{1}{\pi}\,\mathrm{Im}\, G_{aa}(\boldsymbol{k}_{min}, \omega + i\delta)$, to see whether we get a single peak at $\omega = 0$ for a frequency grid step of 0.0005.

3.2.2 TPSC applied to graphene under strain

In undistorted graphene, the value of hopping is independent of the direction of the bond. But, when we apply strain along the zigzag direction, the hopping parameters ($t_1 = t_3$) reduce, while the hopping parameter along the third bond (t_2) increase. This obviously

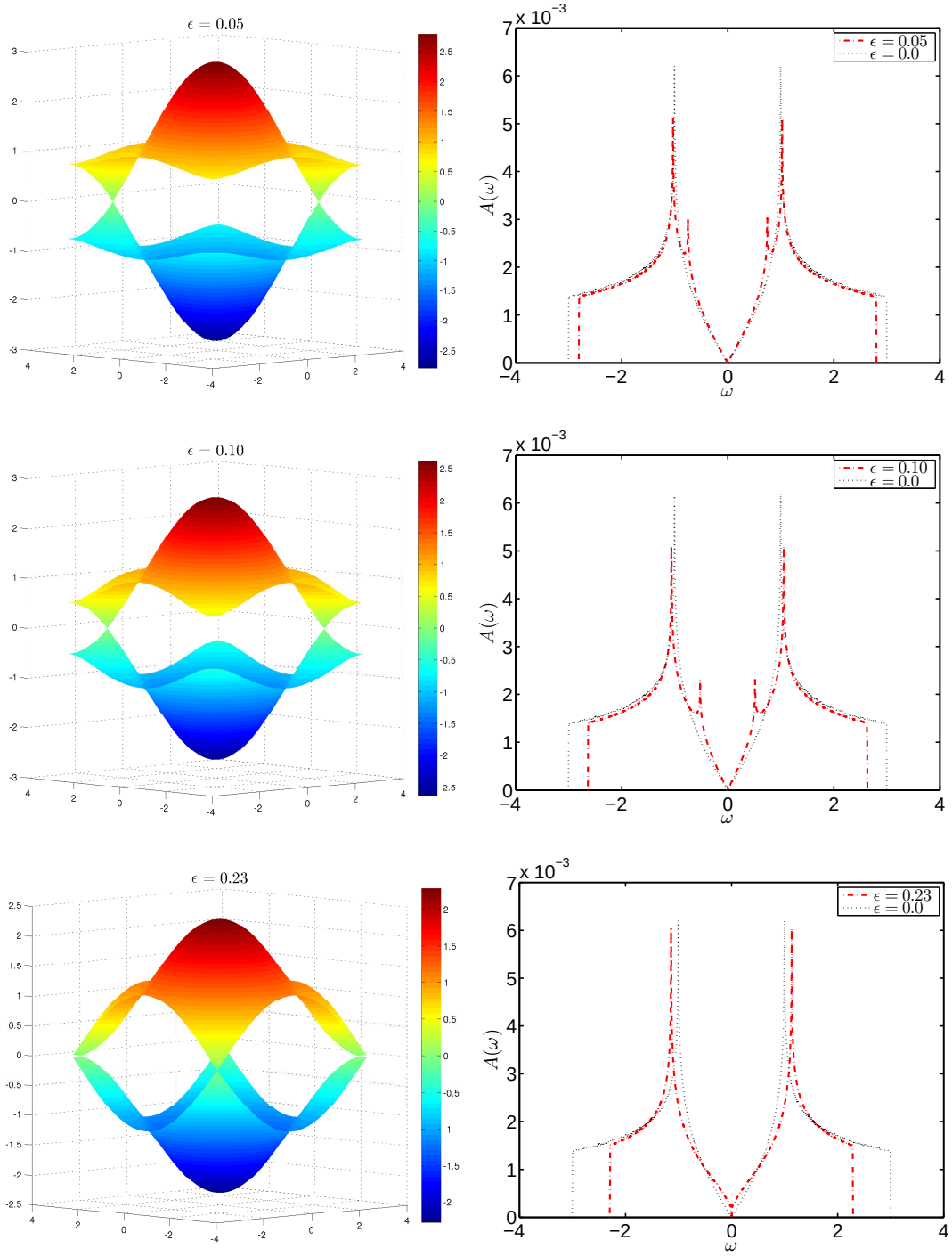

Figure 3.2: Band structure and DOS for for the tight-binding Hamiltonian on the honeycomb lattice for various values of ϵ along the zigzag direction. The DOS for the undistorted case is shown in black dotted lines.

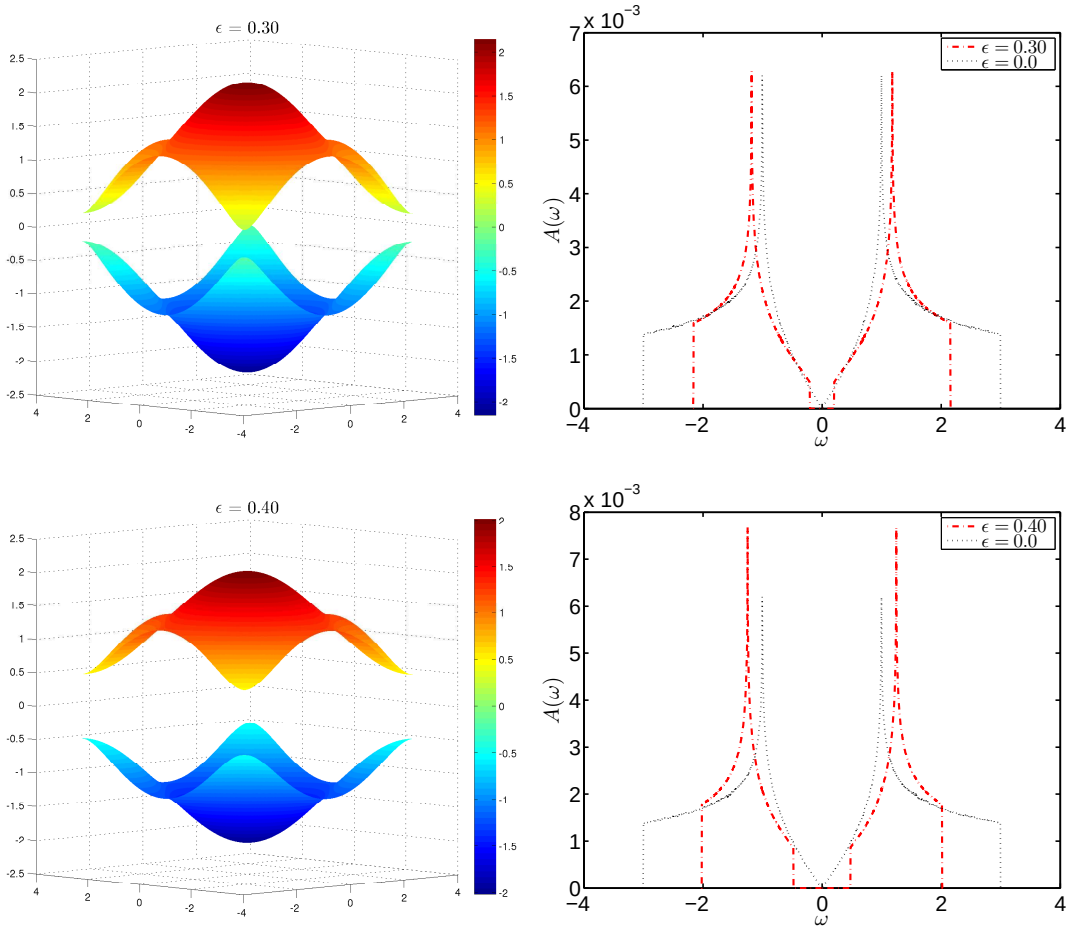

Figure 3.3: Band structure and DOS for for the tight-binding Hamiltonian on the honeycomb lattice for various values of ϵ along the zigzag direction. The DOS for the undistorted case is shown in black dotted lines. The strain is greater than critical strain and the gaps formed are clearly visible from both the bandstructure and DOS plots.

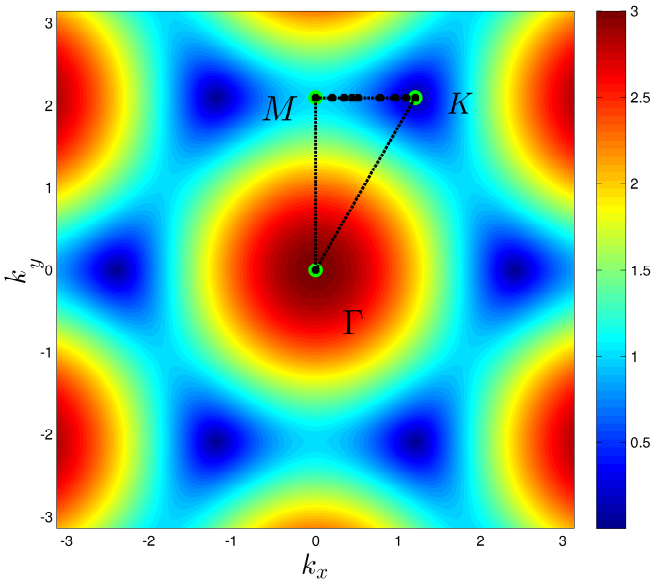

Figure 3.4: The background plot is a contour plot of the energy values of the conduction band for the 'unstrained' case, $\epsilon = 0.0$. The movement of the Dirac point along the direction from K point to M point is shown for some values of strain.

reflects as a change in the dispersion relation and the energy values. In our work, as mentioned previously, we assume the reciprocal lattice is the same as that of the undistorted honeycomb lattice. But, the information regarding the change in bond lengths is taken into account. For a particular value of strain, we find the changed hopping parameters, then evaluate the noninteracting Green function and susceptibilities using these values. These quantities then form the starting point of our TPSC calculations. The rest of the computations proceed as stated previously. For a particular value of interaction U, the double occupancy ($\langle n_\uparrow n_\downarrow \rangle$), is obtained self-consistently. The spin and charge vertices (U_{sp} and U_{ch}) can then be evaluated. The self-energy which includes the effects of these spin and charge fluctuations can be evaluated (detailed derivation given in Appendix B). The second approximation to self-energy including the effects of spin and charge fluctuations can be made as

$$\Sigma_\sigma(k) = U n_{\rho,-\sigma} + \frac{U}{4}\frac{T}{N^2}\sum G^{aa}_\sigma(k+q)\left[U_{sp}\chi^{aaaa}_{sp}(q) + U_{ch}\chi^{aaaa}_{ch}(q)\right] \tag{3.19}$$

3.3 Results

First of all, let us compare the results at two temperatures ($T = 0.1$ and $T = 0.01$). The following figure 3.5 shows plots of double occupancy, $\langle n_\uparrow n_\downarrow \rangle$), irreducible vertices (U_{sp} and U_{ch}) and antiferromagnetic correlation length (given by (2.65)) as functions of strain ϵ for various values of interaction shown in the legends. As expected, antiferromagnetic fluctuations grow in magnitude when the temperature decreases and the interaction increases (the interaction values are given in terms of the isotropic hopping parameter for the unstrained lattice). In addition to this, close to critical strain, $\epsilon \approx 0.235$, we see a discontinuity in the double occupancy and irreducible vertices. Also, the correlation length steadily goes down as the strain crosses the critical strain.

We take a look at the self energy computed using TPSC, for values of strain less than critical strain (3.6). The interaction values implemented vary till $U \sim 3.5$. For the zero strain case, or when the strain is very small ($\epsilon = 0.05$), for small values of U, the Dirac Landau Fermi liquid (LFL) is stable as can be seen from the behavior of self-energy when $\omega_n \to 0$. For $0.1 < \epsilon < 0.23$, when $U < U_c(\epsilon)$ we have a correlated Dirac LFL with Im $\Sigma(\omega_n) = A(\epsilon)\omega_n$. But, once the interaction value goes beyond this strain dependent critical value, the imaginary part of self energy increases as $\omega_n \to 0$. This points to the appearance of a pseudogap in the single-particle density of states.

Fig. 3.7 shows Im Σ for $\epsilon = 0.23$ at $\beta = 100$, the inset shows a plot of $A(\epsilon)$ as a function of ϵ. It can be clearly seen from the inset that the quantity $A(\epsilon)$ develops an anomaly around $U_c/t \approx 3.5$.

Electronic nematic order occurs when the rotational symmetry of the lattice is spontaneously broken. In our problem, the presence of strain destroys the rotational symmetry. So the presence of strain rules out electronic nematic criticality. However, in order to study the feedback effects of strong antiferromagnetic fluctuations on the anisotropic electronic structure resulting from the application of strain, we can compute the quantity, $\mathcal{N} = \frac{\langle (T_{xx} - T_{zz}) \rangle}{\langle (T_{xx} + T_{zz}) \rangle}$. The average kinetic energies along the x- bonds (shown in Fig. 3.1), T_{xx} and the z- bonds, T_{zz} can be evaluated from the interacting Green function. The definition is, $T_{\mu\mu} = \langle b^\dagger_{i,\sigma} a_{i+\mu,\sigma} \rangle$, ($\mu = x, z$). This can be calculated using $G^{ab}(\boldsymbol{r}, \tau)$, for $\mu = z$, we need to evaluate $G^{ab}(\boldsymbol{r} = \boldsymbol{0}, \tau = 0^-)$ and for $\mu = x$ we need $G^{ab}(\boldsymbol{r} = \boldsymbol{a}_1, \tau = 0^-)$. Fig. 3.8 shows the variation of $\mathcal{N}$ with respect to strain for various values of interaction at $\beta = 100$. The upper inset shows the quantity when there is no Hubbard U. For smaller values of strain, this quantity is almost independent of the value of interaction. For $U/t \geq 3.5$, as strain increasingly approaches critical strain, there is a slight enhance-

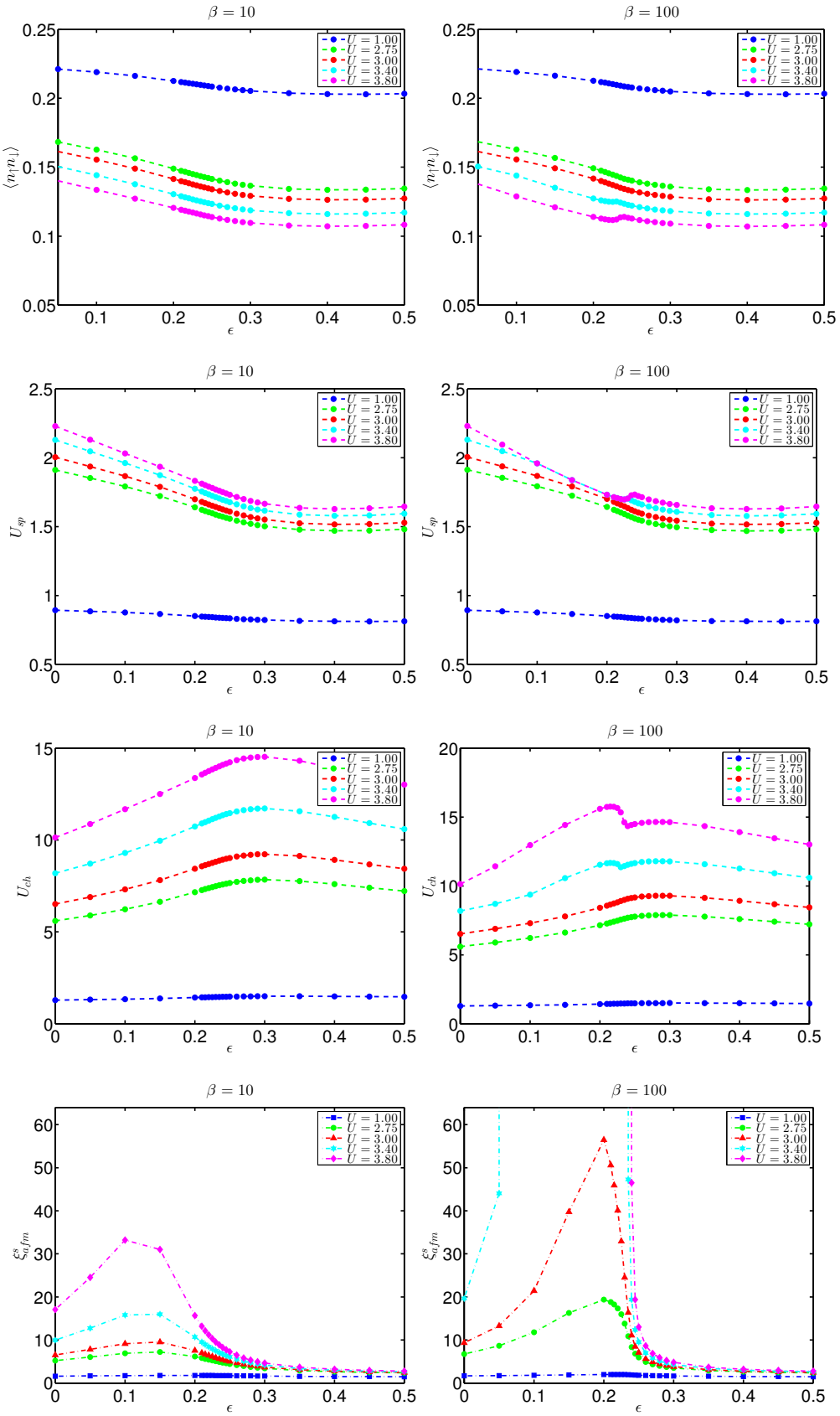

Figure 3.5: Plots of double occupancy ($\langle n_\uparrow n_\downarrow \rangle$) , irreducible vertices (U_{sp}, U_{ch}) and antiferromagnetic correlation length ξ^s_{afm} as functions of strain ϵ at $\beta = 10$ and $\beta = 100$. Interaction values (U) are indicated in the legend.

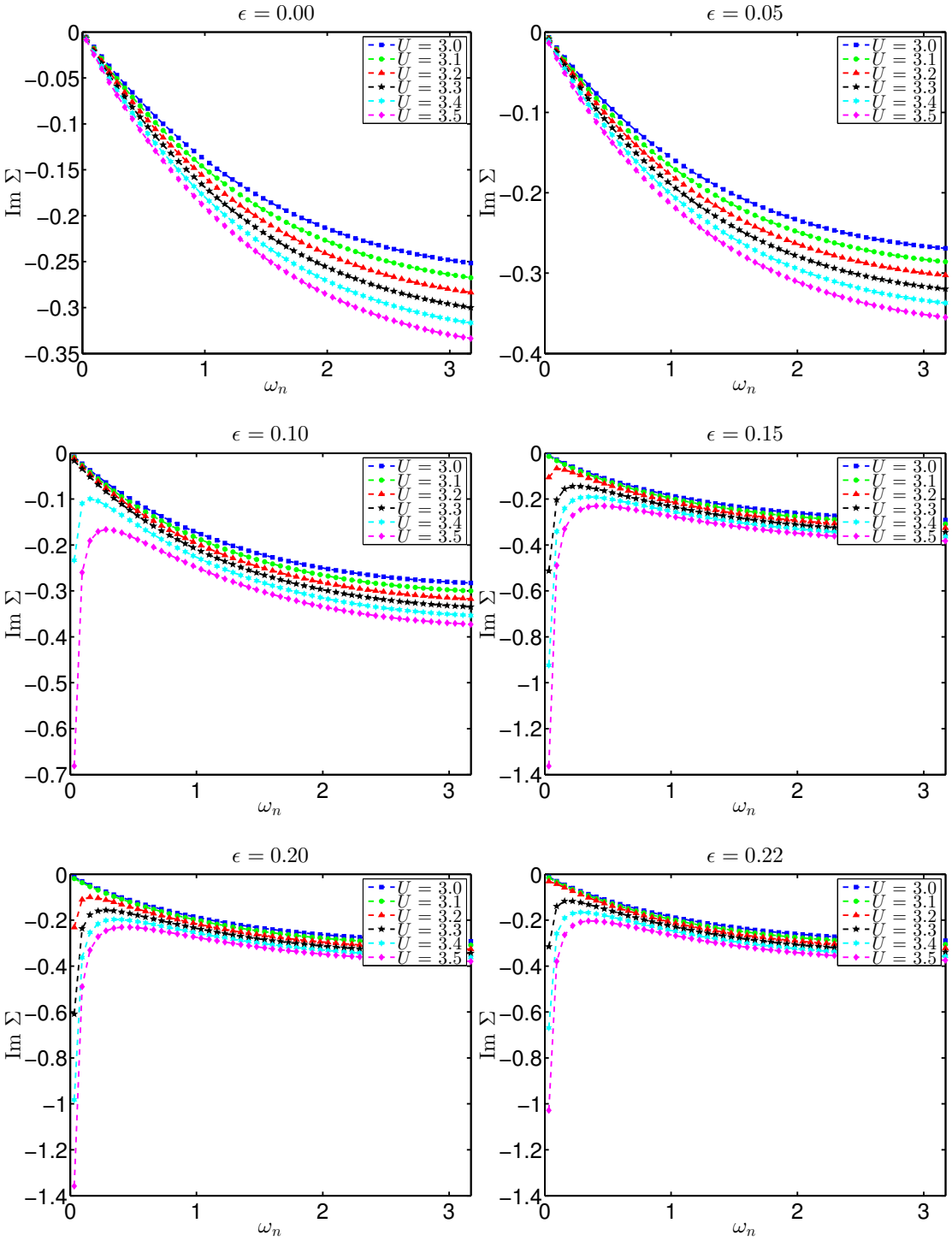

Figure 3.6: Imaginary part of the self energy Σ plotted as a function of Matsubara frequency ω_n, for various values of strain $0.0 \leq \epsilon < 0.23$ for $\beta = 100$. The legend indicates the values of interaction U.

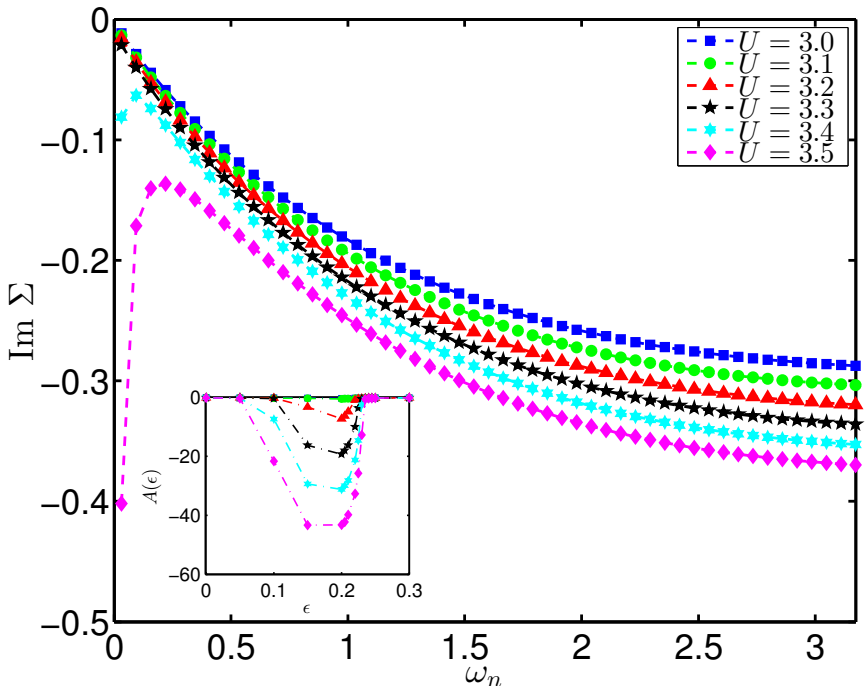

Figure 3.7: Imaginary part of the self-energy Σ as a function of Matsubara frequency ω_n, for $\epsilon = 0.23$. The inset shows how the $A(\epsilon)$ co-efficient of -Im$\Sigma(\omega_n)$ develops clear anomaly around $U/t = 3.4$.

ment in this parameter. This results from a feedback of the growing antiferromagnetic fluctuations. From the lower inset we can see that, the nematic susceptibility $\chi_N = \frac{d\mathcal{N}}{d\epsilon}$ shows singular behavior near $U_c(\epsilon)$. Thus we see that a nematic quantum criticality exists in the system, driven by the large antiferromagnetic fluctuations near the critical interaction strength

This criticality can be observed by studying the magneto-volume and the thermal expansion coefficient. A magneto-elastic interaction occurs because of the coupling of antiferromagnetic fluctuations to strain. The spin fluctuation contribution to the magneto-volume is defined as $\Omega_m(T) = \frac{\delta V(T)}{V}$, and the thermal expansion coefficient is defined as its derivative, $\alpha_m(T) = \frac{\partial \Omega_m}{\partial T}$. From Moriya - Usami theory [57] the magneto-volume is given by $\Omega_m = (D_0/B)\langle S_z^2 \rangle$ where D_0 is related to the strain dependence of bandwidth ($D_0 = \partial ln(W)/\partial \epsilon$) and is negative and of the order of 1, and B is the bulk modulus (for graphene, it is $200 Nm^{-1}$).

$\langle S_z^2 \rangle$ can be evaluated from the spin sum rule connecting it to double occupancy, (2.25). The plots of $\langle S_z^2 \rangle$ and those of $\frac{d\langle S_z^2 \rangle}{dT}$ are given in Figs. 3.9 and 3.10 respectively. These quantities are plotted as functions of temperature

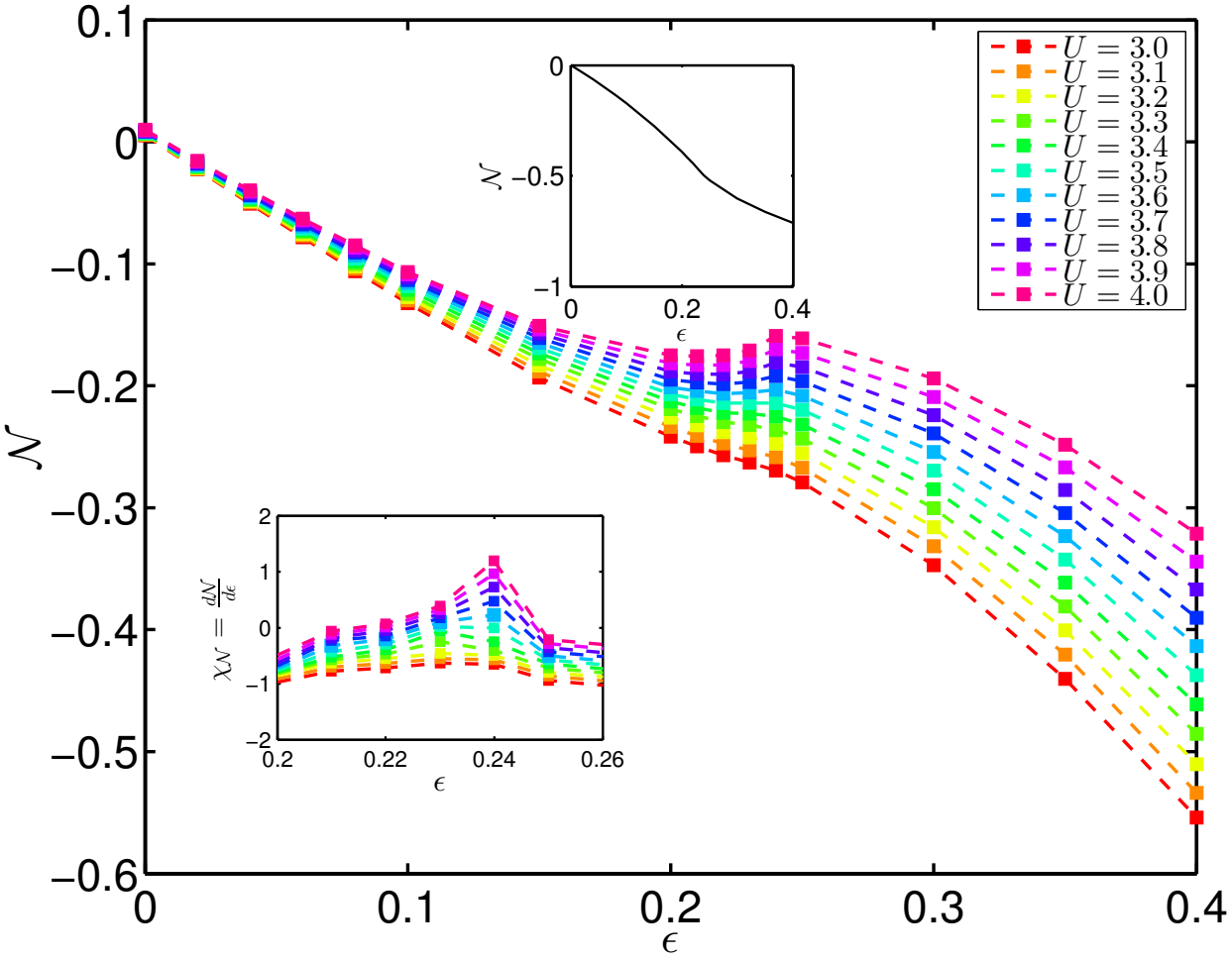

Figure 3.8: $\mathcal{N} = \frac{\langle (T_{xx} - T_{zz}) \rangle}{\langle (T_{xx} + T_{zz}) \rangle}$, plotted as a function of strain ϵ for given values of interaction. The upper inset shows $\mathcal{N}$ for $U = 0$. The lower inset shows the nematic susceptibility, $\chi_N = \frac{d\mathcal{N}}{d\epsilon}$, which shows singular behavior around critical strain due to interplay between anisotropic band structure and critical AFSF.

From these plots, we can see that, there will be a sizable contribution from magnetic fluctuations to the magneto-volume and thermal expansion coefficient at small strains, but this vanishes as $T \to 0$. For $\epsilon = 0.2$, we plot Ω_m and α_m in Fig. 3.11 as functions of temperature. We can see that as strain increases, beyond the strain dependent critical interaction, these quantities show a divergence.

By looking at the derivative of $\langle S_z^2 \rangle$ with respect to strain ϵ, ($\frac{d\langle S_z^2 \rangle}{d\epsilon}$), as a function of strain, we can further substantiate the quantum criticality associated with large antiferromagnetic fluctuations close to critical strain. In Fig. 3.12, the plot shows singular behavior close to critical strain when the interaction is more than the critical interaction strength. Since the magnetic Grüneisen coefficient is defined as $\Gamma_m(T) = \alpha_m(T)/C_{el}(T)$ where $C_{el}(T)$ is the electronic specific heat, we anticipate a divergence in $\Gamma_m(T)$ also. $C_{el}(T) \approx T^2$ up to logarithmic corrections in two dimensions, if this is valid as we approach critical values of strain and interaction, then , as $T \to 0$, the magnetic Grüneisen parameter will also show a critical divergence.

3.3.1 Scenario beyond critical strain

The features of quantum criticality vanish beyond critical strain. For values of strain beyond the critical strain $\epsilon \geq 0.24$, the system becomes a band insulator. Even at low temperatures with growing values of interaction, the antiferromagnetic fluctuations do not become huge as seen previously in Fig. 3.5. These corroborate the statement that the features of quantum criticality are influenced by the growing antiferromagnetic fluctuations in the system. Since the antiferromagnetic fluctuations do not become huge, we do not expect the self energy to show any anomalous feature as $\omega_n \to 0$. This can be seen clearly from Fig. 3.13 where we have plotted imaginary part of the self-energy as a function of the fermionic Matsubara frequency, for values of strain beyond the critical strain. The plots of $\langle S_z^2 \rangle$ in Fig. 3.14 and the derivative of $\frac{d\langle S_z^2 \rangle}{dT}$ in Fig. 3.15 also give us the same information. From the plots of Fig. 3.14, we can see that $\langle S_z^2 \rangle$ is almost temperature independent, for the same values of interaction at which we see large antiferromagnetic fluctuations in the system below critical strain. And, $\frac{d\langle S_z^2 \rangle}{dT}$ does not diverge as $T \to 0$, and is almost independent of the value of interaction.

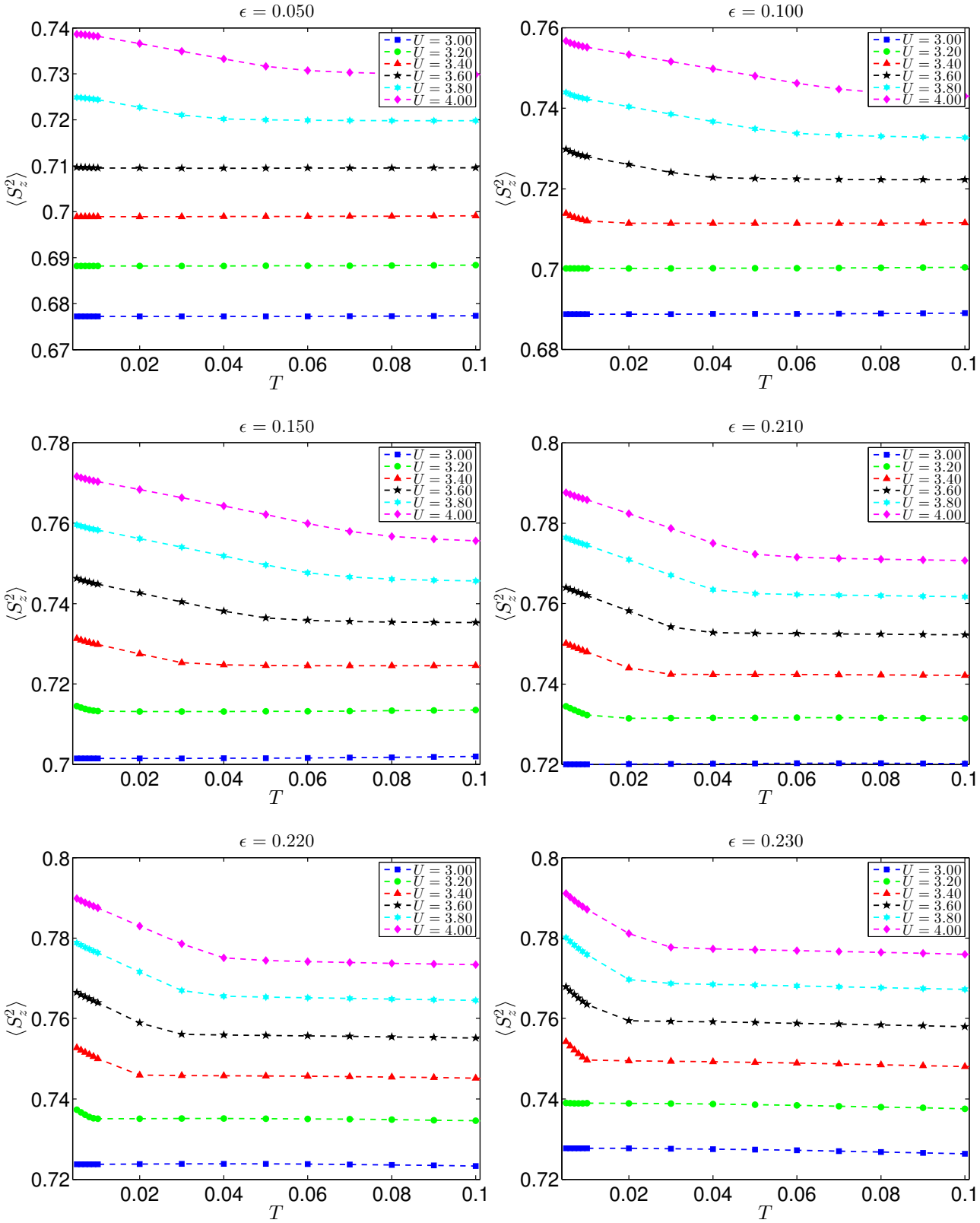

Figure 3.9: Plots of $\langle S_z^2 \rangle = 1 - 2\langle n_\uparrow n_\downarrow \rangle$ as a function of temperature T, for various values of strain ϵ below the critical strain. The legends indicate the values of interaction U.

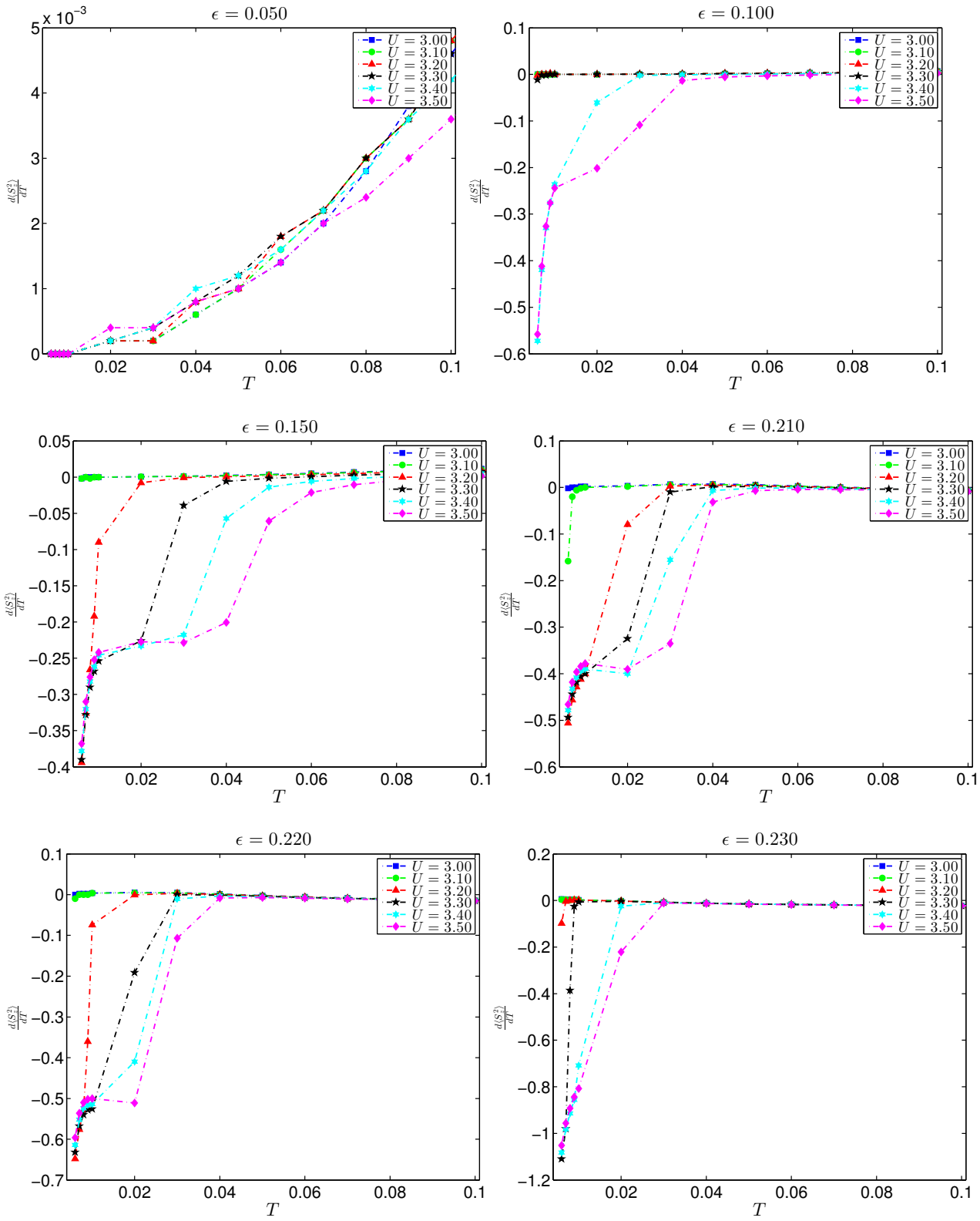

Figure 3.10: Plots of $\frac{d\langle S_z^2\rangle}{dT}$ as a function of temperature T, for various values of strain ϵ below the critical strain. The legend indicates the values of interaction U.

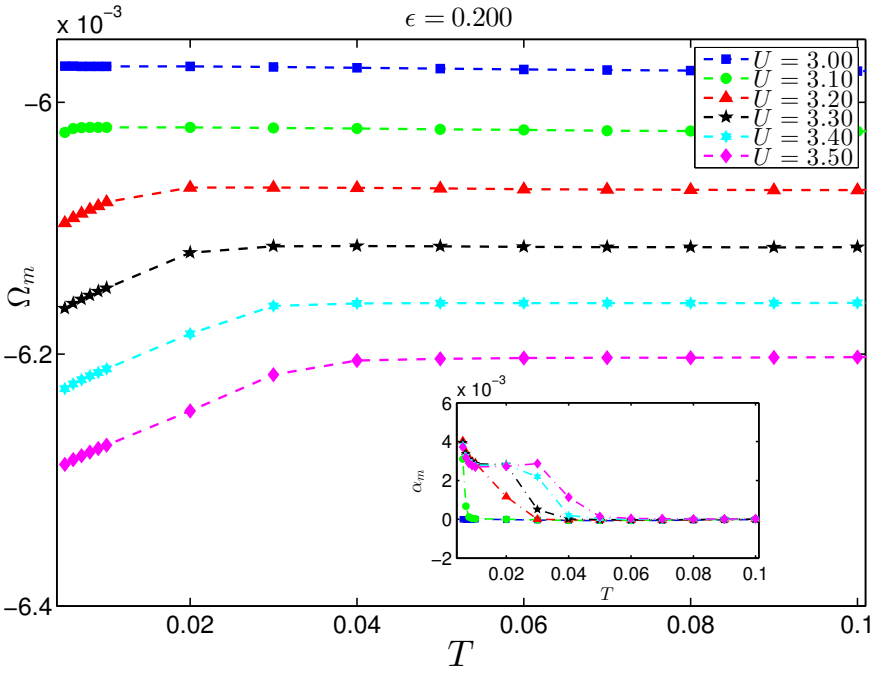

Figure 3.11: Magneto-volume, Ω_m as a function of temperature T. The inset shows a plot of thermal expansion co-efficient, α_m as a function of T, showing how it diverges as $T \rightarrow 0$ due to coupling of strin to critical AFSF for $U \geq 3.2$ near critical strain ($\epsilon = 0.20$).

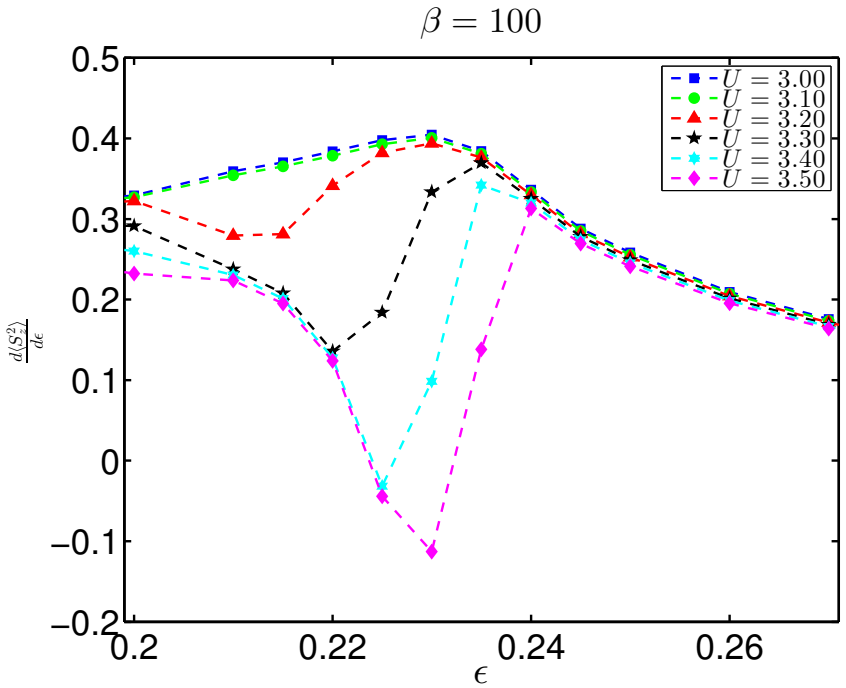

Figure 3.12: Plot of $\frac{d\langle S_z^2\rangle}{d\epsilon}$ as a function of strain ϵ, for $\beta = 100$. The values of interaction U are given in the legend.

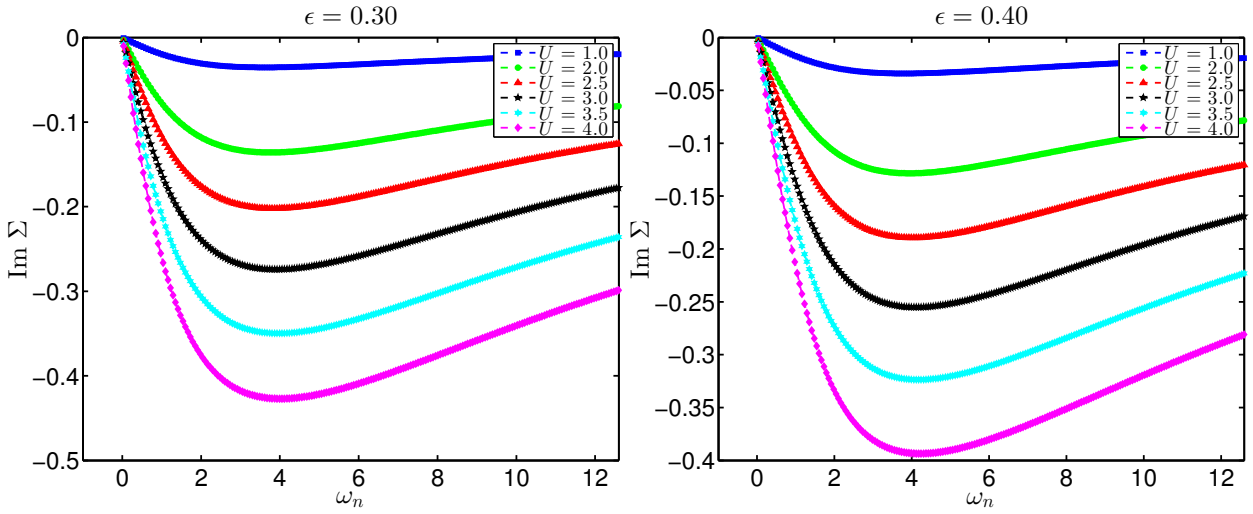

Figure 3.13: Imaginary part of the self energy Σ plotted as a function of Matsubara frequency ω_n, for various values of strain ϵ greater than critical strain for $\beta = 100$. The values of interaction U are shown in the legend.

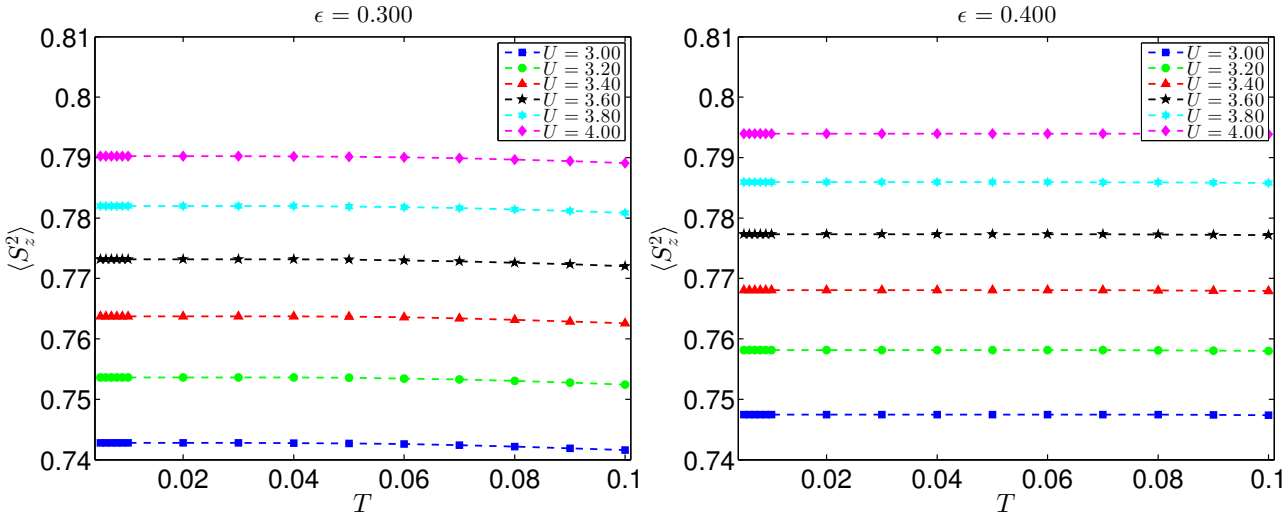

Figure 3.14: Plots of $\langle S_z^2 \rangle = 1 - 2\langle n_\uparrow n_\downarrow \rangle$ as a function of temperature T, for various values of strain ϵ greater than the critical strain. The legend indicates the values of interaction U.

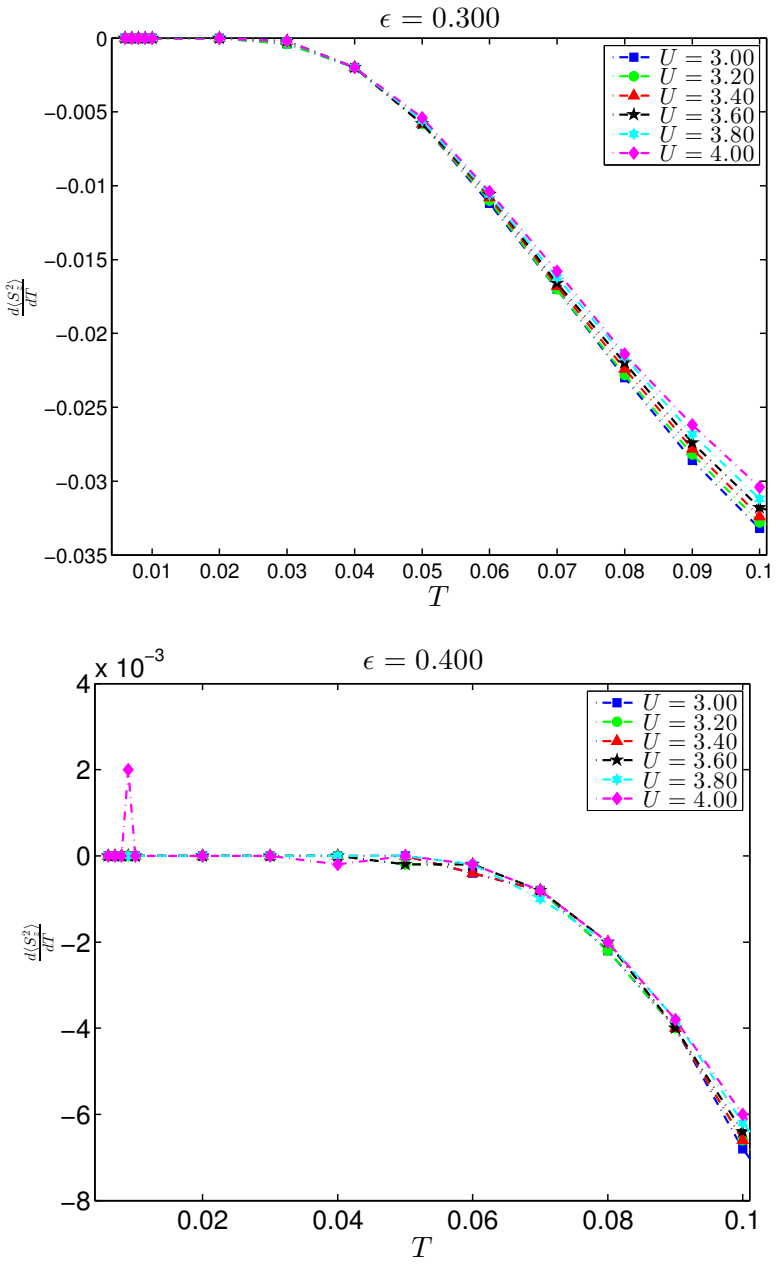

Figure 3.15: Plots of $\frac{d\langle S_z^2\rangle}{dT}$ as a function of temperature T, for various values of strain ϵ greater than the critical strain. The legend indicates the values of interaction U.

3.4 Summary

The formalism of TPSC which was generalized previously to study the multi-band case of graphene was implemented to study the Hubbard model on the honeycomb lattice under uniaxial strain. Focusing on the case where strain is applied along the zigzag direction, taking into account only the change in the hopping parameters, the method was executed. As usual, the double occupancy, the irreducible vertices and the antiferromagnetic correlation length were computed. The self-energy containing the effects of spin and charge fluctuations was also evaluated.

For small values of strain, for $0 < U/t < 3.5$, the Dirac Landau Fermi liquid is stable. For $0.1 < \epsilon < 0.23$, although at low values of interaction we have a Landau Fermi liquid, as interaction exceeds a strain-dependent critical interaction strength, a pseudogap develops in the single-particle density of states. All these are clearly seen from the imaginary part of self-energy. The growing antiferromagnetic fluctuations, with decreasing temperature and increasing interaction causes this pseudogap.

Further, close to critical strain, the electronic nematic order parameter (defined in terms of the kinetic energies along the bonds) is seen to be enhanced by the influence of strong antiferromagnetic fluctuations. The nematic susceptibility shows a divergence near the critical interaction strength. Thus the transition from Dirac metal to an incoherent metal near critical strain, is connected to the nematic quantum criticality driven by large antiferromagnetic fluctuations.

In order to observe this quantum criticality, the magneto-volume and the thermal expansion and magnetic Grüneisen parameters can be studied. Using the value of double occupancy obtained from TPSC, the spin fluctuation in the system is studied. Close to zero temperature, antiferromagnetic fluctuations enhance the spin fluctuation contribution to the magneto-volume. The divergence of the thermal expansion coefficient near zero temperature substantiates this quantum criticality. By taking a look at the derivative of the spin fluctuation with respect to strain, this quantum criticality can be confirmed by the singular behavior close to critical strain. Once the applied strain opens up a gap the antiferromagnetic fluctuations never grow large. Therefore, when strain is greater than critical strain, all these features of quantum criticality vanish.

Chapter 4

Pairing in the single-band Hubbard model with extended hopping

4.1 Introduction

The most repeated lore in condensed matter physics might be that of high-temperature superconductivity, and three decades have passed since the discovery of the phenomenon in hole-doped cuprates [58] in the 1980's. The discovery of high-temperature superconductivity in electron-doped cuprates followed soon [59, 60]. As far as cuprates are concerned, the single-band Hubbard model on the square lattice is said to be the basic model which captures the relevant physics of the CuO planes [31]. Starting from an antiferromagnetic Mott insulator at half-filling, the system is doped away from this half-filled state. Antiferromagnetism is destroyed and superconductivity emerges in the system.

One of the important puzzles is the asymmetry in the phase diagram for hole-doped and electron-doped systems. Antiferromagnetism seems to be more prominent on the electron-doped side compared to the hole-doped side. The hole-doped systems are said to lie in the strongly coupled region and superexchange mediates the pairing. In contrast to this, the electron-doped materials are supposed to lie in the weak to intermediate region of coupling [21, 61]. The pairing glue is made up of antiferromagnetic fluctuations. Such a pairing mediated by growing antiferromagnetic fluctuations near an instability had been discussed earlier in the context of heavy-fermion compounds and organic superconductors [62–65].

While modeling cuprates, in addition to nearest neighbor hopping, extended hopping t' and t'' to the second nearest and third nearest neighbors is deemed essential to explain the results from bandstructure calculations and many experiments like ARPES [61, 66–

71]. A multitude of techniques have been applied to the study of the single-band Hubbard model - theories based on the idea of pairing mediated by magnetic fluctuations [72–76], renormalization group methods [77–80], quantum cluster approaches [61, 81–86], Monte Carlo studies [87–89], density matrix embedding theory (DMET) [90] to name a few, to better understand superconductivity in the system.

The incorporation of additional hopping might explain the observed asymmetry in the phase diagram [91]. In fact, extended hopping seems to stabilize antiferromagnetism on the electron-doped side [92–96]. Various numerical methods - variational Monte Carlo methods[96], Cellular Dynamical Mean Field theory(CDMFT) [86], Variational Cluster Perturbation Theory (VCPT)[81] - have been applied to this problem which bring out the asymmetry in the phase diagram and emphasize antiferromagnetism on the electron-doped side.

Since electron-doped cuprates lie in the region of weak to intermediate interaction, the problem is amenable to study by TPSC. TPSC has already been successfully implemented in computing the pairing mediated by antiferromagnetic fluctuations in the single-band Hubbard model. The results for pairing susceptibility χ_d from TPSC agree well with those from QMC calculations. The study by Kyung *et al.* [21] done on the single-band Hubbard model on the square lattice with only nearest neighbor hopping t, concludes that antiferromagnetic fluctuations aid pairing in the system. But, when the fluctuations are very large, the pseudogap which opens up is detrimental to pairing. The plot for the superconducting transition temperature T_c as a function of doping is dome-shaped. As we increase U, the value of the estimated T_c increases. This sheds light on the negative pressure derivative observed in electron-doped high T_c superconductors. This further cements the idea that these are weakly coupled in contrast to their hole-doped counterparts which lie in the strongly coupled regime. A subsequent study by Kyung and coworkers [22] apply TPSC to the t-t'-t''-U Hubbard model, and obtain results which are in excellent agreement with experimental results. The reduced spectral weight at the hotspots observed in ARPES experiments are attributed to the growing antiferromagnetic fluctuations. Antiferromagnetic correlation length results obtained from neutron scattering also agree quite well with results from TPSC. Later, the effect of the variation in t' on the nature of magnetic fluctuations and the resultant pairing at half-filling were studied by Hassan *et al* [23]. The doping dependence of the transition temperature T_c in this study for a) $d_{x^2-y^2}$ pairing at low values of frustration mediated by commensurate fluctuations and b) d_{xy} pairing mediated by fluctuations near $(0, \pi)$ had a dome-shape. Thus the variation in frustration at half-filling acts like a change in doping.

Recently Ogura and colleagues [97], using TPSC, studied the doping dependence of T_c for both types of doping. The formalism used in this work is not entirely similar to that used previously - in this work the eigenvalue of the linearized Eliashberg equation is used as a measure of T_c. Their motivation was to shed light on the experimental results where T_c on the hole-doped side was dome-shaped, while on the electron-doped side it showed monotonic variation. Despite using realistic band structure parameters, according to them a single-band Hubbard model is insufficient to bring out this contrast. The results are claimed to match those from experiments, when a three-band model is used to depict the system.

4.2 Pairing susceptibility in TPSC

Using TPSC, so far, we have looked at correlations in the particle-hole channel. The formalism can be extended to study pairing mediated by antiferromagnetic fluctuations. We already know how the self-energy can be written in an improved approximation by incorporating the effects of spin and charge fluctuations. By introducing a source field in the particle-particle channel, two-particle correlations in the particle-particle channel - the so-called pairing channel - can be looked at.

We start from the most general generating function with source fields of particle-hole fluctuations, as well as pairing fluctuations. The first step is the computation of spin and charge susceptibilities. These two-particle correlation functions have the same form as before. In the second step, we can express the self-energy by including the effects of the spin and charge fluctuations calculated in the first step. The expression for pairing susceptibility is [21–23],

$$\begin{aligned}\chi_d(\boldsymbol{q}=\mathbf{0}, i\nu_n=0) = &\frac{1}{\beta N^2}\sum_k g_d^2(\boldsymbol{k}) G_\uparrow^{(2)}(-k) G_\downarrow^{(2)}(k) \\ &- \frac{U}{4}\left(\frac{1}{\beta N^2}\right)^2 \sum_{k,k'} g_d(\boldsymbol{k})\, G_\uparrow^{(2)}(-k)\, G_\downarrow^{(2)}(k) \\ &\times \left(\frac{3}{1-\frac{U_{sp}}{2}\chi_0(k-k')} + \frac{1}{1+\frac{U_{ch}}{2}\chi_0(k-k')}\right) \\ &\times g_d(\boldsymbol{k'})\, G_\uparrow^{(1)}(-k')\, G_\downarrow^{(1)}(k') \end{aligned} \tag{4.1}$$

Here, k (k') indicates both the momentum and fermionic Matsubara frequency. g_d is the form factor for d-wave pairing and we take it to be that corresponding to $d_{x^2-y^2}$ symmetry.

Therefore $g_d(\boldsymbol{k}) = \cos(k_x) - \cos(k_y)$. $G^{(2)}(k)$ is the interacting Green function, and $G^{(1)}(k)$ is the noninteracting Green function.

We can see that the pairing susceptibility contains two terms. The first term is the eponymous direct term which gives the direct pairing between two particles. The Green function in the first term is the interacting Green function, including the self-energy effects of spin and charge fluctuations. Therefore, as the fluctuations grow in magnitude, the lifetime of the particles decreases, and the contribution from this term decreases.

Meanwhile, the second term is the pairing mediated by some kind of vertex. The vertex, as we can see, is in terms of spin and charge susceptibilities and hence mediates the pairing via the exchange of particle-hole fluctuations. The increase in the magnitude of antiferromagnetic fluctuations results in an increased contribution of this term to the overall pairing.

4.3 Results

4.3.1 Commensurate and incommensurate fluctuations

Let us start with some results obtained directly from the noninteracting (spin) susceptibility $\chi_0(q)$. The position of the maximum of the noninteracting susceptibility at zero frequency, tells us whether the fluctuations are commensurate or incommensurate in nature. If the peak lies at the momentum vector (π, π), the fluctuations are commensurate and are antiferromagnetic in nature. As the fluctuations become incommensurate, the peak position shifts from (π, π), and the peak gets split into more than one. The transition temperature T_i from commensurate to incommensurate fluctuations, for various values of filling on both sides of half-filling is studied for different values t' and t'' (t is taken as unity).

The transition temperature can be determined by looking at the microscopic length ξ_0 associated with the noninteracting susceptibility given by,

$$\xi_0^2 = -\frac{1}{2\chi_0^{max}} \left. \frac{\partial^2 \chi_0(\boldsymbol{q}, i\nu_n)}{\partial q_x^2} \right|_{(\boldsymbol{q}=\boldsymbol{Q}_{max}, i\nu_n=0)} \tag{4.2}$$

In order to find T_i for a particular value of filling (n), we calculate ξ_0 at (π, π) and scan the entire temperature grid for a change in the sign of this quantity. The temperature at which the sign change occurs is picked as $T_i(n)$. Fig. 4.1 shows the curves of T_i as a

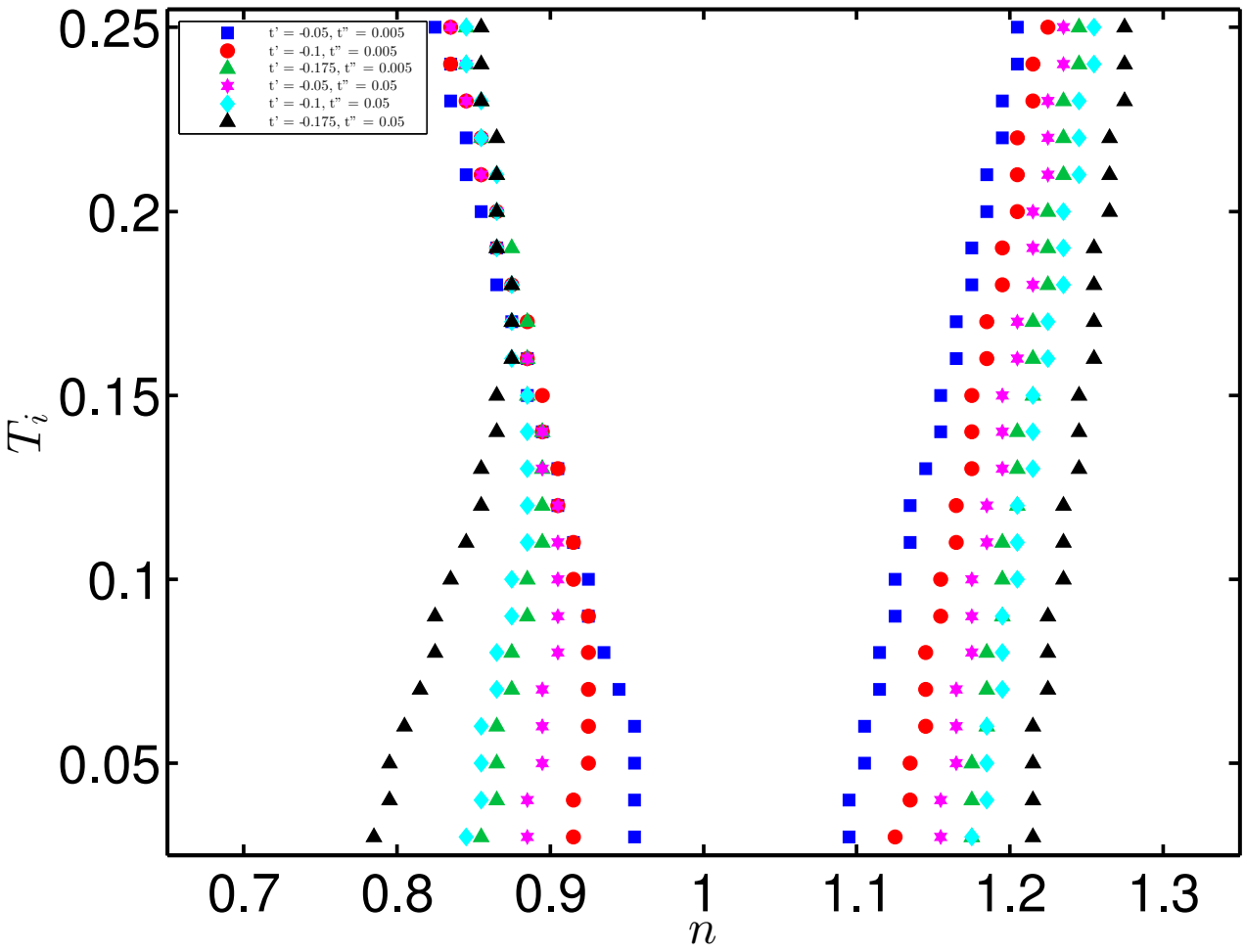

Figure 4.1: Comparison of the plots of T_i as a function of filling n, for given values of t' and t''.

function of filling n for various values of t' and t''. The area around half-filling bounded by the T_i curves is the area of parameter space with commensurate fluctuations. From the plots, it is clear that the area of commensurate fluctuations increases with an increase in the magnitude of t' and t''. That means, antiferromagnetism is stabilized as a result of extended hopping.

This result can be checked from a plot of the noninteracting Fermi Surface(FS) for various values of filling also. If the FS intersects with the antiferromagnetic Brillouin zone(AFMBZ), the peak of the susceptibility lies at (π, π). Fig. 4.2 shows the plots for FS at $T = \frac{1}{64}$ for $t' = -0.175$ and $t'' = 0.05$. The FS intersects the AFMBZ for all values of filling studied $1.0 \leq n \leq 1.2$. These values of t' and t'' are used further in our calculations.

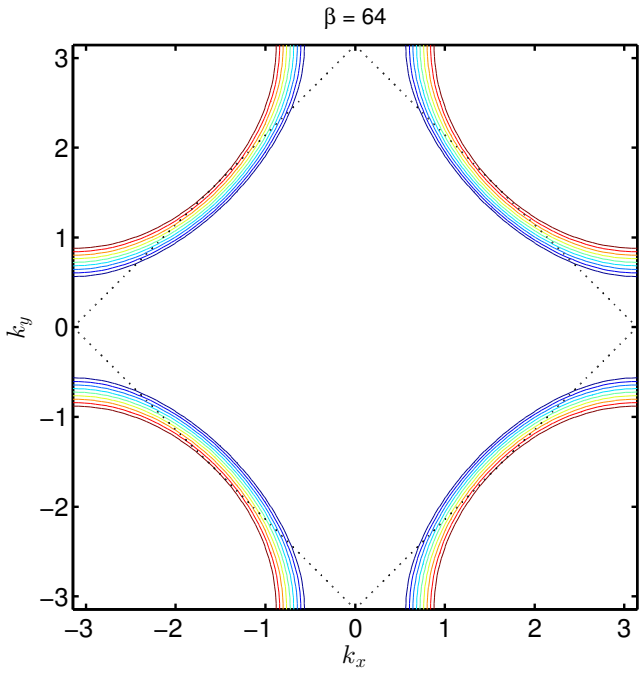

Figure 4.2: Non-interacting Fermi surfaces for $1.0 \leq n \leq 1.2$. $t' = -0.175$ and $t'' = 0.05$, $T = 1/64$. The antiferromagnetic Brillouin zone is shown in black dotted lines.

4.3.2 Antiferromagnetic correlation length and crossover to the renormalized classical regime

The hopping parameters are set to $t = 1.0$, $t' = -0.175$ and $t'' = 0.05$, and we look at values of filling $1.0 \leq n \leq 1.2$. The lattice size chosen is 256×256. The number of Matsubara frequencies we include in numerical calculations has to be set at a high value so that this cutoff does not affect our results. As the temperature is lowered, we are forced to access more number of frequencies. This calls for imaginary frequency grids with more number of points, therefore calculations at lower temperature require more computational resources. RG acceleration is implemented to deal with this crunch [21, 98].

RG is implemented on the imaginary frequency axis. Suppose we have a sequence of temperatures, $T_1 > T_2 > T_3 > \ldots$, and let $Q_1 \leq Q_2 \leq Q_3 \leq \ldots$ be the corresponding frequency cutoff. We have $Q_i = 2\pi T_i N_q(T_i)$ and $Q_{i-1} = 2\pi T_i M_q(T_i)$. From these conditions, we can see that $M_q(T_i) \leq N_q(T_i)$. In order to preserve the length of frequency axis, at every step the temperature has to be halved, and the cutoff also has to be halved. $\frac{T_i}{T_{i-1}} = \frac{1}{2}$ and $\frac{Q_i}{Q_{i-1}} = \frac{1}{2}$. The number $N_q(T_i)$ does not change at each step. Therefore, the computational time needed for each step remains roughly the same.

As the value of interaction increases and the temperature gets smaller, the antiferromagnetic fluctuations in the system grow rapidly. In order to see this, the antiferromagnetic correlation length ξ_{sp} plotted as a function of temperature. There can be various measures to quantify this correlation length. As the interaction increases, the irreducible spin vertex U_{sp} nearly reaches the mean field critical interaction strength U_{mf} to an instability, but never exceeds it. This idea is contained in the following in the definition

$$\xi_{sp} = \xi_0 \sqrt{\frac{U_{sp}}{\delta U}} \tag{4.3}$$

$$\delta U = U_{mf} - U_{sp} \tag{4.4}$$

$$U_{mf} = \frac{2}{\chi_0^{max}} \tag{4.5}$$

When δU becomes really small, the correlation length becomes really large.

Another measure of the correlation length is

$$\xi_{sp} = \sqrt{\frac{\chi_{sp}^{max}}{\chi_0^{max}}} \tag{4.6}$$

This comes from the scaling form of the spin susceptibility for the square lattice (reference). With the thermal de Broglie wavelength approximated as,

$$\xi_{th} \sim \frac{1}{T} \tag{4.7}$$

we can check when the antiferromagnetic correlation length exceeds ξ_{th}, and track down the crossover to the renormalized classical regime. In this regime, the characteristic spin fluctuation frequency is smaller than the temperature. This crossover is accompanied by a pseudogap in the single particle density of states [13, 14, 22]. Once in the renormalized classical regime, the results from TPSC are no longer valid. Fig. 4.3 shows the plots for the antiferromagnetic correlation length plotted alongside the thermal de Broglie wavelength for various values of filling. The value of interaction is $U = 6.55$.

The crossover is a finite temperature (T_X) signature of the zero temperature quantum phase transition. We can plot a crossover plot as a function of filling. By extrapolating the crossover plot to the zero temperature we can obtain the critical strength of filling n_c at which the quantum phase transition occurs. Beyond this quantum critical point, the system is not antiferromagnetic. It must be noted that for $U = 5.05$ and $U = 5.55$, two values of interaction we looked at, no crossover to the renormalized classical regime is

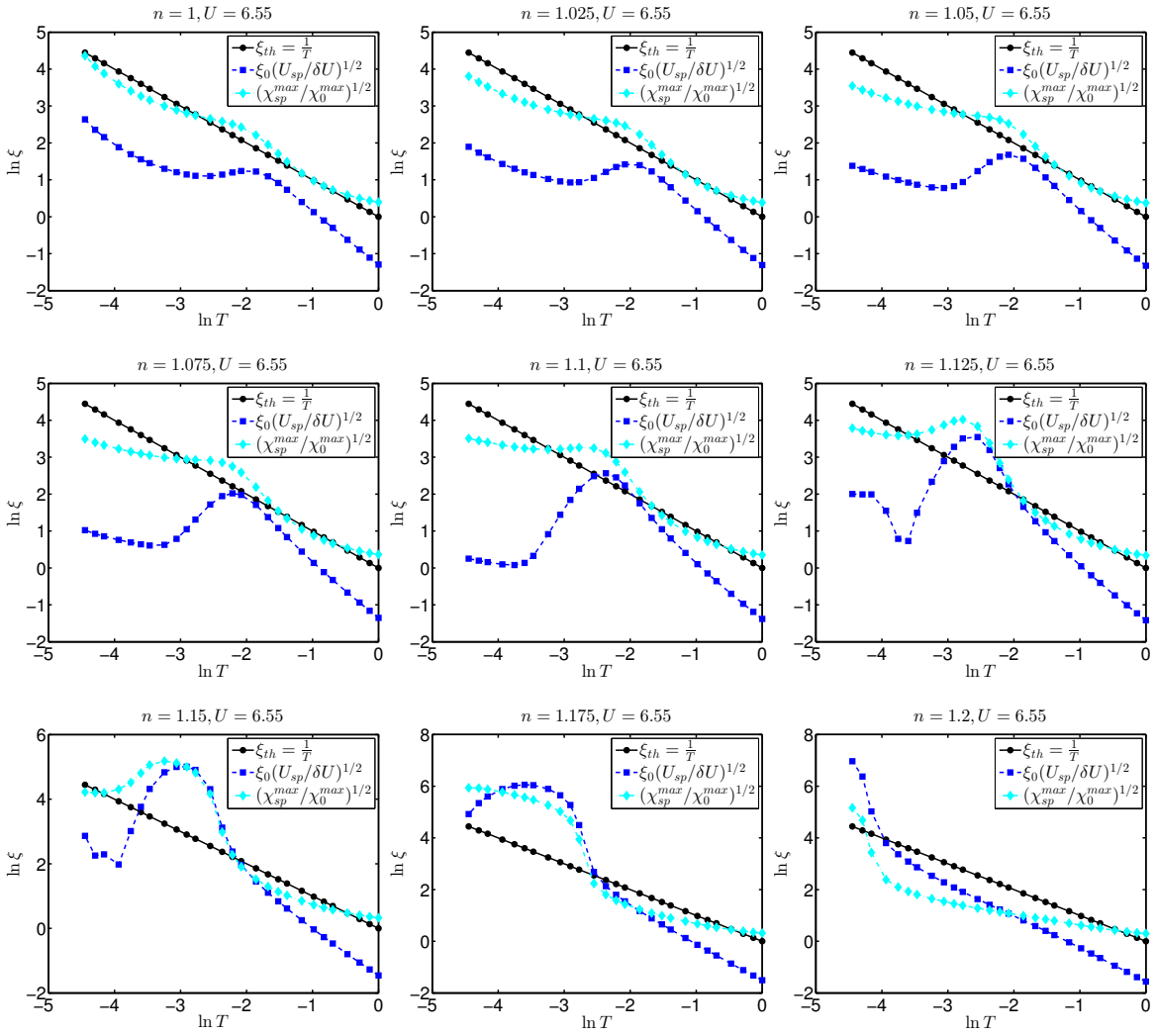

Figure 4.3: Plots of $\ln \xi$ as a function of $\ln T$ for various n, $U = 6.55$, $t' = -0.175$ and $t'' = 0.05$.

observed. The crossover plot for $U = 6.55$ is shown in Fig. 4.4. This plot, upon linear extrapolation gives $n_c = 1.218$ and upon quadratic extrapolation gives $n_c = 1.211$.

4.3.3 Pairing susceptibility χ_d

The pairing susceptibility $\chi_d(0)$ given by (4.1) is plotted for $U = 6.05$ and $U = 6.55$ in Fig. 4.5. The pairing is mediated by antiferromagnetic fluctuations as mentioned earlier. Close to half-filling, when the fluctuations grow large, the quasiparticle lifetime falls accordingly. This results in a decrease in the direct contribution. As we move away from half-filling, this contribution increases. Similarly, near half-filling, since the anti-

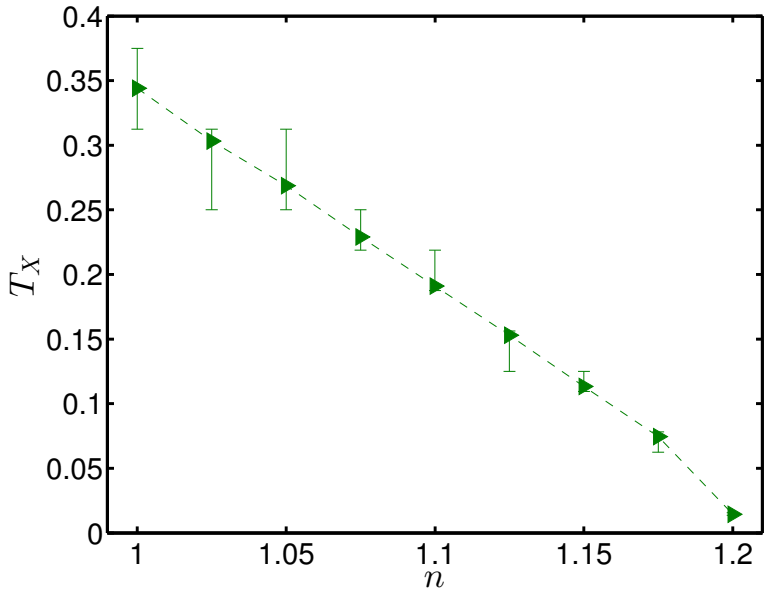

Figure 4.4: Crossover plot as a function of filling for $U = 6.55$, $t' = -0.175$ and $t'' = 0.05$.

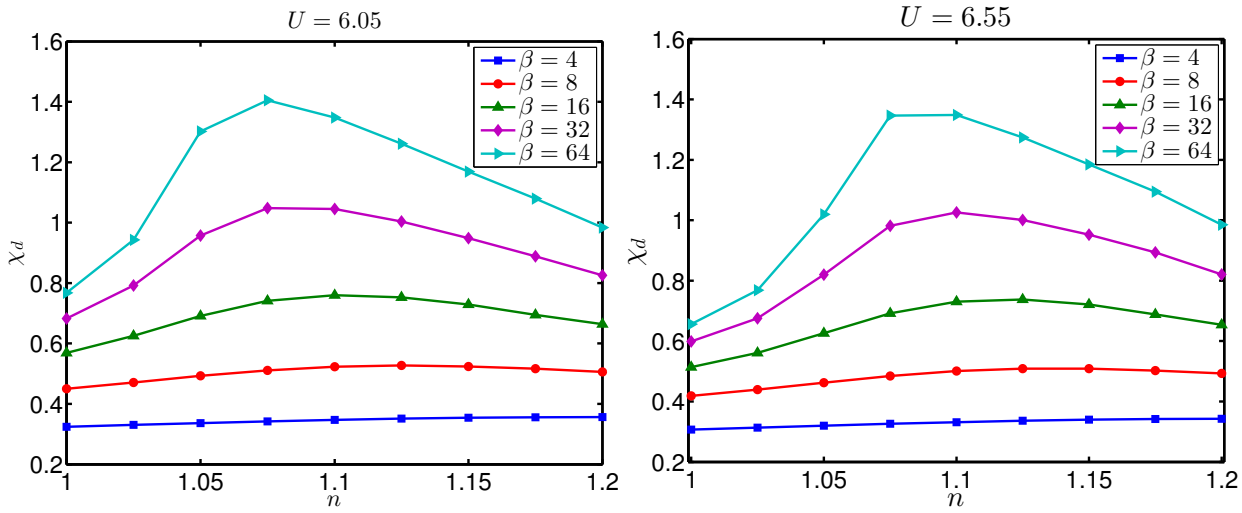

Figure 4.5: Pairing susceptibility $\chi_d(0)$ as a function of filling n, for various values of β, $t' = -0.175$ and $t'' = 0.05$.

ferromagnetic fluctuations are the largest at those points on the Fermi surface where the pseudogap opens up (hotspots), the vertex contribution is also small [21]. Far away from half-filling, around $n = 1.2$, because of the decreasing magnitude of these fluctuations, the vertex contribution again decreases. Therefore the vertex contribution is dome-shaped as a function of filling and the total pairing susceptibility follows this trend. Since for a

larger value of U, the fluctuations are larger, the pairing susceptibility close to half-filling for $U = 6.05$ is seen to be larger than that for $U = 6.55$.

4.3.4 Superconducting transition temperature T_c

The transition temperature to the superconducting phase, T_c is given by the temperature at which the direct contribution and the vertex contribution are equal in magnitude. For instance, the series $\frac{1}{1-x}$, diverges when $x = 1$. If we approximate the series by the first two terms as $\frac{1}{1-x} \sim 1 + x$, whether the series diverges can be checked from the equality of the first two terms. This analogy helps us understand the choice of T_c [23].

For a particular value of interaction U and for a specific value of filling n, we plot the ratio of the direct term to the vertex term as a function of temperature and pick that value of temperature where this ratio is equal to unity as T_c corresponding to that value of U. T_c can be plotted as a function of filling for various values of interaction. The plots are depicted in Fig. 4.6. It is clear that the transition temperature increases as the interaction increases. This emphasizes the weakly coupled nature of the superconductivity mediated by antiferromagnetic fluctuations [21]. If we fix the filling, for a larger value of interaction, as we scan down the temperature axis, we can see that the fluctuations become sufficiently large at higher values of temperature. It was previously observed that T_c has

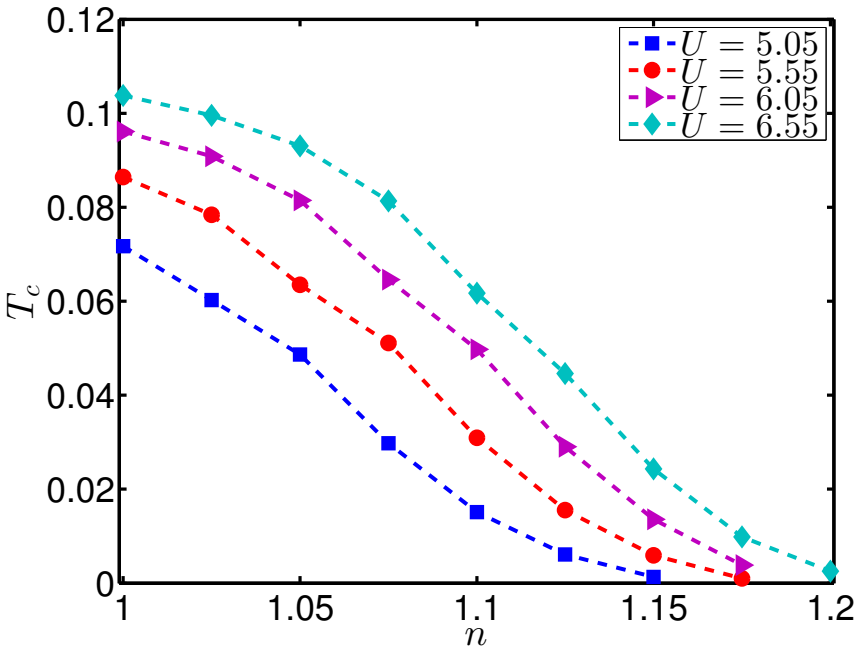

Figure 4.6: Plot of the superconducting transition temperature T_c as a function of filling n for various values of U, $t' = -0.175$ and $t'' = 0.05$.

a dome-shaped variation with respect to filling in the case of the single-band Hubbard model with only nearest-neighbor hopping [21]. In total contrast to that result and the commonly seen experimental results, we obtain a monotonic variation of T_c as a function of doping. When there is no extended hopping, at half-filling the FS coincides totally with the AFMBZ and the pseudogap effects are detrimental to superconductivity. But, when there is extended hopping, these pseudogap effects are limited to the hotspots and are not catastrophic to pairing. The steady decrease in antiferromagnetic fluctuations as a function of filling is reflected in this monotonic variation.

Experimentally, a monotonic variation in the superconducting transition temperature has been observed [99–101], with even claims of an undoped parent compound which shows superconductivity. The difference in structures of the parent compounds - T structure of the hole-doped cuprates and T' structure of the electron-doped cuprates - appears to be crucial. If excess oxygen is removed by reduction processes, the doping range where superconductivity occurs in electron-doped systems can be enhanced. This suggests that the co-ordination of copper can be a new degree of freedom [101].

4.4 Summary

The method of TPSC has been used previously to study pairing mediated by antiferromagnetic fluctuations under electron doping in the single-band Hubbard model. We revisit the problem of electron doping in the single-band Hubbard model with hopping to the second (t') and third (t'') nearest neighbors in addition to the usual hopping (t) to the nearest neighbors, making use of the same method. A glimpse at the sign of the microscopic length associated with the noninteracting susceptibility, helps us determine the transition temperature between the region of commensurate fluctuations and that of incommensurate fluctuations. The extended hopping seems to stabilize commensurate fluctuations around half-filling. This can be verified by plots of the noninteracting Fermi surface - the nesting vector between the points of intersection of the Fermi surface and the antiferromagnetic Brillouin zone helps us locate the maximum of the noninteracting susceptibility.

We can compute the spin vertex self-consistently using TPSC, and thereby take a look at the antiferromagnetic spin correlation length. The correlation length increases rapidly when the interaction is increased and the temperature is lowered. The growing antiferromagnetic fluctuations cause a crossover to the renormalized classical regime, where the antiferromagnetic correlation length exceeds the thermal de Broglie wavelength. Once

the system enters the renormalized classical regime, a pseudogap can be observed in the single particle density of states. The crossover plot is extrapolated to determine the critical value of filling where antiferromagnetism disappears.

The pairing mediated by the growing fluctuations given as the total of a direct term and a vertex term, is seen to have a dome-shaped variation. Near half-filling, because of pseudogap effects, the pairing is reduced, near a filling of $n = 1.2$ the decreasing magnitude of fluctuations cause a reduction in pairing. Contrary to previous work using TPSC which got a dome shaped variation in the superconducting transition temperature, we get a monotonic variation in T_c. The extended hopping changes the noninteracting Fermi surface - the Fermi surface intersects the antiferromagnetic Brillouin zone only at the hotspots. The pseudogap effects are limited to these hotspots, and therefore the antiferromagnetic fluctuations are not fully detrimental to pairing.

Chapter 5

Summary and Outlook

In this thesis, using the two-particle self-consistent method, we have studied a handful of problems. As a non-perturbative method which satisfies many physical constraints, including the Mermin-Wagner theorem, this method is very powerful and had already given results which gave good agreement with Quantum Monte Carlo results [14]. The physics of the growing antiferromagnetic fluctuations, and the effects of these fluctuations on the system are aptly captured using this method.

As mentioned in Chapter 1 the two-particle self-consistent (TPSC) approach was initially developed to study the single-band Hubbard model. In this work, this approach has been generalized to study the multi-band case of the Hubbard model on the honeycomb lattice. In Chapter 2, we present in detail how the semi-metal to antiferromagnet transition of the half-filled Hubbard model on the honeycomb lattice was studied using this method. The critical interaction strength for the transition was computed, and the intermediate spin liquid phase was ruled out.

Further, in Chapter 3, again using TPSC for the honeycomb lattice, we study graphene under uniaxial strain along the zigzag direction. The interplay of strain and strong antiferromagnetic fluctuations results in a novel quantum criticality.

TPSC can also be used to study pairing mediated by the antiferromagnetic fluctuations. In Chapter 4 we return to TPSC for the single-band case to study the Hubbard model with extended hopping to second and third nearest neighbors. Contrary to earlier results from TPSC which gave a dome-shaped variation in the superconducting transition temperature as a function of filling, we get a monotonic variation.

The generalized multi-band version of TPSC can be further extended to study pairing mediated by antiferromagnetic fluctuations. Also, application of this method to study the transport properties in graphene seems to be interesting. Also, it would be exciting to gen-

eralize the method even more by including the effects of spin-orbit coupling. This method can not only be used to look at antiferromagnetic fluctuations, but can be broadened to study ferromagnetism also. Further, the possibility of developing time-dependent TPSC sounds fascinating. For instance, using such a time-dependent version of this approach, we can study the effect of quenching on the antiferromagnetic fluctuations near the Mott transition. Thus, the two-particle self-consistent method still holds a lot of promise and offers a variety of possibilities for the future.

Appendix A

TPSC for the single-band Hubbard model

A.1 Self Energy and two-particle correlation functions

The Hamiltonian is given by,

$$H = H_0 + H_{int} \tag{A.1}$$

$$H_0 = \sum_{i,j,\sigma} -t_{ij} \left(c^\dagger_{i\,\sigma} c_{j\,\sigma} + h.c \right) \tag{A.2}$$

$$H_{int} = U \sum_i n_{i\uparrow} n_{i\downarrow} \tag{A.3}$$

Here H_0 is the noninteracting Hamiltonian and H_{int} is the Hubbard interaction term. The noninteracting Hamiltonian (A.2) describes the hopping of electrons on the lattice, here t_{ij} is the hopping term. Usually, the hopping between nearest neighbors $\langle i, j \rangle$ is considered and $t_{ij} = t$. The interaction term penalizes the double occupation of a site by two electrons - whenever a site is occupied by two electrons, a potential energy 'cost' U has to be paid.

The Green function is defined as the time ordered product,

$$G_\sigma(1,2) = -\langle T_\tau c_\sigma(1) c^\dagger_\sigma(2) \rangle \tag{A.4}$$

$$= -\theta(\tau_1 - \tau_2) \langle c_\sigma(1) c^\dagger_\sigma(2) \rangle + \theta(\tau_2 - \tau_1) \langle c^\dagger_\sigma(2) c_\sigma(1) \rangle \tag{A.5}$$

Here we have assumed a four vector notation where $1 = (\boldsymbol{r}_1, \tau_1)$ - comprising both position and imaginary time. Let us consider the equation of motion of the Green's

function. Using the Heisenberg equation of motion for the time evolution of an operator in the Heisenberg representation.

$$\begin{aligned}\frac{\partial}{\partial\tau_1}G_\sigma(1,2) &= -\frac{\partial}{\partial\tau_1}\langle T_\tau c_\sigma(1)c_\sigma^\dagger(2)\rangle \\ &= \frac{\partial}{\partial\tau_1}\left[-\theta(\tau_1-\tau_2)\langle c_\sigma(1)c_\sigma^\dagger(2)\rangle + \theta(\tau_2-\tau_1)\langle c_\sigma^\dagger(2)c_\sigma(1)\rangle\right] \\ &= -\langle T_\tau\frac{\partial}{\partial\tau_1}c_\sigma(1)c_\sigma^\dagger(2)\rangle \;-\; \delta_{\boldsymbol{r}_1\boldsymbol{r}_2}\delta(\tau_1-\tau_2) \\ &= -\langle T_\tau[H-\mu\mathcal{N}, c_\sigma(1)]c_\sigma^\dagger(2)\rangle \end{aligned} \tag{A.6}$$

where μ is the chemical potential, and $\mathcal{N}$ is the total number of particles. We have,

$$\begin{aligned}[H_0, c_\sigma(1)] &= [\sum_{\langle ij\rangle,\sigma'} -t\,\left(c_{i\,\sigma'}^\dagger c_{j\,\sigma'} + h.c\right), c_\sigma(1)] \\ &= t\sum_{\Delta} c_{\boldsymbol{r}_1+\Delta,\sigma}\end{aligned} \tag{A.7}$$

where the summation is over all the nearest neighbors of the site $\boldsymbol{r}_1$. Similarly,

$$\begin{aligned}[H_{int}, c_\sigma(1)] &= [U\sum_i n_{i\uparrow}n_{i\downarrow}, c_\sigma(1)] \\ &= -Uc_\sigma(1)n_{-\sigma}(1)\end{aligned} \tag{A.8}$$

and,

$$[-\mu\mathcal{N}, c_\sigma(1)] = \mu c_\sigma(1) \tag{A.9}$$

Concisely,

$$\begin{aligned}\left([-\frac{\partial}{\partial\tau_1}+\mu]\delta(\Delta) + t_{\boldsymbol{r}_1,\boldsymbol{r}_{1+\Delta}}\right)G_\sigma(\boldsymbol{r}_{1+\Delta}-\boldsymbol{r}_2,\tau_1-\tau_2) &= \delta_{\boldsymbol{r}_1\boldsymbol{r}_2}\delta(\tau_1-\tau_2) \\ &\quad - U\langle n_{-\sigma}(1)c_\sigma(1)c_\sigma^\dagger(2)\rangle\end{aligned} \tag{A.10}$$

From the Dyson equation, relating the interacting Green function (G_σ) is related to the

noninteracting Green function (G^0_σ) via the self-energy (Σ_σ),

$$\begin{aligned} G^{-1}_\sigma(1,\bar{2}) &= (G^0_\sigma)^{-1}(1,\bar{2}) - \Sigma_\sigma(1,\bar{2}) \\ (G^0_\sigma)^{-1}(1,\bar{2})G_\sigma(\bar{2},2) &= \delta(1-2) + \Sigma_\sigma(1,\bar{2})G_\sigma(\bar{2},2) \end{aligned} \tag{A.11}$$

where a bar over an index means that index will be summed over - a summation over the space index and an integration over the imaginary time index is assumed. From Eqs. (A.10) and (A.11), we arrive at an exact relation between the self energy, Σ and two-particle correlation functions.

$$\Sigma_\sigma(1,\bar{2})G_\sigma(\bar{2},2) = -U\langle n_{-\sigma}(1)c_\sigma(1)c^\dagger_\sigma(2)\rangle \tag{A.12}$$

This exact relation is the starting point of the approximation in TPSC.

A.2 Spin and charge susceptibilities

The spin response function is defined as,

$$\begin{aligned} \chi_{sp}(1,2) &= \langle\, T_\tau S_z(1)S_z(2)\,\rangle \\ &= \langle T_\tau\,(\,n_\uparrow(1) - n_\downarrow(1)\,)\,(\,n_\uparrow(2) - n_\downarrow(2)\,)\rangle \\ &= \langle T_\tau\, n_\uparrow(1)n_\uparrow(2) \;-\; n_\uparrow(1)n_\downarrow(2) \;-\; n_\downarrow(1)n_\uparrow(2) \;+\; n_\downarrow(1)n_\downarrow(2)\,)\,\rangle \end{aligned} \tag{A.13}$$

Using spin rotational invariance,

$$\chi_{sp}(1,2) = 2\;(\,\langle T_\tau\, n_\uparrow(1)n_\uparrow(2)\,\rangle \;-\; \langle\, T_\tau\, n_\uparrow(1)n_\downarrow(2)\,\rangle\,) \tag{A.14}$$

Similarly, for the charge response function,

$$\begin{aligned} \chi_{ch}(1,2) &= \langle\, n(1)n(2)\,\rangle - \langle\, n(1)\rangle\langle n(2)\,\rangle \\ &= \langle T_\tau\,(\,n_\uparrow(1) + n_\downarrow(1)\,)\,(\,n_\uparrow(2) + n_\downarrow(2)\,)\rangle - \langle\, n(1)\rangle\langle n(2)\,\rangle \end{aligned} \tag{A.15}$$

$$= 2\;(\,\langle T_\tau\, n_\uparrow(1)n_\uparrow(2)\,\rangle \;+\; \langle\, T_\tau\, n_\uparrow(1)n_\downarrow(2)\,\rangle\,) - \langle\, n(1)n(2)\,\rangle \tag{A.16}$$

The two-particle correlation functions on the RHS of the spin and charge response functions, Eqs. (A.14) and (A.16) can be written in terms of functional derivatives of the Green function with respect to source fields.

A.3 Bethe-Salpeter equation

Taking into account a source field Φ of particle-hole fluctuations in the system, we can define susceptibilities in the particle-hole channel as functional derivatives of the Green function with respect to these source fields. The source fields are set to zero at the end of calculations. The source field is given by,

$$\Phi = \begin{bmatrix} \phi_\uparrow & 0 \\ 0 & \phi_\downarrow \end{bmatrix} \tag{A.17}$$

and the partition function in the presence of this source field is

$$Z[\Phi] = Tr[e^{-\beta(H-\mu\mathcal{N})} T_\tau e^{-c^\dagger_{\bar{\sigma}}(\bar{1})\phi_{\bar{\sigma}}(\bar{1},\bar{2})c_{\bar{\sigma}}(\bar{2})}] \tag{A.18}$$

The Green function is,

$$G_\sigma(1,2;\Phi) = \frac{Tr[e^{-\beta(H-\mu\mathcal{N})} T_\tau e^{-c^\dagger_{\bar{\sigma}}(\bar{1})\phi_{\bar{\sigma}}(\bar{1},\bar{2})c_{\bar{\sigma}}(\bar{2})} c_\sigma(1) c^\dagger_\sigma(2)]}{Tr[e^{-\beta(H-\mu\mathcal{N})} T_\tau e^{-c^\dagger_{\bar{\sigma}}(\bar{1})\phi_{\bar{\sigma}}(\bar{1},\bar{2})c_{\bar{\sigma}}(\bar{2})}]} \tag{A.19}$$

$$= -\langle T_\tau c_\sigma(1) c^\dagger_\sigma(2)\rangle \tag{A.20}$$

The response function written as the functional derivative of the Green function with respect to ϕ_σ,

$$\frac{\partial G_\sigma(1,2;\Phi)}{\partial \phi_{\sigma'}(3,4)} = G_{\sigma'}(4,3;\Phi) G_\sigma(1,2;\Phi) - \langle T_\tau c^\dagger_{\sigma'}(3) c_{\sigma'}(4) c^\dagger_\sigma(2) c_\sigma(1)\rangle_\Phi \tag{A.21}$$

Taking the functional derivative of,

$$G_\sigma(1,\bar{1};\Phi) G^{-1}_\sigma(\bar{1},2;\Phi) = \delta(1-2) \tag{A.22}$$

we have,

$$\frac{\partial G_\sigma(1,\bar{1};\Phi)}{\partial \phi_{\sigma'}(3,4)} G^{-1}_\sigma(\bar{1},2;\Phi) = -G_\sigma(1,\bar{1};\Phi) \frac{\partial G^{-1}_\sigma(\bar{1},2;\Phi)}{\partial \phi_{\sigma'}(3,4)} \tag{A.23}$$

$$\frac{\partial G_\sigma(1,2;\Phi)}{\partial \phi_{\sigma'}(3,4)} = -G_\sigma(1,\bar{1};\Phi) \frac{\partial G^{-1}_\sigma(\bar{1},\bar{2};\Phi)}{\partial \phi_{\sigma'}(3,4)} G_\sigma(\bar{2},2;\Phi) \tag{A.24}$$

In order to rewrite the above equation, we make use of the Dyson equation in the presence

of the source field,

$$G_\sigma(1,2,\Phi) = (G_\sigma^{(0)})^{-1}(1,2;\Phi) - \Sigma(1,2;\Phi) - \phi_\sigma(1,2) \tag{A.25}$$

$$\frac{\partial G_\sigma^{-1}(1,2;\Phi)}{\partial \phi_{\sigma'}(3,4)} = -\delta(1-3)\delta(2-4)\delta_{\sigma\sigma'} - \frac{\partial \Sigma_\sigma(1,2;\Phi)}{\partial \phi_{\sigma'}(3,4)} \tag{A.26}$$

Hence, the response function can be written as,

$$\begin{aligned}\frac{\partial G_\sigma(1,2;\Phi)}{\partial \phi_{\sigma'}(3,4)} &= G_\sigma(1,\bar{1};\Phi)G_\sigma(\bar{2},2;\Phi)\delta(\bar{1}-3)\delta(\bar{2}-4)\delta_{\sigma\sigma'} \\ &\quad + G_\sigma(1,\bar{1};\Phi)\frac{\partial \Sigma_\sigma(\bar{1},\bar{2};\Phi)}{\partial \phi_{\sigma'}(3,4)}G_\sigma(\bar{2},2;\Phi)\end{aligned} \tag{A.27}$$

Applying chain rule to evaluate the functional derivative of the self energy

$$\begin{aligned}\frac{\partial G_\sigma(1,2;\Phi)}{\partial \phi_{\sigma'}(3,4)} &= G_\sigma(1,3;\Phi)G_\sigma(4,2;\Phi)\delta_{\sigma\sigma'} \\ &\quad + G_\sigma(1,\bar{1};\Phi)\frac{\partial \Sigma_\sigma(\bar{1},\bar{2};\Phi)}{\partial G_{\bar{\sigma}}(\bar{3},\bar{4};\Phi)}\frac{\partial G_{\bar{\sigma}}(\bar{3},\bar{4};\Phi)}{\partial \phi_{\sigma'}(3,4)}G_\sigma(\bar{2},2;\Phi)\end{aligned} \tag{A.28}$$

The functional derivative of the self energy with respect to the Green function gives us the irreducible vertex,

$$\Gamma_{\sigma\sigma'}(1,2;3,4) = \frac{\partial \Sigma_\sigma(1,2)}{\partial G_{\sigma'}(3,4)} \tag{A.29}$$

Hence,

$$\begin{aligned}\frac{\partial G_\sigma(1,2;\Phi)}{\partial \phi_{\sigma'}(3,4)} &= G_\sigma(1,3;\Phi)G_\sigma(4,2;\Phi)\delta_{\sigma\sigma'} \\ &\quad + G_\sigma(1,\bar{1};\Phi)\Gamma_{\sigma\bar{\sigma}}(\bar{1},\bar{2},\bar{3},\bar{4};\Phi)\frac{\partial G_{\bar{\sigma}}(\bar{3},\bar{4};\Phi)}{\partial \phi_{\sigma'}(3,4)}G_\sigma(\bar{2},2;\Phi)\end{aligned} \tag{A.30}$$

This is the Bethe-Salpeter equation, which is the integral equation for the response functions in the particle - hole channel.

Let us consider the following combination of response functions at zero source field,

$$\chi_\pm(1,2;3,4) = -2\left(\frac{\partial G_\uparrow(1,2;\Phi)}{\partial \phi_\uparrow(3,4)} \pm \frac{\partial G_\uparrow(1,2;\Phi)}{\partial \phi_\downarrow(3,4)}\right)\Bigg|_{\Phi=0} \tag{A.31}$$

Substituting the expression for the response function from Eq. (A.30) in the above, we

can write an integral equation for response functions $\chi_\pm$. In writing this 'new' Bethe-Salpeter equation, we can make use of spin rotational invariance,

$$G_\uparrow = G_\downarrow = G$$

The integral equations are,

$$\chi_\pm(1,2;3,4) = -2G(1,3)G(2,4) \pm \Gamma_{sp,ch}(1,2;3,4)G(1,\bar{1})G(\bar{2},2)\chi_\pm(\bar{3},\bar{4},3,4) \tag{A.32}$$

where the irreducible vertices in the spin and charge channel are given by,

$$\Gamma_{sp}(1,2;3,4) = \frac{\partial\Sigma_\uparrow(1,2)}{\partial G_\downarrow(3,4)} - \frac{\partial\Sigma_\uparrow(1,2)}{\partial G_\uparrow(3,4)} \tag{A.33}$$

$$\Gamma_{ch}(1,2;3,4) = \frac{\partial\Sigma_\uparrow(1,2)}{\partial G_\downarrow(3,4)} + \frac{\partial\Sigma_\uparrow(1,2)}{\partial G_\uparrow(3,4)} \tag{A.34}$$

The spin and charge response functions are special cases of the response functions given by $\chi_\pm$ and Eqs. (A.14) and (A.16) can be rewritten as,

$$\chi_{sp,ch}(1,2) = -2\left(\frac{\partial G_\uparrow(1,1^+)}{\partial\phi_\uparrow(2^+,2)} \pm \frac{\partial G_\uparrow(1,1^+)}{\partial\phi_\downarrow(2^+,2)}\right)\Bigg|_{\Phi=0} \tag{A.35}$$

In the four-point correlation function, a couple of points are identified to be the same except for a minor change in the time so that we get the correct time ordering in the correlation function.

A.4 TPSC ansatz

From the exact relation given by Eq. (A.12), we can write an approximation to the two-particle correlation function on the RHS. TPSC does a mean-field or Hartree-Fock approximation to the two-particle correlation function, but with a twist. On the RHS of Eq. (A.12) if $2 \to 1^+$, i.e., $\boldsymbol{r}_2 = \boldsymbol{r}_1$ and $\tau_2 = \tau_1 + \epsilon$ where ϵ is an infinitesimal increment which we have for the proper time ordering, the equation can be rewritten as

$$\Sigma_\sigma(1,\bar{2})G_\sigma(\bar{2},2) = -U\langle n_{-\sigma}(1)c_\sigma(1)c^\dagger_\sigma(1^+)\rangle \tag{A.36}$$

$$= U\langle n_{-\sigma}(1)c^\dagger_\sigma(1^+)c_\sigma(1)\rangle \tag{A.37}$$

$$= U\langle n_\uparrow(1)n_\downarrow(1)\rangle \tag{A.38}$$

The exact result on the RHS involving the double occupancy is retained in TPSC by a modified approximation. This resembles the Hartree-Fock approximation, but reproduces the exact result when $2 \to 1^+$. This is the TPSC ansatz,

$$\Sigma_\sigma(1,\bar{2})G_\sigma(\bar{2},2) = \mathcal{A}\, G^{-\sigma}(1,1^+)G^\sigma(1,2) \tag{A.39}$$

We have replaced the bare interaction by a renormalized interaction such that the exact relation is reproduced when $2 \to 1^+$. So we have

$$U\,\langle n_\uparrow(1)n_\downarrow(1)\rangle = \mathcal{A}\, G^{-\sigma}(1,1^+)G^\sigma(1,1^+) \tag{A.40}$$

$$= \mathcal{A}\langle n_\uparrow(1)\rangle\langle n_\downarrow(1)\rangle \tag{A.41}$$

which gives us

$$\mathcal{A} = U\frac{\langle n_\uparrow n_\downarrow\rangle}{\langle n_\uparrow\rangle\langle n_\downarrow\rangle} \tag{A.42}$$

Therefore, the first approximation to the self-energy is local and frequency-independent.

$$\Sigma_\sigma(1,2) = U\frac{\langle n_\uparrow n_\downarrow\rangle}{\langle n_\uparrow\rangle\langle n_\downarrow\rangle}\, G_{-\sigma}(1,1^+)\delta(1-2) \tag{A.43}$$

When we evaluate the spin vertex from (A.33), we get a local, frequency-independent quantity $U_{sp} = U\frac{\langle n_\uparrow n_\downarrow\rangle}{\langle n_\uparrow\rangle\langle n_\downarrow\rangle}$. The higher order correlations from the derivative of $\frac{\langle n_\uparrow n_\downarrow\rangle}{\langle n_\uparrow\rangle\langle n_\downarrow\rangle}$ cancel because of the minus sign. But, as far as the charge vertex is concerned (A.34), this does not happen. For simplicity, we assume that the charge vertex (U_{ch}) is also local.

A.5 Improved approximation for the self-energy

The exact relation between the self-energy and two-particle correlation function given by Eq. (A.12) can be rewritten from the information available in Eq. (A.21) as,

$$\Sigma_\sigma(1,\bar{2})G_\sigma(\bar{2},2) = -U\left[\frac{\partial G_\sigma(1,2)}{\partial\phi_{-\sigma'}(1^+,1;\Phi)} - G_{-\sigma}(1,1^+;\Phi)G_\sigma(1,2;\Phi)\right] \tag{A.44}$$

$$\Sigma_\sigma(1,2) = -U\left[G_\sigma(1,\bar{1};\Phi)\frac{\partial\Sigma_\sigma(\bar{1},2;\Phi)}{\partial G_{\bar{\sigma}}(\bar{3},\bar{4};\Phi)}\frac{\partial G_{\bar{\sigma}}(\bar{3},\bar{4};\Phi)}{\partial\phi_{-\sigma}(1^+,1)} - G_{-\sigma}(1,1^+;\Phi)\delta(1-2)\right] \tag{A.45}$$

Suppose, $\sigma = \uparrow$. Then the RHS contains the combination $\Gamma_{\uparrow\uparrow}\chi_{\uparrow\downarrow} + \Gamma_{\uparrow\downarrow}\chi_{\downarrow\downarrow}$. From the equation of spin and charge vertices and response functions, we can rewrite this as,

$$\Gamma_{\uparrow\uparrow} = \frac{1}{2}\left(\Gamma_{ch} - \Gamma_{sp}\right) \tag{A.46}$$

$$\Gamma_{\uparrow\downarrow} = \frac{1}{2}\left(\Gamma_{ch} + \Gamma_{sp}\right) \tag{A.47}$$

$$\chi_{\uparrow\uparrow} = -\frac{1}{4}\left(\chi_{+} + \chi_{-}\right) \tag{A.48}$$

$$\chi_{\uparrow\downarrow} = -\frac{1}{4}\left(\chi_{+} - \chi_{-}\right) \tag{A.49}$$

Lets us set the source field to zero. We can use the fact that the irreducible vertices are local $\Gamma_{ch,sp}(\bar{1}, 2, \bar{3}, \bar{4}) = U_{ch,sp}\delta(\bar{1} - 2)\delta(\bar{1} - \bar{3})\delta(2 - \bar{4})$, and we have the special case of $\chi_{\pm}(\bar{3}, \bar{4}, 1, 1^{+}) = \chi_{ch,sp}(2, 1)$. Therefore,

$$\Sigma_{\sigma}(1, 2) = \frac{U}{4}\left[G_{\sigma}(1, 2)U_{sp}\chi_{sp}(2, 1) + U_{ch}\chi_{ch}(2, 1)\right] + UG_{-\sigma}(1, 1^{+})\delta(1 - 2) \tag{A.50}$$

This can be written in the momentum - imaginary frequency space as,

$$\Sigma_{\sigma}(k) = Un_{-\sigma} + \frac{U}{4}\frac{T}{N}\sum_{q}\left[U_{sp}\chi_{sp}(q) + U_{ch}\chi_{sp}(q)\right]G_{\sigma}(k + q) \tag{A.51}$$

The above derivation of the self-energy is when the source field is in the longitudinal channel. Source fields can be introduced in the transverse channel also.

Appendix B

TPSC for the multi-band case of the Hubbard model on the honeycomb lattice

B.1 Self-energy and two-particle correlations

The honeycomb lattice is in reality a triangular Bravais lattice with two sublattices, A and B. Hence, when we consider the noninteracting tight-binding Hamiltonian, we get two bands which touch at the Dirac points. The Hamiltonian for the Hubbard model on the honeycomb lattice which comprises the nearest neighbor hopping Hamiltonian and the Hubbard term is given by,

$$H = H_0 + H_{int} \tag{B.1}$$

$$H_0 = -t \sum_{i,\Delta,\sigma} \left(a^\dagger_{i\sigma} b_{i+\Delta,\sigma} + h.c \right) \tag{B.2}$$

$$H_{int} = U \sum_{i \in A,B} \left(a_{i\uparrow} a_{i\downarrow} + b_{i\uparrow} b_{i\downarrow} \right) \tag{B.3}$$

H_0 describes the hopping of an electron from site i on A (B) to the three nearest neighbors given by $i+\Delta$ on B (A). The Green function is a matrix in a and b indices. Assuming spin rotational invariance, we can write the Green function as a 2×2 matrix in the sublattice

space as

$$\mathbf{G}(1,2) = \begin{pmatrix} G^{aa}(1,2) & G^{ab}(1,2) \\ G^{ba}(1,2) & G^{bb}(1,2) \end{pmatrix} \tag{B.4}$$

where each element is a time ordered product of the following form

$$G^{\rho\lambda}_{\sigma\sigma'}(1,2) = -\langle T_\tau \rho_\sigma(1)\lambda^\dagger_{\sigma'}(2)\rangle \delta_{\sigma\sigma'} \tag{B.5}$$

where $\rho, \lambda = a, b$.

Let us consider the equation of motion for the element given by Eq. (B.5)

$$\frac{\partial}{\partial\tau_1} G^{\rho\lambda}_{\sigma\sigma'}(1,2) = -\frac{\partial}{\partial\tau_1}\left(\langle T_\tau \rho_\sigma(1)\lambda^\dagger_{\sigma'}(2)\rangle \delta_{\sigma\sigma'}\right) \tag{B.6}$$

$$= -\delta(1-2)\delta_{\sigma\sigma'}\delta_{\rho\lambda} - \langle T_\tau \frac{\partial}{\partial\tau_1}\rho_\sigma(1)\lambda^\dagger_{\sigma'}(2)\rangle \delta_{\sigma\sigma'} \tag{B.7}$$

Using Heisenberg equation of motion for the operator, we can write

$$\frac{\partial}{\partial\tau_1} a_\sigma(1) = [H - \mu\mathcal{N}, a_\sigma(1)] \tag{B.8}$$

$$= \left(t\sum_\Delta b_\sigma(\boldsymbol{r}_1 + \Delta, \tau_1)\right) - U n_{a,-\sigma}(1) a_\sigma(1) + \mu a_\sigma(1) \tag{B.9}$$

$$\frac{\partial}{\partial\tau_1} b_\sigma(1) = [H - \mu\mathcal{N}, b_\sigma(1)] \tag{B.10}$$

$$= \left(t\sum_\Delta a_\sigma(\boldsymbol{r}_1 + \Delta, \tau_1)\right) - U n_{b,-\sigma}(1) b_\sigma(1) + \mu b_\sigma(1) \tag{B.11}$$

$$\tag{B.12}$$

We must be able to rewrite the equation of motion of the Green function in terms of the Dyson equation to get the most general relation between self-energy and two-particle correlation functions. For this, we define

$$h^{\rho\lambda}_{\sigma\sigma'}(1,2) = \sum_\Delta t\, \delta_{\boldsymbol{r}_1+\Delta,\boldsymbol{r}_2}\delta(\tau_1 - \tau_2)\zeta^x_{\rho\lambda}\delta_{\sigma\sigma'} \tag{B.13}$$

where

$$\zeta^x = \begin{pmatrix} 0 & 1 \\ 1 & 0 \end{pmatrix}$$

and using

$$\left(\mathbf{G}^{(0)}\right)^{-1}(1,2) = \left(-\frac{\partial}{\partial\tau_1} + \mu\right)\mathbf{I} - \mathbf{h}(1,2) \tag{B.14}$$

we can rewrite the equation of motion of the Green function as

$$\left(-\frac{\partial}{\partial\tau_1} + \mu\right)\delta(1-\bar{2})G^{\rho\lambda}_{\sigma\sigma'}(\bar{2},2) - h^{\rho\eta}_{\sigma\sigma''}(1,\bar{2})\,G^{\eta\lambda}_{\sigma''\sigma'}(\bar{2},2) = \delta(1-2)\delta_{\sigma\sigma'}\delta_{\rho\lambda} - U\langle T_\tau \rho^\dagger_{-\sigma}(1)\rho_{-\sigma}(1)\rho_\sigma(1)\lambda^\dagger_{\sigma'}(2)\rangle\delta_{\sigma\sigma'} \tag{B.15}$$

Thus,

$$\left(\mathbf{G}^{(0)}\right)^{-1}(1,\bar{2})\,\mathbf{G}(\bar{2},2) = \delta(1-2)\mathbf{I} - \mathbf{u}(1,2) \tag{B.16}$$

where

$$u^{\rho\lambda}_{\sigma\sigma'}(1,2) = -U\langle T_\tau \rho^\dagger_{-\sigma}(1)\rho_{-\sigma}(1)\rho_\sigma(1)\lambda^\dagger_{\sigma'}(2)\rangle\delta_{\sigma\sigma'} \tag{B.17}$$

From the Dyson equation

$$\mathbf{G}^{-1}(1,2) = \left(\mathbf{G}^{(0)}\right)^{-1}(1,2) - \mathbf{\Sigma}(1,2) \tag{B.18}$$

the exact relation between self-energy and the two-particle correlation function is given by

$$\mathbf{\Sigma}(1,\bar{2})\,\mathbf{G}(\bar{2},2) = \mathbf{u}(1,2) \tag{B.19}$$

B.1.1 Bethe-Salpeter equation

The partition function in the presence of a source which produces particle-hole fluctuations, for the multi-band case is

$$Z[\Phi] = Tr\left[e^{-\beta(H-\mu\mathcal{N})}T_\tau e^{-\eta^\dagger_{\bar{\sigma}}(\bar{1})\phi^{\eta\gamma}_{\bar{\sigma}}(\bar{1},\bar{2})\gamma_{\bar{\sigma}}(\bar{2})}\right] \tag{B.20}$$

Here the source field for each spin species, is a 2×2 matrix

$$\Phi = \begin{bmatrix} \phi_\uparrow & 0 \\ 0 & \phi_\downarrow \end{bmatrix} \tag{B.21}$$

where

$$\phi_\sigma = \begin{bmatrix} \phi_\sigma^{aa} & \phi_\sigma^{ab} \\ \phi_\sigma^{ba} & \phi_\sigma^{bb} \end{bmatrix} \tag{B.22}$$

The Green function can be written as

$$G_\sigma^{\rho\lambda}(1,2;\Phi) = \frac{Tr[e^{-\beta(H-\mu\mathcal{N})}T_\tau e^{-\eta_{\bar{\sigma}}^\dagger(\bar{1})\phi_{\bar{\sigma}}^{\eta\gamma}(\bar{1},\bar{2})\gamma_{\bar{\sigma}}(\bar{2})}\rho_\sigma(1)\lambda_\sigma^\dagger(2)]}{Tr[e^{-\beta(H-\mu\mathcal{N})}T_\tau e^{-\eta_{\bar{\sigma}}^\dagger(\bar{1})\phi_{\bar{\sigma}}^{\eta\gamma}(\bar{1},\bar{2})\gamma_{\bar{\sigma}}(\bar{2})}]} \tag{B.23}$$

$$= -\langle T_\tau \rho_\sigma(1)\lambda_\sigma^\dagger(2)\rangle \tag{B.24}$$

To derive the integral equation for the response function in the multi-band case

$$\frac{\partial G_\sigma^{\rho\lambda}(1,2;\Phi)}{\partial \phi_{\sigma'}^{\eta\gamma}(3,4)} = G_{\sigma'}^{\gamma\eta}(4,3;\Phi)G_\sigma^{\rho\lambda}(1,2;\Phi) - \langle T_\tau \eta_{\sigma'}^\dagger(3)\gamma_{\sigma'}(4)\lambda_\sigma^\dagger(2)\rho_\sigma(1)\rangle_\Phi \tag{B.25}$$

we start from the identity,

$$G_\sigma^{\rho\kappa}(1,\bar{1};\Phi)(G_\sigma^{-1})^{\kappa\zeta}(\bar{1},2;\Phi) = \delta(1-2)\delta_{\rho\zeta} \tag{B.26}$$

and take its functional derivative with respect to the source field

$$\frac{\partial G_\sigma^{\rho\kappa}(1,\bar{1};\Phi)}{\partial \phi_{\sigma'}^{\eta\gamma}(3,4)}(G_\sigma^{-1})^{\kappa\zeta}(\bar{1},2;\Phi) = -G_\sigma^{\rho\kappa}(1,\bar{1};\Phi)\frac{\partial (G_\sigma^{-1})^{\kappa\zeta}(\bar{1},2;\Phi)}{\partial \phi_{\sigma'}^{\eta\gamma}(3,4)}$$

$$\frac{\partial G_\sigma^{\rho\lambda}(1,2;\Phi)}{\partial \phi_{\sigma'}^{\eta\gamma}(3,4)} = -G_\sigma^{\rho\kappa}(1,\bar{1};\Phi)\frac{\partial (G_\sigma^{-1})^{\kappa\zeta}(\bar{1},\bar{2};\Phi)}{\partial \phi_{\sigma'}^{\eta\gamma}(3,4)}G_\sigma^{\zeta\lambda}(\bar{2},2;\Phi) \tag{B.27}$$

From the Dyson equation,

$$(G_\sigma^{-1})^{\kappa\zeta}(1,2) = ((G_\sigma^{(0)})^{-1})^{\kappa\zeta}(1,2) - \phi_\sigma^{\kappa\zeta}(1,2) - \Sigma_\sigma^{\kappa\zeta}(1,2) \tag{B.28}$$

This lets us write,

$$\frac{\partial(G_\sigma^{-1})^{\kappa\zeta}(1,2;\Phi)}{\partial\phi_{\sigma'}^{\eta\gamma}(3,4)} = -\delta_{\kappa\eta}\delta_{\zeta\gamma}\delta_{\sigma\sigma'}\delta(\bar{1}-3)\delta(\bar{2}-4) - \frac{\partial\Sigma_\sigma^{\kappa\zeta}(1,2;\Phi)}{\partial\phi_{\sigma'}^{\eta\gamma}(3,4)} \tag{B.29}$$

Making use of this relation we can rewrite the expression for the response function as

$$\begin{aligned}\frac{\partial G_\sigma^{\rho\lambda}(1,2;\Phi)}{\partial\phi_{\sigma'}^{\eta\gamma}(3,4)} &= G_\sigma^{\rho\kappa}(1,\bar{1};\Phi)G_\sigma^{\zeta\lambda}(\bar{2},2;\Phi)\delta_{\kappa\eta}\delta_{\zeta\gamma}\delta_{\sigma\sigma'}\delta(\bar{1}-3)\delta(\bar{2}-4) \\ &\quad + G_\sigma^{\rho\kappa}(1,\bar{1};\Phi)\frac{\partial\Sigma_\sigma^{\kappa\zeta}(\bar{1},\bar{2};\Phi)}{\partial\phi_{\sigma'}^{\eta\gamma}(3,4)}G_\sigma^{\zeta\lambda}(\bar{2},2;\Phi)\end{aligned} \tag{B.30}$$

Using chain rule,

$$\begin{aligned}\frac{\partial G_\sigma^{\rho\lambda}(1,2;\Phi)}{\partial\phi_{\sigma'}^{\eta\gamma}(3,4)} &= G_\sigma^{\rho\eta}(1,3;\Phi)G_\sigma^{\gamma\lambda}(4,2;\Phi)\delta_{\sigma\sigma'} \\ &\quad + G_\sigma^{\rho\kappa}(1,\bar{1};\Phi)\frac{\partial\Sigma_\sigma^{\kappa\zeta}(\bar{1},\bar{2};\Phi)}{\partial G_{\bar{\sigma}}^{\iota\upsilon}(\bar{3},\bar{4};\Phi)}\frac{\partial G_{\bar{\sigma}}^{\iota\upsilon}(\bar{3},\bar{4};\Phi)}{\partial\phi_{\sigma'}^{\eta\gamma}(3,4)}G_\sigma^{\zeta\lambda}(\bar{2},2;\Phi)\end{aligned} \tag{B.31}$$

The functional derivative of the self-energy with respect to the Green function is the irreducible vertex,

$$\Gamma_{\sigma\sigma'}^{\kappa\zeta\iota\upsilon}(1,2;3,4) = \frac{\partial\Sigma_\sigma^{\kappa\zeta}(1,2)}{\partial G_{\sigma'}^{\iota\upsilon}(3,4)} \tag{B.32}$$

Hence, the integral equation for the response function

$$\begin{aligned}\frac{\partial G_\sigma^{\rho\lambda}(1,2;\Phi)}{\partial\phi_{\sigma'}^{\eta\gamma}(3,4)} &= G_\sigma^{\rho\eta}(1,3;\Phi)G_\sigma^{\gamma\lambda}(4,2;\Phi)\delta_{\sigma\sigma'} \\ &\quad + G_\sigma^{\rho\kappa}(1,\bar{1};\Phi)\Gamma_{\sigma\bar{\sigma}}^{\kappa\zeta\iota\upsilon}(\bar{1},\bar{2};\bar{3},\bar{4})\frac{\partial G_{\bar{\sigma}}^{\iota\upsilon}(\bar{3},\bar{4};\Phi)}{\partial\phi_{\sigma'}^{\eta\gamma}(3,4)}G_\sigma^{\zeta\lambda}(\bar{2},2;\Phi)\end{aligned} \tag{B.33}$$

This is a matrix generalization of the scalar equations we got in the single-band case. Therefore, here also we can consider the following combination of the response functions at zero source field,

$$\chi_\pm^{\rho\lambda\eta\gamma}(1,2;3,4) = -2\left(\frac{\partial G_\uparrow^{\rho\lambda}(1,2;\Phi)}{\partial\phi_\uparrow^{\eta\gamma}(3,4)} \pm \frac{\partial G_\uparrow^{\rho\lambda}(1,2;\Phi)}{\partial\phi_\downarrow^{\eta\gamma}(3,4)}\right)\Bigg|_{\Phi=0} \tag{B.34}$$

Substituting the expression for the response function from Eq. (B.33) in the above, we can write an integral equation for the response functions $\chi_\pm$. In writing this 'new' Bethe-

Salpeter equation, we can make use of spin rotational invariance,

$$G^{\rho\lambda}_{\uparrow} = G^{\rho\lambda}_{\downarrow} = G^{\rho\lambda}$$

The integral equations are,

$$\begin{aligned}\chi^{\rho\lambda\eta\gamma}_{\pm}(1,2;3,4) = &-2G^{\rho\eta}(1,3)G^{\gamma\lambda}(2,4) \\ &\pm \Gamma^{\kappa\zeta\iota\upsilon}_{sp,ch}(1,2;3,4)G^{\rho\kappa}(1,\bar{1})G^{\zeta\lambda}(\bar{2},2)\chi^{\iota\upsilon\eta\gamma}_{\pm}(\bar{3},\bar{4},3,4) \end{aligned} \tag{B.35}$$

where the irreducible vertices in the spin and charge channel are given by,

$$\Gamma^{\kappa\eta\iota\upsilon}_{sp}(1,2;3,4) = \frac{\partial\Sigma^{\kappa\eta}_{\uparrow}(1,2)}{\partial G^{\iota\upsilon}_{\downarrow}(3,4)} - \frac{\partial\Sigma^{\kappa\eta}_{\uparrow}(1,2)}{\partial G^{\iota\upsilon}_{\uparrow}(3,4)} \tag{B.36}$$

$$\Gamma^{\kappa\eta\iota\upsilon}_{ch}(1,2;3,4) = \frac{\partial\Sigma^{\kappa\eta}_{\uparrow}(1,2)}{\partial G^{\iota\upsilon}_{\downarrow}(3,4)} + \frac{\partial\Sigma^{\kappa\eta}_{\uparrow}(1,2)}{\partial G^{\iota\upsilon}_{\uparrow}(3,4)} \tag{B.37}$$

The spin and charge response functions are special cases of the response functions given by $\chi_{\pm}$.

B.2 TPSC ansatz

Consider a single element in the most general relation between the self-energy matrix and the two-particle correlation matrix. Suppose we have $2 \to 1^{+}$, which implies $\boldsymbol{r}_1 = \boldsymbol{r}_2$ and $\tau_2 = \tau_1 + \epsilon$ where ϵ is an infinitesimal increment for the right time ordering and in the multi-band case $\lambda = \rho$. The RHS of the above equation can be written in terms of double occupancy at (1).

$$[\boldsymbol{\Sigma}(1,\bar{2})\,\mathbf{G}(\bar{2},2)]^{\rho\lambda}_{\sigma\sigma'}\,\delta_{\sigma\sigma'}\delta_{\rho\lambda} = u^{\rho\lambda}(1,2) \tag{B.38}$$

$$= -U\langle T_\tau \rho^{\dagger}_{-\sigma}(1)\rho_{-\sigma}(1)\rho_{\sigma}(1)\lambda^{\dagger}_{\sigma'}(2)\rangle\delta_{\sigma\sigma'} \tag{B.39}$$

$$= U\langle n_{\rho,\uparrow}(1)n_{\rho,\downarrow}(1)\rangle\delta_{\rho\lambda}\delta_{\sigma\sigma'} \tag{B.40}$$

We can extend the TPSC ansatz to the multi-band case and write

$$\Sigma^{\rho\eta}_{\sigma}(1,\bar{2})G^{\eta\lambda}_{\sigma}(\bar{2},2) = \mathcal{A}\,G^{\rho\rho}_{-\sigma}(1,1^{+})G^{\rho\lambda}_{\sigma}(1,2) \tag{B.41}$$

such that the exact expression involving the double occupancy is obtained on the RHS. When $2 \to 1^+$ ($\rho = \lambda$), we have

$$\mathcal{A}\, G^{\rho\rho}_{-\sigma}(1,1^+)G^{\rho\rho}_{\sigma}(1,1^+) = \mathcal{A}\langle n_{\rho,-\sigma}(1)\rangle\langle n_{\rho,\sigma}(1)\rangle\delta_{\rho\lambda} \tag{B.42}$$

$$= U\langle n_{\rho,\uparrow}(1)n_{\rho,\downarrow}(1)\rangle\delta_{\rho\lambda} \tag{B.43}$$

Therefore, we have

$$\mathcal{A} = \frac{U\langle n_{\rho,\uparrow}n_{\rho,\downarrow}\rangle}{\langle n_{\rho,\uparrow}\rangle\langle n_{\rho,\downarrow}\rangle} \tag{B.44}$$

and

$$\Sigma^{\rho\eta}_{\sigma}(1,\bar{2})G^{\eta\lambda}_{\sigma}(\bar{2},2) = \frac{U\langle n_{\rho,\uparrow}n_{\rho,\downarrow}\rangle}{\langle n_{\rho,\uparrow}\rangle\langle n_{\rho,\downarrow}\rangle}\, G^{\rho\rho}_{-\sigma}(1,\bar{2})G^{\rho\lambda}_{\sigma}(\bar{2},2)$$

$$\Sigma^{\rho\eta}_{\sigma}(1,2) = \frac{U\langle n_{\rho,\uparrow}n_{\rho,\downarrow}\rangle}{\langle n_{\rho,\uparrow}\rangle\langle n_{\rho,\downarrow}\rangle}\, G^{\rho\rho}_{-\sigma}(1,1^+)\delta(1-2)\delta_{\rho\lambda} \tag{B.45}$$

From this the spin and charge vertices can be computed. The spin vertex has a matrix structure where only the $aaaa$ and $bbbb$ terms are non-zero and equal to each other because of sublattice symmetry. This term denoted by $U_{sp} = \frac{\langle n_\uparrow n_\downarrow\rangle}{\langle n_\uparrow\rangle\langle n_\downarrow\rangle}$is local and frequency-independent. We assume the charge vertex has such a structure with only $aaaa$ and $bbbb$ elements denoted by U_{ch}, despite the fact that we get higher order correlation functions if we evaluate the functional derivatives as shown in the above equations.

B.2.1 Improved approximation for the self-energy

The self-energy expression given by

$$\Sigma^{\rho\eta}_{\sigma}(1,\bar{2})\, G^{\eta\lambda}_{\sigma}(\bar{2},2) = -U\langle T_\tau \rho^{\dagger}_{-\sigma}(1)\rho_{-\sigma}(1)\rho_{\sigma}(1)\lambda^{\dagger}_{\sigma'}(2)\rangle$$

$$= UG^{\rho\rho}_{-\sigma}(1,1^+;\Phi)G^{\rho\lambda}_{\sigma}(1,2;\Phi)$$

$$- UG^{\rho\kappa}_{\sigma}(1,\bar{1};\Phi)\Gamma^{\kappa\zeta\iota\upsilon}_{\sigma\bar{\sigma}}(\bar{1},\bar{2};\bar{3},\bar{4})\frac{\partial G^{\iota\upsilon}_{\bar{\sigma}}(\bar{3},\bar{4};\Phi)}{\partial\phi^{\rho\rho}_{-\sigma}(1^+,1)}G^{\zeta\lambda}_{\sigma}(\bar{2},2;\Phi) \tag{B.46}$$

can be simplified making use of Eqs. (B.25) and (B.33)

$$\begin{aligned}\langle T_\tau \eta^\dagger_{\sigma'}(3)\gamma_{\sigma'}(4)\lambda^\dagger_\sigma(2)\rho_\sigma(1)\rangle_\Phi &= G^{\gamma\eta}_{\sigma'}(4,3;\Phi)G^{\rho\lambda}_{\sigma}(1,2;\Phi) - \frac{\partial G^{\rho\lambda}_\sigma(1,2;\Phi)}{\partial \phi^{\eta\gamma}_{\sigma'}(3,4)} \\ &= G^{\gamma\eta}_{\sigma'}(4,3;\Phi)G^{\rho\lambda}_{\sigma}(1,2;\Phi) - G^{\rho\eta}_{\sigma}(1,3;\Phi)G^{\gamma\lambda}_{\sigma}(4,2;\Phi)\delta_{\sigma\sigma'} \\ &- G^{\rho\kappa}_{\sigma}(1,\bar{1};\Phi)\Gamma^{\kappa\zeta\iota\upsilon}_{\sigma\bar{\sigma}}(\bar{1},\bar{2};\bar{3},\bar{4})\frac{\partial G^{\iota\upsilon}_{\bar{\sigma}}(\bar{3},\bar{4};\Phi)}{\partial \phi^{\eta\gamma}_{\sigma'}(3,4)}G^{\zeta\lambda}_{\sigma}(\bar{2},2;\Phi)\end{aligned} \tag{B.47}$$

Therefore the self-energy matrix element is,

$$\begin{aligned}\Sigma^{\rho\gamma}_\sigma(1,2) &= UG^{\rho\rho}_{-\sigma}(1,1^+;\Phi)\delta(1-2)\delta_{\rho\gamma} \\ &- UG^{\rho\kappa}_{\sigma}(1,\bar{1};\Phi)\Gamma^{\kappa\gamma\iota\upsilon}_{\sigma\bar{\sigma}}(\bar{1},2;\bar{3},\bar{4})\chi^{\iota\upsilon\rho\rho}_{\bar{\sigma},-\sigma}(\bar{3},\bar{4};1^+,1)\end{aligned} \tag{B.48}$$

Since the vertices are local, the above expression can be written as,

$$\begin{aligned}\Sigma^{\rho\gamma}_\sigma(1,2) &= UG^{\rho\rho}_{-\sigma}(1,1^+;\Phi)\delta(1-2)\delta_{\rho\gamma} \\ &- UG^{\rho\gamma}_{\sigma}(1,2;\Phi)\Gamma^{\gamma\gamma\gamma\gamma}_{\sigma\bar{\sigma}}(2,2;2,2)\chi^{\gamma\gamma\rho\rho}_{\bar{\sigma},-\sigma}(2,2;1^+,1)\end{aligned} \tag{B.49}$$

We also make use of the expressions for the spin and charge vertices and susceptibilities, to get the final form as,

$$\Sigma^{\rho\gamma}_\sigma(1,2) = UG^{\rho\rho}_{-\sigma}\delta(1-2) + \frac{1}{4}UG^{\rho\gamma}_\sigma(1,2)\left[U_{sp}\chi^{\gamma\gamma\rho\rho}_{sp}(2,1) + U_{ch}\chi^{\gamma\gamma\rho\rho}_{ch}(2,1)\right] \tag{B.50}$$

In the momentum - frequency representation, the self-energy takes the form

$$\Sigma^{\rho\gamma}_\sigma(k) = Un_{\rho,-\sigma} + \frac{U}{4}\frac{T}{N^2}\sum G^{\rho\gamma}_\sigma(k+q)\left[U_{sp}\chi^{\gamma\gamma\rho\rho}_{sp}(q) + U_{ch}\chi^{\gamma\gamma\rho\rho}_{ch}(q)\right] \tag{B.51}$$

Bibliography

[1] E. H. Lieb and F. Y. Wu, "Absence of mott transition in an exact solution of the short-range, one-band model in one dimension," *Physical Review Letters*, vol. 20, no. 25, p. 1445, 1968.

[2] W. Metzner and D. Vollhardt, "Correlated lattice fermions in d=âĹđ dimensions," *Physical review letters*, vol. 62, no. 3, p. 324, 1989.

[3] R. D. Mattuck, *A guide to Feynman diagrams in the many-body problem*. Courier Corporation, 2012.

[4] A. L. Fetter and J. D. Walecka, *Quantum theory of many-particle systems*. Courier Corporation, 2003.

[5] J. Hubbard, "Electron correlations in narrow energy bands," in *Proceedings of the royal society of london a: mathematical, physical and engineering sciences*, vol. 276, pp. 238–257, The Royal Society, 1963.

[6] J. Hubbard, "Electron correlations in narrow energy bands. ii. the degenerate band case," in *Proceedings of the Royal Society of London A: Mathematical, Physical and Engineering Sciences*, vol. 277, pp. 237–259, The Royal Society, 1964.

[7] J. Hubbard, "Electron correlations in narrow energy bands. iii. an improved solution," in *Proceedings of the Royal Society of London A: Mathematical, Physical and Engineering Sciences*, vol. 281, pp. 401–419, The Royal Society, 1964.

[8] J. Hubbard, "Electron correlations in narrow energy bands. iv. the atomic representation," in *Proceedings of the Royal Society of London A: Mathematical, Physical and Engineering Sciences*, vol. 285, pp. 542–560, The Royal Society, 1965.

[9] J. Hubbard, "Electron correlations in narrow energy bands. v. a perturbation expansion about the atomic limit," in *Proceedings of the Royal Society of London A:*

Mathematical, Physical and Engineering Sciences, vol. 296, pp. 82–99, The Royal Society, 1967.

[10] J. Kanamori, "Electron correlation and ferromagnetism of transition metals," *Progress of Theoretical Physics*, vol. 30, no. 3, pp. 275–289, 1963.

[11] M. C. Gutzwiller, "Effect of correlation on the ferromagnetism of transition metals," *Phys. Rev. Lett.*, vol. 10, pp. 159–162, Mar 1963.

[12] Y. M. Vilk, L. Chen, and A.-M. S. Tremblay, "Theory of spin and charge fluctuations in the hubbard model," *Phys. Rev. B*, vol. 49, pp. 13267–13270, May 1994.

[13] Y. Vilk and A.-M. Tremblay, "Non-perturbative many-body approach to the hubbard model and single-particle pseudogap," *Journal de Physique I*, vol. 7, no. 11, pp. 1309–1368, 1997.

[14] A.-M. S. Tremblay, "Two-particle-self-consistent approach for the hubbard model," in *Strongly Correlated Systems*, pp. 409–453, Springer, 2012.

[15] N. D. Mermin and H. Wagner, "Absence of ferromagnetism or antiferromagnetism in one- or two-dimensional isotropic heisenberg models," *Phys. Rev. Lett.*, vol. 17, pp. 1133–1136, Nov 1966.

[16] P. C. Hohenberg, "Existence of long-range order in one and two dimensions," *Phys. Rev.*, vol. 158, pp. 383–386, Jun 1967.

[17] *Destruction of Fermi liquid by spin fluctuations in two dimensions*, vol. 56, 12/1995 1995.

[18] Y. Vilk and A. M. S. Tremblay, "Destruction of fermi-liquid quasiparticles in two dimensions by critical fluctuations," *Europhysics Letters*, vol. 33, no. 2, p. 159–164, 1996.

[19] S. Allen and A. M. S. Tremblay, "Nonperturbative approach to the attractive hubbard model," *Physical Review B*, vol. 64, no. 7, p. art. no.–075115, 2001.

[20] B. Kyung, S. Allen, and A. M. S. Tremblay, "Pairing fluctuations and pseudogaps in the attractive hubbard model," *Physical Review B*, vol. 64, no. 7, p. art. no.–075116, 2001.

[21] B. Kyung, J.-S. Landry, and A.-M. S. Tremblay, "Antiferromagnetic fluctuations and d -wave superconductivity in electron-doped high-temperature superconductors," *Phys. Rev. B*, vol. 68, p. 174502, Nov 2003.

[22] B. Kyung, V. Hankevych, A.-M. Daré, and A.-M. S. Tremblay, "Pseudogap and spin fluctuations in the normal state of the electron-doped cuprates," *Phys. Rev. Lett.*, vol. 93, p. 147004, Sep 2004.

[23] S. R. Hassan, B. Davoudi, B. Kyung, and A.-M. S. Tremblay, "Conditions for magnetically induced singlet d-wave superconductivity on the square lattice," *Phys. Rev. B*, vol. 77, p. 094501, Mar 2008.

[24] B. Davoudi and A. M. S. Tremblay, "Nearest-neighbor repulsion and competing charge and spin order in the extended hubbard model," *Physical Review B*, vol. 74, pp. 035113/1–15, 2006 2006.

[25] B. Davoudi and A. M. S. Tremblay, "Non-perturbative treatment of charge and spin fluctuations in the two-dimensional extended hubbard model: Extended two-particle self-consistent approach," *Physical Review B*, vol. 76, pp. 085115/1–12, 2007 2007.

[26] B. Davoudi, S. R. Hassan, and A. M. S. Tremblay, "Competition between charge and spin order in the t-u-v extended hubbard model on the triangular lattice," *Physical Review B*, vol. 77, pp. 214408/1–11, 2008 2008.

[27] D. Bergeron, V. Hankevych, B. Kyung, and A.-M. Tremblay, "Optical and dc conductivity of the two-dimensional hubbard model in the pseudogap regime and across the antiferromagnetic quantum critical point including vertex corrections," *Physical Review B*, vol. 84, no. 8, p. 085128, 2011.

[28] P. Anderson, "Resonating valence bonds: A new kind of insulator?," *Materials Research Bulletin*, vol. 8, no. 2, pp. 153 – 160, 1973.

[29] L. Pauling, *The nature of the chemical bond and the structure of molecules and crystals: an introduction to modern structural chemistry*, vol. 18. Cornell university press, 1960.

[30] L. Balents, "Spin liquids in frustrated magnets," *Nature*, vol. 464, no. 7286, pp. 199–208, 2010.

[31] P. W. ANDERSON, "The resonating valence bond state in la2cuo4 and superconductivity," *Science*, vol. 235, no. 4793, pp. 1196–1198, 1987.

[32] M. J. P. Gingras and P. A. McClarty, "Quantum spin ice: a search for gapless quantum spin liquids in pyrochlore magnets," *Reports on Progress in Physics*, vol. 77, no. 5, p. 056501, 2014.

[33] B. J. Powell and R. H. McKenzie, "Quantum frustration in organic mott insulators: from spin liquids to unconventional superconductors," *Reports on Progress in Physics*, vol. 74, no. 5, p. 056501, 2011.

[34] S. Yan, D. A. Huse, and S. R. White, "Spin-liquid ground state of the s = 1/2 kagome heisenberg antiferromagnet," *Science*, vol. 332, no. 6034, pp. 1173–1176, 2011.

[35] Z. Meng, T. Lang, S. Wessel, F. Assaad, and A. Muramatsu, "Quantum spin liquid emerging in two-dimensional correlated dirac fermions," *Nature*, vol. 464, no. 7290, pp. 847–851, 2010.

[36] S. Sorella, Y. Otsuka, and S. Yunoki, "Absence of a spin liquid phase in the hubbard model on the honeycomb lattice," *Scientific reports*, vol. 2, 2012.

[37] T. Maier, M. Jarrell, T. Pruschke, and M. H. Hettler, "Quantum cluster theories," *Rev. Mod. Phys.*, vol. 77, pp. 1027–1080, Oct 2005.

[38] G. Kotliar, S. Y. Savrasov, K. Haule, V. S. Oudovenko, O. Parcollet, and C. A. Marianetti, "Electronic structure calculations with dynamical mean-field theory," *Rev. Mod. Phys.*, vol. 78, pp. 865–951, Aug 2006.

[39] A.-M. S. Tremblay, B. Kyung, and D. SÃl'nÃl'chal, "Pseudogap and high-temperature superconductivity from weak to strong coupling. towards a quantitative theory (review article)," *Low Temperature Physics*, vol. 32, no. 4, pp. 424–451, 2006.

[40] M.-T. Tran and K. Kuroki, "Finite-temperature semimetal-insulator transition on the honeycomb lattice," *Phys. Rev. B*, vol. 79, p. 125125, Mar 2009.

[41] S. A. Jafari, "Dynamical mean field study of the dirac liquid," *The European Physical Journal B*, vol. 68, no. 4, pp. 537–542, 2009.

[42] M. Ebrahimkhas, "Exact diagonalization study of 2d hubbard model on honeycomb lattice: Semi-metal to insulator transition," *Physics Letters A*, vol. 375, no. 36, pp. 3223 – 3227, 2011.

[43] W. Wu, S. Rachel, W.-M. Liu, and K. Le Hur, "Quantum spin hall insulators with interactions and lattice anisotropy," *Phys. Rev. B*, vol. 85, p. 205102, May 2012.

[44] J. C. Budich, B. Trauzettel, and G. Sangiovanni, "Fluctuation-driven topological hund insulators," *Phys. Rev. B*, vol. 87, p. 235104, Jun 2013.

[45] S.-L. Yu, X. C. Xie, and J.-X. Li, "Mott physics and topological phase transition in correlated dirac fermions," *Phys. Rev. Lett.*, vol. 107, p. 010401, Jun 2011.

[46] W. Wu, Y.-H. Chen, H.-S. Tao, N.-H. Tong, and W.-M. Liu, "Interacting dirac fermions on honeycomb lattice," *Phys. Rev. B*, vol. 82, p. 245102, Dec 2010.

[47] S. Hassan and D. Sénéchal, "Absence of spin liquid in nonfrustrated correlated systems," *Physical review letters*, vol. 110, no. 9, p. 096402, 2013.

[48] A. Liebsch, "Correlated dirac fermions on the honeycomb lattice studied within cluster dynamical mean field theory," *Phys. Rev. B*, vol. 83, p. 035113, Jan 2011.

[49] A. Liebsch and W. Wu, "Coulomb correlations in the honeycomb lattice: Role of translation symmetry," *Phys. Rev. B*, vol. 87, p. 205127, May 2013.

[50] R.-Q. He and Z.-Y. Lu, "Cluster dynamical mean field theory of quantum phases on a honeycomb lattice," *Phys. Rev. B*, vol. 86, p. 045105, Jul 2012.

[51] K. Seki and Y. Ohta, "Variational cluster approach to the hubbard model on a honeycomb lattice," *Journal of the Korean Physical Society*, vol. 62, no. 12, pp. 2150–2154, 2013.

[52] F. F. Assaad and I. F. Herbut, "Pinning the order: The nature of quantum criticality in the hubbard model on honeycomb lattice," *Phys. Rev. X*, vol. 3, p. 031010, Aug 2013.

[53] C. Honerkamp, "Density waves and cooper pairing on the honeycomb lattice," *Phys. Rev. Lett.*, vol. 100, p. 146404, Apr 2008.

[54] S. Raghu, X.-L. Qi, C. Honerkamp, and S.-C. Zhang, "Topological mott insulators," *Phys. Rev. Lett.*, vol. 100, p. 156401, Apr 2008.

[55] Z. H. Ni, T. Yu, Y. H. Lu, Y. Y. Wang, Y. P. Feng, and Z. X. Shen, "Uniaxial strain on graphene: Raman spectroscopy study and band-gap opening," *ACS Nano*, vol. 2, no. 11, pp. 2301–2305, 2008. PMID: 19206396.

[56] V. M. Pereira, A. C. Neto, and N. Peres, "Tight-binding approach to uniaxial strain in graphene," *Physical Review B*, vol. 80, no. 4, p. 045401, 2009.

[57] T. Moriya and K. Usami, "Magneto-volume effect and invar phenomena in ferromagnetic metals," *Solid State Communications*, vol. 34, no. 2, pp. 95 – 99, 1980.

[58] J. Bednorz and K. Müller, "Possible hight c superconductivity in the ba- la- cu- o system," *Zeitschrift für Physik B Condensed Matter*, vol. 64, no. 2, pp. 189–193, 1986.

[59] H. Takagi, S. Uchida, and Y. Tokura, "Superconductivity produced by electron doping in $\mathrm{cuo_2}$-layered compounds," *Phys. Rev. Lett.*, vol. 62, pp. 1197–1200, Mar 1989.

[60] Y. Tokura, H. Takagi, and S. Uchida, "A superconducting copper oxide compound with electrons as the charge carriers," *Nature*, vol. 337, pp. 345–347, Jan 1989.

[61] D. Sénéchal and A.-M. S. Tremblay, "Hot spots and pseudogaps for hole- and electron-doped high-temperature superconductors," *Phys. Rev. Lett.*, vol. 92, p. 126401, Mar 2004.

[62] M. T. Béal-Monod, C. Bourbonnais, and V. J. Emery, "Possible superconductivity in nearly antiferromagnetic itinerant fermion systems," *Phys. Rev. B*, vol. 34, pp. 7716–7720, Dec 1986.

[63] K. Miyake, S. Schmitt-Rink, and C. M. Varma, "Spin-fluctuation-mediated even-parity pairing in heavy-fermion superconductors," *Phys. Rev. B*, vol. 34, pp. 6554–6556, Nov 1986.

[64] D. J. Scalapino, E. Loh, and J. E. Hirsch, "d-wave pairing near a spin-density-wave instability," *Phys. Rev. B*, vol. 34, pp. 8190–8192, Dec 1986.

[65] L. Caron and C. Bourbonnais, "Importance of one-dimensional correlations in the phase diagram of the (tmttf)2-(tmtsf)2-x salts," *Physica B+C*, vol. 143, no. 1, pp. 453 – 455, 1986.

[66] E. Pavarini, I. Dasgupta, T. Saha-Dasgupta, O. Jepsen, and O. K. Andersen, "Band-structure trend in hole-doped cuprates and correlation with $t_{c\max}$," *Phys. Rev. Lett.*, vol. 87, p. 047003, Jul 2001.

[67] A. Ino, C. Kim, T. Mizokawa, Z.-X. Shen, A. Fujimori, M. Takaba, K. Tamasaku, H. Eisaki, and S. Uchida, "Fermi surface and band dispersion in la 2-xsrxcuo 4," *Journal of the Physical Society of Japan*, vol. 68, no. 5, pp. 1496–1499, 1999.

[68] A. Ino, C. Kim, M. Nakamura, T. Yoshida, T. Mizokawa, A. Fujimori, Z.-X. Shen, T. Kakeshita, H. Eisaki, and S. Uchida, "Doping-dependent evolution of the electronic structure of $\mathrm{la}_{2-x}\mathrm{sr}_x\mathrm{cuo}_4$ in the superconducting and metallic phases," *Phys. Rev. B*, vol. 65, p. 094504, Feb 2002.

[69] W. E. Pickett, "Electronic structure of the high-temperature oxide superconductors," *Rev. Mod. Phys.*, vol. 61, pp. 433–512, Apr 1989.

[70] A. Damascelli, Z. Hussain, and Z.-X. Shen, "Angle-resolved photoemission studies of the cuprate superconductors," *Rev. Mod. Phys.*, vol. 75, pp. 473–541, Apr 2003.

[71] T. Yoshida, X. J. Zhou, K. Tanaka, W. L. Yang, Z. Hussain, Z.-X. Shen, A. Fujimori, S. Sahrakorpi, M. Lindroos, R. S. Markiewicz, A. Bansil, S. Komiya, Y. Ando, H. Eisaki, T. Kakeshita, and S. Uchida, "Systematic doping evolution of the underlying fermi surface of $\mathrm{la}_{2-x}\mathrm{sr}_x\mathrm{Cuo}_4$," *Phys. Rev. B*, vol. 74, p. 224510, Dec 2006.

[72] N. E. Bickers, D. J. Scalapino, and S. R. White, "Conserving approximations for strongly correlated electron systems: Bethe-salpeter equation and dynamics for the two-dimensional hubbard model," *Phys. Rev. Lett.*, vol. 62, pp. 961–964, Feb 1989.

[73] D. Scalapino, "The case for dx2 âĹŠ y2 pairing in the cuprate superconductors," *Physics Reports*, vol. 250, no. 6, pp. 329 – 365, 1995.

[74] T. Moriya and K. Ueda, "Antiferromagnetic spin fluctuation and superconductivity," *Reports on Progress in Physics*, vol. 66, no. 8, p. 1299, 2003.

[75] P. Monthoux, A. V. Balatsky, and D. Pines, "Toward a theory of high-temperature superconductivity in the antiferromagnetically correlated cuprate oxides," *Phys. Rev. Lett.*, vol. 67, pp. 3448–3451, Dec 1991.

[76] P. Monthoux and G. G. Lonzarich, "p-wave and d -wave superconductivity in quasi-two-dimensional metals," *Phys. Rev. B*, vol. 59, pp. 14598–14605, Jun 1999.

[77] C. J. Halboth and W. Metzner, "Renormalization-group analysis of the two-dimensional hubbard model," *Phys. Rev. B*, vol. 61, pp. 7364–7377, Mar 2000.

[78] J. Reiss, D. Rohe, and W. Metzner, "Renormalized mean-field analysis of antiferromagnetism and d-wave superconductivity in the two-dimensional hubbard model," *Phys. Rev. B*, vol. 75, p. 075110, Feb 2007.

[79] A. Eberlein and W. Metzner, "Superconductivity in the two-dimensional t-$t^{'}$-hubbard model," *Phys. Rev. B*, vol. 89, p. 035126, Jan 2014.

[80] H. Yamase, A. Eberlein, and W. Metzner, "Coexistence of incommensurate magnetism and superconductivity in the two-dimensional hubbard model," *Phys. Rev. Lett.*, vol. 116, p. 096402, Mar 2016.

[81] D. Sénéchal, P.-L. Lavertu, M.-A. Marois, and A.-M. S. Tremblay, "Competition between antiferromagnetism and superconductivity in high-T_c cuprates," *Phys. Rev. Lett.*, vol. 94, p. 156404, Apr 2005.

[82] T. Maier, M. Jarrell, T. Pruschke, and J. Keller, "d-wave superconductivity in the hubbard model," *Phys. Rev. Lett.*, vol. 85, pp. 1524–1527, Aug 2000.

[83] T. A. Maier, M. Jarrell, T. C. Schulthess, P. R. C. Kent, and J. B. White, "Systematic study of d-wave superconductivity in the 2d repulsive hubbard model," *Phys. Rev. Lett.*, vol. 95, p. 237001, Nov 2005.

[84] K. Haule and G. Kotliar, "Strongly correlated superconductivity: A plaquette dynamical mean-field theory study," *Phys. Rev. B*, vol. 76, p. 104509, Sep 2007.

[85] M. Aichhorn, E. Arrigoni, M. Potthoff, and W. Hanke, "Antiferromagnetic to superconducting phase transition in the hole- and electron-doped hubbard model at zero temperature," *Phys. Rev. B*, vol. 74, p. 024508, Jul 2006.

[86] S. S. Kancharla, B. Kyung, D. Sénéchal, M. Civelli, M. Capone, G. Kotliar, and A.-M. S. Tremblay, "Anomalous superconductivity and its competition with antiferromagnetism in doped mott insulators," *Phys. Rev. B*, vol. 77, p. 184516, May 2008.

[87] A. Paramekanti, M. Randeria, and N. Trivedi, "Projected wave functions and high temperature superconductivity," *Phys. Rev. Lett.*, vol. 87, p. 217002, Nov 2001.

[88] N. Bulut, "d x 2 - y 2 superconductivity and the hubbard model," *Advances in Physics*, vol. 51, no. 7, pp. 1587–1667, 2002.

[89] L. Spanu, M. Lugas, F. Becca, and S. Sorella, "Magnetism and superconductivity in the t-$t^{'}$-j model," *Phys. Rev. B*, vol. 77, p. 024510, Jan 2008.

[90] B.-X. Zheng and G. K.-L. Chan, "Ground-state phase diagram of the square lattice hubbard model from density matrix embedding theory," *Phys. Rev. B*, vol. 93, p. 035126, Jan 2016.

[91] N. P. Armitage, P. Fournier, and R. L. Greene, "Progress and perspectives on electron-doped cuprates," *Rev. Mod. Phys.*, vol. 82, pp. 2421–2487, Sep 2010.

[92] T. Tohyama and S. Maekawa, "Role of next-nearest-neighbor hopping in the *t* - *t* '- *J* model," *Phys. Rev. B*, vol. 49, pp. 3596–3599, Feb 1994.

[93] R. J. Gooding, K. J. E. Vos, and P. W. Leung, "Theory of electron-hole asymmetry in doped cuo_2 planes," *Phys. Rev. B*, vol. 50, pp. 12866–12875, Nov 1994.

[94] T. Tohyama and S. Maekawa, "Electronic states in the antiferromagnetic phase of electron-doped high-T_c cuprates," *Phys. Rev. B*, vol. 64, p. 212505, Nov 2001.

[95] A. Singh and H. Ghosh, "Stability of the doped antiferromagnetic state of the $t - t^{'}$ hubbard model," *Phys. Rev. B*, vol. 65, p. 134414, Mar 2002.

[96] S. Pathak, V. B. Shenoy, M. Randeria, and N. Trivedi, "Competition between antiferromagnetic and superconducting states, electron-hole doping asymmetry, and fermi-surface topology in high temperature superconductors," *Phys. Rev. Lett.*, vol. 102, p. 027002, Jan 2009.

[97] D. Ogura and K. Kuroki, "Asymmetry of superconductivity in hole- and electron-doped cuprates: Explanation within two-particle self-consistent analysis for the three-band model," *Phys. Rev. B*, vol. 92, p. 144511, Oct 2015.

[98] C.-H. Pao and N. E. Bickers, "Renormalization-group acceleration of self-consistent field solutions: Two-dimensional hubbard model," *Phys. Rev. B*, vol. 49, pp. 1586–1599, Jan 1994.

[99] M. Brinkmann, T. Rex, H. Bach, and K. Westerholt, "Extended superconducting concentration range observed in $\mathrm{pr}_{2-x}\mathrm{ce}_x\mathrm{cuo}_{4-\delta}$," *Phys. Rev. Lett.*, vol. 74, pp. 4927–4930, Jun 1995.

[100] T. Adachi, Y. Mori, A. Takahashi, M. Kato, T. Nishizaki, T. Sasaki, N. Kobayashi, and Y. Koike, "Evolution of the electronic state through the reduction annealing in electron-doped pr1.3-xla0.7cexcuo4+ÃŐÂt' (x=0.10) single crystals: Antiferromagnetism, kondo effect, and superconductivity," *Journal of the Physical Society of Japan*, vol. 82, no. 6, p. 063713, 2013.

[101] Y. Krockenberger, H. Irie, O. Matsumoto, K. Yamagami, M. Mitsuhashi, A. Tsukada, M. Naito, and H. Yamamoto, "Emerging superconductivity hidden beneath charge-transfer insulators," *Scientific Reports*, vol. 3, pp. 2235 EP –, Jul 2013. Article.